Doctoral Dissertations   Student Scholarship

Spring 2015

Developing Index Parameters for Cracking in Asphalt Pavements Through Black Space and Viscoelastic Continuum Damage Principles

David Jonathan Mensching
University of New Hampshire, Durham

Follow this and additional works at: https://scholars.unh.edu/dissertation

DEVELOPING INDEX PARAMETERS FOR CRACKING IN ASPHALT PAVEMENTS

THROUGH BLACK SPACE AND VISCOELASTIC CONTINUUM DAMAGE PRINCIPLES

BY

DAVID JONATHAN MENSCHING

B.S. Civil Engineering, Villanova University, 2010

M.S. Civil Engineering, Villanova University, 2011

DISSERTATION

Submitted to the University of New Hampshire

in Partial Fulfillment of

the Requirements for the Degree of

Doctor of Philosophy

in

Civil Engineering

May, 2015

This dissertation has been examined and approved in partial fulfillment of the requirements for the degree of Doctor of Philosophy in Civil Engineering by:

Dissertation Director, Jo Sias Daniel, Professor of Civil Engineering

Eshan V. Dave, Assistant Professor of Civil Engineering

Majid Ghayoomi, Assistant Professor of Civil Engineering

Nelson H. Gibson, Research Engineer, Federal Highway Administration

Leslie Myers McCarthy, Assistant Professor, Villanova University

B. Shane Underwood, Assistant Professor, Arizona State University

On April 28, 2015

Original approval signatures are on file with the University of New Hampshire Graduate School.

DEDICATION

To Lauren, who undertook this journey with me and provided the love, patience, and support I

needed to complete this work.

ACKNOWLEDGEMENTS

TABLE OF CONTENTS

LIST OF TABLES

LIST OF FIGURES

ABSTRACT

DEVELOPING INDEX PARAMETERS FOR CRACKING IN ASPHALT PAVEMENTS

THROUGH BLACK SPACE AND VISCOELASTIC CONTINUUM DAMAGE PRINCIPLES

by

David Jonathan Mensching

University of New Hampshire, May, 2015

Cracking is a major distress for asphalt concrete pavements and presents significant challenges to effective design and maintenance. Fatigue and thermal cracking decrease ride quality of the pavement and allow water to penetrate into underlying layers, which can result in major damage if left unchecked. The primary obstacle in predicting field performance for cracking in asphalt pavements is related to the interaction of material, structural, and environmental components. The major objective of this work is to develop index parameters to relate material and structural parameters, identifying whether a mixture is prone to fatigue or thermal cracking.

A Simplified Viscoelastic Continuum Damage (S-VECD) model, which relates material integrity and damage growth under repeated loading, is used in this project. The structural response is evaluated using layered elastic analysis principles in order to establish a material-structure space, where the pass/fail determination is based. This pass/fail index parameter is operationally efficient and easy to implement at a contractor or owner agency with capacity to test materials in the S-VECD configuration.

A thermal cracking parameter is developed for mixtures through a relation to laboratory and field performances in terms of Black Space. Since Black Space diagrams are able to capture changes in stiffness and relaxation, where separation would be indicative of poorly performing materials, these parameters provide insight into relationships among pavement structures and mixture designs. The results also lend themselves to the formation of performance-related specifications, where agencies can require a certain parameter value based on experimental and field observations. Opportunities exist to extend the parameter definitions among length scales, to further examine the effects of each on cracking performance. The capabilities of the parameter will influence design and funding decisions, resulting in cost savings at the owner agency and contractor levels through enhanced performance and a reduced testing framework.

CHAPTER 1

INTRODUCTION

Pavement engineers hold a societal duty to provide for the safe movement of goods, services, and people while effectively using, managing, and preserving natural, material, and monetary resources. With that said, asphalt concrete is an immensely complex material, where time, temperature, loading rate, and inherent non-homogeneity between the components of the mixture influence field performance and ultimately the experience of the traveling public. Some of the most prominent causes of asphalt pavement failure require conflicting material property accommodations as well, which further complicates design. Localized calibration of performance models and the desire for increased usage of non-traditional components in the asphalt mixture also pose challenges to engineers. Research in the community has focused largely on characterization, modeling, and specification development in an effort to predict and monitor performance to improve design and preservation of the asset. The pressures facing all transportation engineers stem from tighter budgets at state and federal levels and the enormous level of exposure the facilities designed and maintained receive from society.

In the asphalt industry, governmental funding is outlined in accordance with the Moving Ahead for Progress in the 21st Century Act (or MAP-21). The legislation calls for the transformation of policy towards a streamlined and performance-based approach to surface transportation projects, a major shift in the funding methodologies of the past. In the United States, the transportation

industry is at a crossroads – the American Society of Civil Engineers (ASCE) Infrastructure Report Card for 2013 gave roadways in the nation a D (or poor) grade, stating that there is a $79 billion annual deficit in the capital investment being set aside for roadway improvement and the amount the Federal Highway Administration (FHWA) needs to significantly improve conditions and performance (ASCE, 2013). At FHWA, researchers and engineers are exploring ways to encourage cooperation among stakeholders and transition towards the goals of MAP-21, which could help to close this funding gap in the future. In the asphalt materials field, a need for performance-based mixture design is evident, as far too many roadways exhibit premature distress and failure, costing taxpayers time and money due to frequent rehabilitation and increased congestion.

Regarding asphalt pavements, cracking is a major distress type that causes problems throughout the United States. Cracks decrease ride quality, introduce avenues for water to infiltrate and destroy the pavement structure, and cost users millions of dollars in delays due to rehabilitation (or lack thereof) and decreased fuel economy. The two primary types of cracking are low temperature (thermal), which run transverse to the direction of traffic, and fatigue cracking, which usually appear in the direction of traffic. A more detailed description of these distresses and their contributing mechanisms is available in Chapter 2 of this dissertation.

1.1 Statement of Problem

In an aging and under-funded infrastructure, performance-based decisions are vital for the most effective use of taxpayer dollars. In asphalt mixture design, contractors and owner agencies must understand the ramifications of design decisions and receive guidance to reach an optimum proportion of asphalt and associated additives and aggregate for prolonged levels of satisfactory

2

performance. A tool is needed to provide guidance with scientific backing to maximize efficiency in raw materials selection, material design, and structural design to ultimately extend pavement life.

1.2 Objectives

The primary objectives of this dissertation are to:

1. Analyze performance differences between binder and mixture-based methodologies and to evaluate the impact of reclaimed asphalt materials on low temperature and fatigue resistance;

2. To develop a mixture-based low temperature cracking parameter in Black Space, using dynamic modulus ($|E*|$) and phase angle (δ) to account for increased usage of additives and specialized materials and any asphalt-aggregate interactions that cannot be captured in an approach dominated by binder properties;

3. To relate $|E*|$ and the Simplified-Viscoelastic Continuum Damage (S-VECD) model in the form of an index parameter, the purpose of which is to provide agencies with a singular pass/fail prediction for crack resistant mixtures in the field. The parameter will also consider the impacts of pavement structure, temperature, and loading conditions to develop a comprehensive sense of crack resistance;

4. To enhance understanding of cracking phenomena in asphalt concrete as it relates to stiffness and ductility;

5. To provide a robust and efficient system of tools for advanced detection of poorly performing materials and monitoring of degradation of in-place pavements, which can be used in a performance-based framework which can be developed from mixture

design through the end of service. The system should require minimal laboratory testing for characterization of materials and utilize standardized procedures and test equipment.

1.3 Structure of Work

The form of this dissertation is meant to be a series of published or publishable technical papers relating to the formation of parameters for advanced detection of poor-performing asphalt mixtures in bottom-up fatigue and thermal cracking modes. Please note that the author of this dissertation is also the primary author of all technical chapters. Chapter 1 provides an introduction to the problem and significance of cracking characterization for asphalt pavements, the objectives of the dissertation, and the scope. Chapter 2 provides a literature review highlighting critical elements of linear viscoelasticity and thermal and fatigue cracking.

Chapter 3 is in the form of a technical paper published by the Association of Asphalt Paving Technologists and the Journal of Road Materials and Pavement Design, entitled "Low Temperature Properties of Plant-Produced RAP Mixtures in the Northeast". The author of this dissertation was the lead for this work. The relevance of this paper to the overall dissertation and the asphalt technology community is to examine low temperature performance and prediction with respect to materials with RAP. The paper also comments on the variation in these analysis methods compared to field conditions and introduces the idea that binder and mixture performance predictions show notable variation among experimental and predictive techniques, providing a backdrop for the mixture-based parameters developed later in this dissertation.

Chapter 4 presents a technical paper submitted for publication to the American Society of Civil Engineers Journal of Materials in Civil Engineering, entitled "Applying the Glover-Rowe

Parameter to Evaluate Low Temperature Performance of Hot Mix Asphalt LTPP Sections". This chapter is comprised of a validation study initially submitted to the American Society of Civil Engineers Transportation and Development Institute Long Term Pavement Performance International Data Analysis Contest in the summer of 2014. There are also plans to submit an abstract of this chapter to the Petersen Asphalt Conference for presentation. The paper was selected as the runner-up in the Graduate Category of the contest. Several field-aged binders from the Long-Term Pavement Performance (LTPP) database are analyzed using three indicator methods based on rheological properties, one being the Glover-Rowe parameter. The Glover-Rowe parameter is the motivation behind the mixture-based low temperature parameter developed later in the dissertation, and the suitability of this measure for use with LTPP sections is discussed.

Chapter 5 of the dissertation is in the form of a technical paper accepted for publication by the Association of Asphalt Paving Technologists and Journal of Road Materials and Pavement Design, entitled "Exploring Low Temperature Performance in Black Space". The author of this dissertation acted as the lead researcher of the study. In this paper, the effectiveness of the intermediate and low temperature Glover-Rowe parameter is evaluated for several binders from various locations and compared with field data. The initial discussion and exploration of a low temperature mixture-based parameter is shown for 17 plant-produced mixtures by comparing dynamic modulus and phase angle values with laboratory-measured performance characteristics.

Chapter 6 is comprised of a manuscript to be submitted for publication, entitled "A Mixture-Based Black Space Parameter for Low Temperature Performance of Hot Mix Asphalt Sections". The primary focus of this portion of the dissertation is to define the low temperature mixture parameter for available materials so that a single temperature and frequency combination is

required for dynamic modulus and phase angle measurements, coupled in this case with some laboratory performance measure. The paper also uses LTPP sections with measured field performance for validation and refinement purposes. Recommendations are made as to the effectiveness of the parameter, the mixture data available in the database, as well as the conversion methods from binder modulus to mixture modulus. The opportunity for revisions of the parameter itself is also discussed.

Chapter 7 begins the process of defining the mixture-based parameter for fatigue cracking through inclusion of a manuscript to be submitted for publication, entitled "Developing an Indicator for Fatigue Cracking in Hot Mix Asphalt Pavements Using Viscoelastic Continuum Damage Principles". Elements of this chapter are being submitted for publication and presentation at the 8th RILEM International Conference on Mechanisms of Cracking and Debonding in Pavements in Nantes, France. An in-depth analysis of the dynamic modulus and phase angle master curves and the outputs from the Simplified Viscoelastic Continuum Damage (S-VECD) model is executed to develop a material space encompassing stiffness and relaxation considerations for detection of poorly performing materials in bottom-up fatigue cracking. In this piece, pavement structural information from the LTPP database is used to develop strain profiles to be used in conjunction with the asphalt material characterization approach. This approach can be refined and expanded with field performance data to be used to assist in agency decision-making processes for mixture design and ultimately preservation of the pavement system as a whole.

Chapter 8 provides a closing discussion which touches on the author's progression towards a mixture-based parameter and the range of application at this time. Plans for post-graduate work are identified and presented from the perspective of developing a performance-based

specification not only for mixture design, but for construction and life cycle analysis of the pavement asset. Chapter 9 is comprised of a master reference list, while the Appendix includes the raw data used in the dissertation work.

CHAPTER 2

LITERATURE REVIEW

In order to satisfy the objectives of the following research, a review of pertinent literature was undertaken. As mentioned previously, the form of the dissertation is a series of papers of refereed journal quality relating to the formulation of thermal and fatigue cracking parameters for advanced detection of poorly performing binders and mixtures. The material in Chapter 2 is presented in three sections relating to linear viscoelasticity (LVE), thermal cracking, and fatigue cracking. Furthermore, the cracking sections delve briefly into the mechanisms of each distress type and testing of asphalt concrete. Additional literature review (e.g., appropriate modeling) is available in subsequent chapters as required in each technical paper.

2.1 Linear Viscoelasticity

Asphalt is a viscoelastic material, meaning it exhibits time and temperature dependence and possesses capacity to store and dissipate energy under loading (Christensen, 2003). With this in mind, behavior of asphalt under loading is quite complex. For engineering applications, it is often sufficient to model the response by assuming or operating within the LVE region, where stress is proportional to strain at a given time and the linear superposition principle applies (Findley, Lai, and Onaran, 1976). The linear, or Boltzmann, superposition principle expresses the additivity or historical effects of stresses and strains over time through convolution integrals,

shown in Equations 2.1 and 2.2 (Tschoegl, 1989). The premise is also illustrated in Figure 2.4, where the magnitude of the strain response at t_2 is reliant on the strain experienced at t_1.

$$\sigma = \int_0^t E(t - \tau) \frac{d\varepsilon}{d\tau} d\tau \qquad [2.1]$$

$$\varepsilon = \int_0^t D(t - \tau) \frac{d\sigma}{d\tau} d\tau \qquad [2.2]$$

where,

σ = stress;

ε = strain;

t = time;

τ = previous time;

E(t) = relaxation function;

D(t) = creep compliance function.
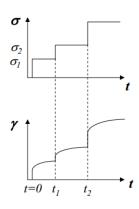
Figure 2.4: Schematic of linear superposition principle (VanLandingham, 2009)

9

2.1.1 Creep Compliance, Relaxation Modulus, and Dynamic Modulus

Generally, viscoelastic materials experience increasing strain under continued load, recover elastic strain instantaneously, and then undergo delayed recovery relating to viscous flow. The ability of the material to resist increasing strains under constant load is modeled through the creep compliance function. The rate of strain increase depends on the region of creep flow (primary, secondary, or tertiary), which is driven by the duration of the load. Under constant strain, the material experiences decreasing stress with time (referred to as stress relaxation). The relaxation modulus function relates the rate of stress decrease under constant strain. Although not discussed in depth here, there exist many combinations of mechanical models to describe the creep and relaxation functions through springs (to represent elasticity) and dashpots (to represent viscous components). Figure 2.5 shows a typical LVE response under a) constant stress and b) constant strain.

(a)

(b)
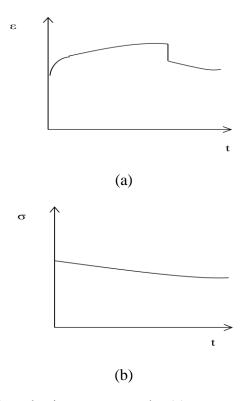
Figure 2.5: Typical linear viscoelastic response under (a) constant stress and (b) constant strain

10

Aside from constant stress and strain loading, LVE characterization can also be achieved through harmonic excitation, either in controlled stress or controlled strain modes. The loading waveform is usually sinusoidal and in shear, tension, or compression. By monitoring stress and strain, researchers can identify two important viscoleastic properties: the complex modulus (E*) and phase angle (δ). The complex modulus is comprised of a real component, representing energy storage, and an imaginary component, representing the energy dissipation per unit volume. In vector space, calculating the magnitude of the storage (E′) and loss (E″) moduli results in the dynamic modulus (|E*|), which is also found by dividing the stress amplitudes by the strain amplitudes. Note that for binders, shear oscillation is primarily used to determine complex shear modulus (G*), dynamic shear modulus (|G*|), storage shear modulus (G′), and loss shear modulus (G″).

The phase angle is important for asphalt characterization due to its ability to indicate dominating elastic or viscous response under loading. The phase angle often represents the time lag of strain response to a stress input, as shown in Figure 2.6. The angle varies from 0 to 90°, with the minimum value corresponding to a purely elastic material and the maximum corresponding to a purely viscous material. The phase angle is used to calculate E′ and E″ from the |E*| by using simple trigonometric manipulations. The same is true in shear loading. A simple equation for calculating phase angle from a particular time lag and loading frequency is shown in Equation 2.3.
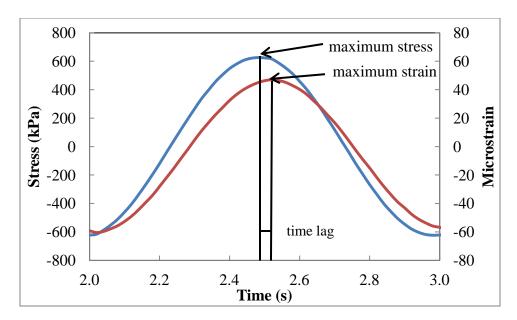
Figure 2.6: Schematic of stress and strain sinusoidal waveforms with time lag used to calculate phase angle

$$\delta = 2\pi f \Delta t$$

[2.3]

where,

δ = phase angle;

f   = loading frequency;

Δt = time lag between stress and strain.

To fit viscoelastic functions for determining material properties over a range of conditions, a Prony (Dirichlet) series is often employed through a series of exponentials. The series is used to model creep compliance through a Generalized Voigt model and storage, loss, and relaxation modulus functions through the Generalized Maxwell (or Wiechert) mechanical models, respectively (Kim, 2009). The forms of these manipulations are shown in Equations 2.4-2.7.

Note the number of retardation/relaxation strengths and times correspond to the number of elements in the mechanical model.

$$D(t) = D_0 + \sum_{m}^{M} D_m (1 - e^{\frac{-t}{\tau_m}}) \qquad [2.4]$$

$$E(t) = E_\infty + \sum_{m=1}^{M} E_m e^{\frac{-t}{\rho_m}} \qquad [2.5]$$

$$E'(\omega) = E_\infty + \sum_{m=1}^{M} \frac{\omega^2 \rho_m^2 E_m}{1 + \omega^2 \rho_m^2} \qquad [2.6]$$

$$E''(\omega) = \sum_{m=1}^{M} \frac{\omega \rho_m E_m}{1 + \omega^2 \rho_m^2} \qquad [2.7]$$

where,

D(t)   = creep compliance function (retardation spectra);

D_0 = glassy (or short-time) compliance;

D_m = retardation strength;

t   = time;

τ_m = retardation time;

E(t)   = relaxation modulus function (relaxation spectra);

E'(ω)   = storage modulus function;

13

$E''(\omega)$ = loss modulus function;

E_∞ = equilibrium (long-time) modulus;

E_m = relaxation strength;

ρ_m = relaxation time.

There are several ways to fit the Prony series to determine the regression coefficients (i.e., retardation strengths and times) and the response functions. One method is the collocation method, initially used by Schapery (1961), which solves a system of nonlinear equations among a range of decades on the log time scale to obtain the retardation/relaxation times and strengths. Once a Prony series for a particular response function is known, interconversions exist to determine other viscoelastic properties. Where appropriate, the matrix manipulations devised by Park and Schapery (1999) and Schapery and Park (1999) are used. Another method using Baumgaertel and Winter's (1989) nonlinear optimization of the regression coefficients is used. This approach uses discrete relaxation and retardation spectra to calculate material properties over a wide range of loading times and frequencies and is part of the analysis procedure in Abatech, Inc.'s Rheology Analysis (RHEA) software, which will be used later on in the dissertation.

2.1.2 Time-Temperature Superposition and Ranges of Linear Viscoelasticity

The time-temperature superposition principle (TTSP) is a well-documented and commonly-used principle in viscoelastic analyses, allowing for reduced testing conditions. By shifting isotherms with a particular time-temperature shift factor, a wide range of temperatures and loading rates/times can be modeled in a single master curve. The master curve becomes dependent on a reduced time or frequency which is related to the isotherms. Reduced frequency is found by

14

multiplying the measured frequency by the time-temperature shift factor, while reduced time is found through division by the shift factor. The shift factors themselves can be obtained through manual manipulation or functional fit. In this work, functional fits are used and are explained further in subsequent chapters. Figure 2.7 demonstrates the application of the TTSP. The isotherms warmer than the reference temperature (in this case 5°C) will shift to the left and be represented by a shift factor less than unity. The opposite is true for isotherms colder than the reference.
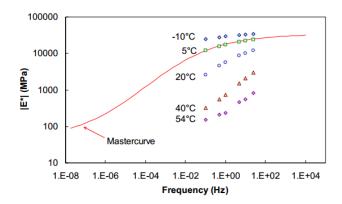
Figure 2.7: Demonstration of the time-temperature superposition principle (Kim et al., 2009)

As it relates to material testing to develop a master curve, researchers strive to operate within the microstrain range where LVE behavior is present. Otherwise, the material is not thermorheologically simple and the shift factor relationships are void. Generally, the LVE limit is believed to be from about 50-100 microstrain (Monismith 1966; AASHTO 2012i). However, recent studies have found that asphalt concrete holds its thermorheologically simple behavior in conditions when large strain and growing damage is incurred (Chehab et al., 2002; Gibson et al., 2003; Gibson, 2006).

2.2 Thermal Cracking

In colder climates, transverse cracking caused by thermal loading is a major distress mode. As temperatures decrease, thermal stress increases and can eventually exceed the tensile strength of the material. Cracks typically manifest themselves in the perpendicular direction (with respect to the travel way) and in somewhat evenly spaced distances. As is the case with any surface crack, the discontinuity in the pavement structure provides an avenue for infiltration of water. It has been documented that water causes advanced deterioration of pavements, whether it be through the material itself or pumping of fines from underlying layer (Fromm and Phang, 1972). Recently, researchers postulate that thermal cracks result in a stress localization that can reduce resistance to longitudinal cracking (Marasteanu et al., 2004). Figure 2.8 provides a schematic of thermal cracking.

Figure 2.8: Thermal cracks in asphalt pavement (Dongré and D'Angelo, 2003)

2.2.1 Mechanical Background for Thermal Cracking

In the most general sense, transverse cracks result from a shrinkage associated with cold temperature events. Specifications, testing, and modeling efforts have sought to capture the effects of relaxation and stiffness in three primary ways to determine thermal cracking

16

resistance: 1) using a stiffness threshold at a particular time (or frequency) and temperature combination; 2) determining thermal stress build-up and comparing that to the tensile strength; and 3) a fracture mechanics-based approach (Anderson et al., 2001).

The stiffness-based approach is founded on the notion of a limiting modulus at very low temperatures, commonly referred to as the glassy modulus. The glassy modulus is a theoretical asymptote representing the purely elastic condition at very short loading times or very low temperatures. In the 1960s, Heukelom (1966) extrapolated a correlation in stiffness versus elongation at break to a common glassy modulus of 3 GPa. This data was also used to develop tensile strength versus stiffness curves for binders. One criticism of the study involves the time-temperature dependence of stiffness, which is not directly accounted for in the data (Glover et al., 2005).

Hills and Brien (1966) worked from Heukelom's data to determine a limiting stiffness and limiting stiffness temperature. The authors also realized that tensile stresses are generated during cooling of asphalt pavements which could exceed the tensile strength of the material. By noting that thermal strains in asphalt pavements are about 1 percent (using a typical coefficient of thermal contraction), the research proposed a corresponding limiting stiffness modulus of 400 MPa. Since then, many researchers have used time-temperature superposition to formulate limiting stiffness values based on specific loading times for binder specifications, the most prevalent of which is part of the Superpave grading system (Anderson et al., 1994; Fromm and Phang, 1970; McLeod, 1972; Readshaw, 1972; Anderson et al., 1994).

In the late 1980s and early 1990s, researchers associated with the Strategic Highway Research Program (SHRP) evaluated the stiffness modulus-based approach and found that the time-

dependency of the asphalt binder also held an integral role in the formation of shrinkage stresses. Therefore, the m-value (log-log slope of the creep stiffness curve) was used to aid in the assignment of performance-graded binders, as it sheds light onto the stress relaxation capabilities of the binder (Anderson et al., 2001). Later on, the m-value was determined to be related to phase angle, shear rate dependency, and rheological type of the binder, which lends itself to additional discussion in Chapters 4, 5, and 6 of the dissertation (Marasteanu and Anderson, 1999). The bending beam rheometer (BBR) is the standard piece of equipment to find the creep stiffness curve and m-value for binders.

Another approach to determine resistance to low temperature cracking involves linear elastic fracture mechanics (LEFM). Fracture mechanics is the study of the mechanical behavior of cracked materials under loading. LEFM, more specifically, assumes a material is homogeneous and isotropic with linear elastic behavior (Perez, 2004). Of the three fracture types (opening crack, sliding, or tearing), asphalt concrete exhibits opening (tension/Mode-I) cracks under thermal loads and sliding (or in-plane shear/Mode-II) cracks under vehicular loading (Braham, 2008; Perez, 2004). Griffith (1921) recognized that cracks will only grow when the released energy surpasses the energy required to form a new surface.

Later on, Irwin (1957) described the stress intensity factor, K, which can be used for LEFM conditions to describe a stress field near the crack tip (Anderson et al., 1994). The critical stress value, where crack propagation will begin, is known as the fracture toughness or K_C (Li, 2006). Another parameter used to characterize fracture behavior of materials is the critical strain energy release rate, J_C, or the J-integral (Rice, 1968). According to the literature, the fracture toughness cannot model fracture behavior in nonlinear cases, and hence the J-integral is more useful

(Anderson et al., 1994). Schapery (1984) modified the J-integral formulation to apply to viscoelastic materials, where time dependence influences the behavior under loading.

2.2.2 Testing for Thermal Cracking Resistance

Many tests are currently used to characterize the nature of low temperature performance for binders and mixture, featuring a range of geometries, loading configurations, and temperature protocols. A common issue in the asphalt materials community pertains to selecting the test that best correlates with field performance. The tests described below are options to use in the formulation of a low temperature parameter as a cracking measure, which can be separated into tests to measure thermal stress and strain, tests to measure material properties (e.g., strength, modulus), and tests to measure fracture properties. Of course, each test comes with its own challenges as it relates to time of preparation, ease of testing, and modeling. Introductions to these tests are provided to identify potential methods to use for a low temperature index parameter, either as a means to identify material properties or as a performance measure to aid in the definition of failure criteria. As the objectives of this dissertation relate to developing performance indicators for asphalt mixture, this section will not delve into binder testing methods in detail.

2.2.2.1 Direct Measures of Thermal Stress and Strain

A prevalent method to measure thermal stress accumulation with changes in temperature is the Thermal Stress Restrained Specimen Test (TSRST), specified by American Association of State Highway and Transportation Officials (AASHTO) Provisional Standard TP10. The test in its current form was developed as part of SHRP, after Vinson et al. (1990) decided the TSRST held the greatest potential for accurate characterization of low temperature performance for mixture

(Jung and Vinson, 1994). The earliest work with the test was done by Monismith et al. (1965), who measured thermal stress through restrained asphalt beam testing and predicted thermal stress from creep compliance curves. The test restricts contraction in the specimen, which in turn causes thermal tensile stresses to increase as temperatures drop, ultimately resulting in fracture of the specimen. A thermal stress curve can be derived, as well as the critical cracking temperature for comparison with other test methods. Figure 2.9 is an image of a typical TSRST setup.

Figure 2.9: Sample TSRST setup (Asphalt Research Consortium, 2007)

A variation of the TSRST, the uniaxial thermal stress strain test (UTSST), has been developed by researchers at the University of Nevada, Reno. The primary difference among the two tests is in the introduction of an unrestrained specimen to measure thermal strain. By monitoring thermal strain and stress, thermovolumetric properties of the mixture can be obtained. More information is provided in Chapter 3.

A similar premise is used by the Asphalt Thermal Cracking Analyzer, developed by researchers at University of Wisconsin-Madison. The test, shown in Figure 2.10, uses an unrestrained sample to measure thermal strain, glass transition temperature, and coefficient of thermal contraction. A restrained beam is used to capture thermal stress build-up. The mechanism can

also measure fracture temperature and thermal stress relaxation directly (through a particular testing regimen), which are useful for low temperature study (Tabatabaee et al., 2012).
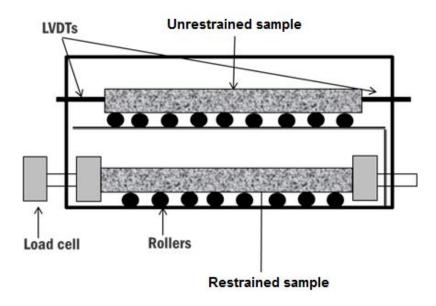
Figure 2.10: Asphalt Thermal Cracking Analyzer setup (Tabatabaee et al., 2012)

Another test possessing the capability to measure thermal stress/strain is the Asphalt Concrete Cracking Device (ACCD), which is a ring-shaped device capable of restraining the specimen (Figure 2.11). The test uses a steel ring surrounded by compacted hot mix asphalt (HMA), which eliminates the need for cutting and use of epoxy in the test preparation stages. The ring holds a strain gage and temperature sensor inside. A notch in the HMA sample introduces a stress concentration point for fracture to occur. The thermal strain curve allows the user to model thermal stress through LVE principles and to determine the fracture temperature. A study by Kim, Wargo, and Powers (2010) found the ACCD correlates well with TSRST results.

38 mm notch

Figure 2.11: Asphalt Concrete Cracking Device setup (Kim, Sargand, and Wargo, 2009)

2.2.2.2 Material Property Characterization

As mentioned previously, material properties for low temperature considerations primarily include relaxation modulus (typically converted from dynamic modulus or creep compliance) and tensile strength. Knowledge of the mixture material properties is important for estimating thermal stress development. Dynamic modulus testing is typically done in uniaxial compression at various temperatures and frequencies, in some fashion similar to AASHTO T342 (AASHTO, 2012g). Dynamic modulus can also be measured through diametral loading via indirect tension (IDT), usually with the test geometry specified in AASHTO T322 (AASHTO, 2012h). A master curve is then constructed and other LVE properties can be approximated from this relationship.

Creep compliance of the mixture is being measured at low temperatures using two methods primarily: IDT and BBR. The IDT setup applies a constant load for duration of 100 seconds, with a data acquisition system capturing displacement (or strain) with time. The Thermal Cracking Model (TCModel) methodology specifies the IDT creep testing be conducted at 0, -10, and -20°C. At this stage, the strain output can be used to calculate creep compliance for each linear variable differential transducer (LVDT) using the elastic solution specified in AASHTO

T322 itself, or a LVE-based method derived by researchers at North Carolina State University (AASHTO 2012h; Elwardany, 2012; Kim, Daniel, and Wen, 2002). Poisson's ratio is also calculated from the specimen dimensions and displacements (AASHTO, 2012h). The indirect tensile strength of the mixture can also be obtained using AASHTO T322 standards by loading an IDT specimen at a constant rate and recording load, displacement, and time. For low temperature considerations, the test is typically conducted at -10°C. The area under the load-displacement curve can be used to calculate the fracture energy of a sample, while the peak load is used to calculate the tensile strength (AASHTO, 2012h).

Recently, researchers have investigated the feasibility of using the BBR for asphalt mixtures, in attempts to find creep compliance and tensile strength at low temperatures (Marasteanu et al., 2009; Marasteanu et al., 2012b; Clendennen and Romero, 2013; Romero and Jones, 2013). To determine creep compliance (or stiffness), the midpoint deflection of a beam is monitored over the course of a 1000 second, constant-load test. The proposed specimen size is 6.25 mm thick by 12.5 mm wide by 125 mm long (Marasteanu et al., 2012b). The draft standard developed in 2009 calls for a particular load at a high temperature level (representing the low temperature PG grade + 22°C) and an intermediate temperature level (low temperature PG grade + 10°C). A low temperature level can be approximated using time-temperature superposition. The researchers have found that a linear relationship exists between IDT and BBR creep stiffness, and the magnitudes of IDT stiffness are generally smaller than the BBR values (Marasteanu et al., 2009). The BBR is also being proposed as a method to find tensile strength of mixture. In Marasteanu et al.'s work (2012a), the loading rate should be set so that the specimen fails within 15-20 seconds, to eliminate viscoelastic effects. IDT strength was found to be significantly lower than the BBR strength. The researchers argue that IDT strength testing has limitations due to a size

dependence that is not relevant in beam testing (Marasteanu et al., 2012b). The use of BBR for mixture is a controversial topic due to the specimen size, which may be smaller than the representative volume element (RVE) for a particular mixture type. The beam dimensions have been found to not be an RVE for strength testing, which requires modeling to extrapolate the characteristics to represent the whole (Marasteanu et al., 2012b). It has been confirmed that BBR creep testing for the mixture meets RVE requirements (Marasteanu et al., 2009; Clendennen and Romero, 2013).

2.2.2.3 Fracture-Based Testing

There are multiple testing methodologies which characterize low temperature susceptibility of HMA using fracture mechanics. The first tests featured the single edge notched beam (SE(B)) approach, where a notch is created at midspan and LEFM conditions are assumed (Marasteanu et al., 2007). During SHRP, Labuz and Dai (1994) conducted fracture tests using an unloading-reloading procedure to obtain multiple K_C values. However, the SE(B) testing is becoming less useful due to the Superpave Gyratory Compactor, which prepares cylindrical specimens (Marasteanu et al., 2007).

A cylindrical sample fracture test is the disk-shaped compact tension (DC(T)) test, which was developed at University of Illinois and is standardized in ASTM D7313 (Wagoner et al., 2005; ASTM, 2013). As Figure 2.12 shows, 25 mm holes are bored into the specimen on either side of a notched crack. The holes are used to load the specimen, which is in a crack mouth opening displacement (CMOD)-controlled setup, where the CMOD rate must remain constant throughout the test. From the acquired CMOD, load, and time data, fracture energy can be calculated. As stated in Wagoner, Buttlar, and Paulino (2005), the DC(T) holds potential for use as a laboratory

24

and field specimen test. The testing procedure is currently being implemented in Minnesota and

Iowa as a low temperature cracking specification, by citing minimum fracture energy values for

a given traffic design (Clyne, 2012; Marasteanu et al., 2012a).
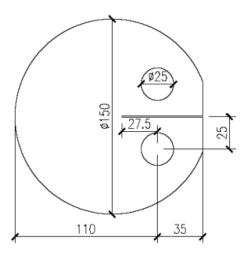
Figure 2.12: Disk-shaped compact tension test setup, with dimensions in mm (Marasteanu et al., 2007)

Another prevalent fracture mechanics-based test for low temperature cracking is the semi-

circular bend (SCB) test, first proposed by Chong and Kurrupu (1984). The test consists of a

semi-circular cylindrical specimen with an edge notch subjected to three point bending, as shown

in Figure 2.13. The test allows for the determination of the fracture energy, fracture toughess,

and stiffness of the material in Modes I and II. Similarly to the DC(T) test, the CMOD rate is

controlled throughout the test, with the load, time, and load line displacement being measured

(West, Willis, and Marasteanu, 2013). Researchers in Minnesota have elected to use the DC(T)

as a new low temperature specification over the SCB due to variability concerns and the fact that

the DC(T) is already an accepted standard test by ASTM (Clyne, 2012). Note that as part of the

NCHRP Project 9-46 report, a draft standard for the SCB has been developed (West, Willis, and

Marasteanu, 2013). The SCB is also being used at intermediate temperatures to analyze fatigue

resistance (Molenaar and Molenaar, 2000; Kim, Mohammad, and Elseifi, 2012; Huang, Shu, and Zuo, 2013).
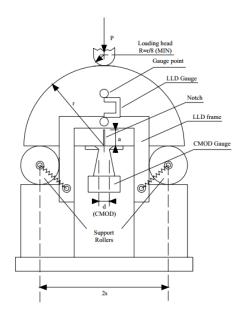
Figure 2.13: Semi-circular bend test setup (West, Willis, and Marasteanu, 2013)

2.3 Fatigue Cracking

In the case of traditional bottom-up fatigue (alligator) cracking, horizontal tensile strains develop under repetitive loading at the bottom of the asphalt layer that are below the ultimate strength of the material, forming microcracks in the pavement structure (Yoder and Witczak, 1975; Huang, 2004; Mallick and El-Korchi, 2013). These microcracks coalesce, localize, and propagate through the asphalt layer, eventually reaching the surface (Daniel, 2001; Underwood et al., 2009; Underwood, 2011). Fatigue cracking causes major problems in an asphalt pavement, ranging from decreased ride quality to the introduction of water into the underlying layers, which in turn can result in more bottom-up fatigue cracks. In this section, tests for fatigue characterization will be identified for mixture. The theory and applications behind the Viscoelastic Continuum Damage (VECD) model will also be discussed. Since the fatigue cracking portion of this

dissertation deals specifically with VECD theory, descriptions of other fatigue tests and modeling will be brief.

2.3.1 Mechanisms for Fatigue Cracking

Designing a crack-resistant flexible pavement can be a daunting task. While there are certain design inputs that can be altered for better crack resistance, these inputs often carry a detriment to permanent deformation potential. It is well-known that asphalt binder content and air voids are significant factors with regard to cracking performance (Epps and Monismith, 1969; Harvey et al., 1995; Pell and Taylor, 1969; Zeiada et al., 2013). For load-associated cracking, additional factors which are expected to impact performance include: pavement structure, rheological properties, aggregate characteristics of mixture, in place properties of unbound layers, rest periods, temperature, and traffic (ARA, Inc., 2004; Brown et al., 2009).

Generally, design of crack-resistant mixtures is separated into two categories: thin asphalt sections and thick asphalt sections. For a thin asphalt section, constant strains are assumed, as the effect of the underlying layer stiffness is more pronounced. Therefore, it is important to use a mixture with lower stiffness, and analysis conducted in a constant strain mode (Brown et al., 2009; Huang, 2004; Mallick and El-Korchi, 2013). For thick pavement sections, strains at the bottom of the asphalt layer increase rapidly with a decrease in mixture stiffness. In this case, constant stress analysis is seen as more suitable (Brown et al., 2009; Epps and Monismith, 1969; Mallick and El-Korchi, 2013).

2.3.2 Tests to Assess Fatigue Cracking Resistance

Perhaps the most commonly used test type to quantify fatigue cracking resistance involves flexural beam loading, typically done in a trapezoidal cantilever, three-point, or four-point

bending setup. Generally, beams of asphalt concrete are loaded in a cyclic fashion at a specific strain level until failure, which allows for a strain versus cycles to failure plot to be developed. When mapped on a log-log scale, a linear relationship between applied tensile strain (or stress) and cycles to failure exists. Empirical models can be used to predict cycles to failure for a given stress or strain input, typically in an exponential form. Analysis methods also utilize the dissipated energy approach because it is independent of loading mode and evaluates damage accumulation per cycle (Baburamani, 1999).

A test method that is used for reflective and fatigue cracking is the Texas Overlay Test (OT). Direct tension is applied in a cyclic triangular pattern by introducing a setup with one stationary plate and one sliding plate, set to a maximum displacement value. A spacer bar simulates the underlying concrete slab for reflective cracking considerations. The test is run until 93 percent of the peak load is reached, and the number of cycles is used as a subjective measure of cracking resistance (Texas DOT, 2014). Several studies have utilized the OT to improve the method itself (Walubita et al., 2012; Ma, 2014), verify field performance, and evaluated its use as a crack initiation and propagation test (Zhou, Hu, and Scullion, 2007). Ma (2014) has conducted an in-depth literature review of the test procedure and past studies relating to variability, robustness, and application.

Several tests to examine the fracture characteristics of mixtures for intermediate temperatures are also used for fatigue characterization. Roque et al. (1999) modified the IDT setup by boring a hole through the center of the specimen. By measuring the stress intensity factor (in Mode-I) at various loading cycles, crack growth was able to be predicted by Paris' Law (Paris and Erdogan, 1963), which was later deemed to be unreasonable at a testing temperature of 10°C due to permanent deformation (Zhang et al., 2001). As a result, the analysis procedure was altered to

include the dissipated creep strain energy and fracture energy limits (Roque et al., 2001). Recently, researchers have determined that the fracture toughness from the modified IDT and the J integral correlate well with laboratory-produced specimen (Kim, Mohammad, and Elseifi, 2012), allowing for some transferability across test methods.

2.3.3 Viscoelastic Continuum Damage

Over the course of the last 25 years, significant strides have been made in fatigue characterization through the development of the Viscoelastic Continuum Damage model (VECD), initially proposed by Kim and Little (1990). The method applies Schapery's constitutive relations for nonlinear materials, coupled with work potential theory, the extended elastic-viscoelastic correspondence principle and the time-temperature superposition (TTSP) principle with growing damage to evaluate the effect of damage on deformation (Daniel and Kim, 2002). The model is able to relate material integrity and damage growth under repeated loading, and is independent of loading mode, temperature, and frequency (Daniel and Kim, 2002). Recently, a simplified VECD (S-VECD) model was developed to formulate the damage characteristic curve (DCC) using the Simple Performance Tester (also known as the Asphalt Mixture Performance Tester (AMPT)) for asphalt concrete in direct tension (Underwood et al., 2010). However, a shortcoming in the model is the ability to directly relate and explain the interaction between stiffness and fatigue properties. Currently, one can predict relative fatigue resistance from either the DCC from an empirical model relating the DCC and N_f for a given loading condition (controlled stress or controlled strain). A single parameter combining the effects of stiffness with the DCC components has not yet been developed.

2.3.3.1 Viscoelastic Continuum Damage Introduction

The basis of the VECD model was originally put forth by Kim and Little (1990). The authors successfully applied Schapery's constitutive relations for nonlinear viscoelastic materials to sand asphalt under cyclic loading. The model describes the effect of microcracking on the constitutive behavior and can be applied to various types of cyclic loading (controlled stress versus controlled strain), temperatures, frequencies, and modes of loading (cyclic versus monotonic) (Lee and Kim, 1998a, 1998b; Daniel and Kim, 2002). More recently, the S-VECD has reduced analysis time, established compatibility with the AMPT, and maintained the mathematical rigor needed for proper fatigue characterization through the VECD scheme (Underwood et al., 2010). The DCC presents a material-dependent parameter relating material integrity (through pseudo secant modulus) to an internal state variable representing damage growth in a specimen subjected to repetitive loading. A typical DCC is shown in Figure 2.14. The basic theory behind each of the three key VECD development principles, as well as a background of the S-VECD, is provided below.
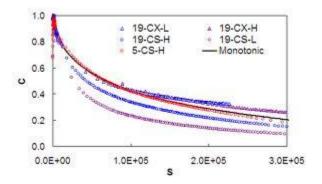
Figure 2.14: Sample damage characteristic curve (Kim et al., 2009)

2.3.3.2 Elastic-Viscoelastic Correspondence Principle

For viscoelastic materials, stress-strain relationships can be represented similarly to those of elastic materials through proper conversion. A common procedure is to use the Laplace transform, which can be analytically difficult to determine. Through the introduction of pseudo variables, Schapery (1984) was able to represent viscoelastic stress-strain relations in a form closer to that of elastic materials through an extended elastic-viscoelastic correspondence principle (Daniel, 2001). The uniaxial pseudo strain (ε^R), presented in the form of a convolution integral, is shown in Equation 2.8:

$$\varepsilon^R = \frac{1}{E_R} \int_0^\xi E(\xi - \xi') \frac{\partial \varepsilon}{\partial \xi'} d\xi' \qquad [2.8]$$

where,

E_R = arbitrary reference modulus (usually set to unity);

$\xi = \dfrac{t}{a_T}$ = reduced time;

t = physical time;

a_T = time-temperature shift factor;

$E(\xi)$ = relaxation modulus;

ξ' = integration variable;

ε = uniaxial strain.

Subsequently, the stress response can be written as a function of pseudo strain and reference modulus:

$$\sigma = E_R \varepsilon^R \qquad [2.9]$$

The utility of the pseudo strain is obvious when considering hysteretic responses for a viscoelastic material. When strains are converted to pseudo strains, a relationship exists between stress and pseudo strain, similar to that of Hooke's Law for elastic materials. In the case of linear viscoelastic (LVE) behavior, there is no damage accumulation, meaning that the hysteretic loops share the same slope and can be collapsed to a single line with a slope of 1 (when $E_R = 1$). Therefore, the viscoelasticity of the material is captured in the pseudo strain calculation, meaning that any deviation from the line of equality can be related to damage induction (Daniel, 2001). Damage can be represented by a reduction in pseudo stiffness, as shown in Equation 2.10.

$$\sigma = C(S) \varepsilon^R \qquad [2.10]$$

where,

$C(S)$ = pseudo stiffness as a function of a damage parameter, S.

2.3.3.3 Work Potential Theory

Based on Schapery's (1990) work potential theory, which used the method of thermodynamics of irreversible processes, a rate type damage evolution law can be found to determine S as it relates to ε^R. Note that S is an internal state variable designed to account for microstructural damage in the specimen. The formulation of a damage evolution law is shown by Equations 2.11-2.13:

Pseudo strain energy density function

$$W^R = f(\varepsilon^R, S) \hspace{4cm} [2.11]$$

Stress-pseudo strain relationship

$$\sigma = \frac{\partial W^R}{\partial \varepsilon^R} \hspace{4cm} [2.12]$$

Damage evolution law

$$\frac{dS}{dt} = \left(-\frac{\partial W^R}{\partial S}\right)^\alpha \hspace{3cm} [2.13]$$

where,

α = material property based on viscoelastic behavior, function of log-log slope of relaxation modulus with respect to reduced time.

Several researchers (Chehab et al., 2002; Underwood et al., 2006) have confirmed that the time-temperature superposition principle is valid in tension with significant levels of time-dependent damage. Note that by ensuring that asphalt concrete exhibits thermorheologically simple behaviors outside of the LVE range, the material property master curves remain valid, reducing testing time and enhancing modeling effectiveness. It also reinforces the notion that damage is a universal property of asphalt concrete (Underwood et al., 2006).

2.3.3.4 Simplified Viscoelastic Continuum Damage Model

The S-VECD is a specialized version of the VECD model for use on cylindrical specimens subjected to a cyclic fatigue test in controlled crosshead (actuator displacement), controlled stress, or controlled strain loading. The S-VECD method reduces analysis time while

maintaining the mathematical rigor associated with the VECD model, and is also compatible with the AMPT. The method also possesses the potential to relate the DCC for a mixture to the traditional fatigue model, which is an empirical formulation to determine N_f for controlled-strain or controlled-stress modes.

The primary output of the S-VECD analysis, as is the case with other VECD platforms, is the DCC. The methodology relates damage, S, to a pseudo secant modulus (material integrity), C. The value of the pseudo secant modulus lies in that it is a function of stress and pseudo strain, which is not reliant on the time-dependency of the material (Underwood et al., 2010).

With this in mind, a "basic concept" of the S-VECD formulation centers around the separation of damage into transient (first loading path) and cyclic (repeated loading) components (Kim et al., 2009). This is a useful approach in that the VECD derivation states that damage occurs in the first loading path, and during the loading portion of a particular strain cycle (Kim et al., 2009; Underwood et al., 2010).

In the transient realm (referred to as Dataset 1 in AASHTO TP107), the loading path is treated as a constant rate loading where potentially significant damage levels are expected to occur (AASHTO, 2014). Therefore, the S-VECD methodology considers pseudo strain, pseudo secant modulus, and damage evolution calculations in transient and cyclic portions. The primary relations needed to determine the DCC are shown in Equations 2.14-2.16 (Underwood, 2011):

$$\varepsilon^R = \begin{cases} \varepsilon^R = \dfrac{1}{E_R} \displaystyle\int_0^\xi E(\xi - \tau)\dfrac{d\xi}{d\tau}\,d\tau & \xi \leq \xi_p \\[4mm] \varepsilon^R_{0,ta_{cycle\ i}} = \dfrac{1}{E_R}\dfrac{\beta + 1}{2}\left((\varepsilon_{0,pp})_i |E^*|_{LVE}\right) & \xi > \xi_p \end{cases} \qquad [2.14]$$

$$C = \begin{cases} C = \dfrac{\sigma}{\varepsilon^R DMR} & \xi \leq \xi_p \\[2mm] C^* = \dfrac{\sigma_{0,ta}}{\epsilon_{0,ta}^R DMR} & \xi > \xi_p \end{cases} \qquad [2.15]$$

$$dS = \begin{cases} (dS_{transient})_{timestep\ j} = (-\dfrac{DMR}{2}(\varepsilon^R)_j \Delta C_j)^{\frac{\alpha}{1+\alpha}}(\Delta \xi_j)^{\frac{1}{1+\alpha}} & \xi \leq \xi_p \\[2mm] (dS_{cyclic})_{cycle\ i} = (-\dfrac{DMR}{2}(\varepsilon_{0,ta}^R)^2 \Delta C_i)^{\frac{\alpha}{1+\alpha}}(\Delta \xi_p K_1)^{\frac{1}{1+\alpha}} & \xi > \xi_p \end{cases} \qquad [2.16]$$

where,

$\varepsilon_{0,ta}^R$ = tension amplitude of pseudo strain for given cycle;

β = quantity to determine proportion of tensile loading in cycle;

C^* = pseudo secant modulus in cyclic portion;

DMR = dynamic modulus ratio from LVE testing;

$\varepsilon_{0,pp}$ = peak-to-peak strain for given cycle;

ξ_p = pulse time;

$\sigma_{0,ta}$ = tension amplitude of stress for given cycle.

It is also important to note K_1, a form adjustment factor, shown in Equation 2.17:

$$K_1 = \frac{1}{\xi_f - \xi_i} \int_{\xi_i}^{\xi_f} (f(\xi))^{2\alpha} d\xi \qquad [2.17]$$

where,

$f(\xi)$ = loading function.

Once the pseudo strain, pseudo secant modulus (or pseudostiffness), and damage evolution characteristics are determined, a fit can be applied to determine the DCC. The S-VECD is capable of fitting the DCC in exponential or power law form, shown in Equations 2.18 and 2.19, respectively:

$$C(S) = e^{aS^b}$$ [2.18]

$$C(S) = 1 - C_{11}S^{C_{12}}$$ [2.19]

where,

a, b = fit coefficients for the exponential form;

C_{11}, C_{12} = fit coefficients for the power law form.

At this stage, the DCC for different specimen and mixtures can be compared. Another useful technique included in the S-VECD model is the ability to calculate N_f as it relates to the classical empirical models for fatigue cracking. As stated in Underwood (2011), this prediction can be performed using a single stress or strain value, or an array of measurements at various temperatures or frequencies. The N_f prediction is then used to determine the coefficients of the empirical model, which can be used as inputs into the Mechanistic-Empirical Design Guide (MEPDG) for distress prediction (Jadoun, 2011; Underwood, 2011).

CHAPTER 3

LOW TEMPERATURE PROPERTIES OF PLANT-PRODUCED RAP MIXTURES IN THE

NORTHEAST

3.1 Introduction

Recently, the asphalt materials community has placed increasing emphasis on the development and research of materials incorporating the use of Reclaimed Asphalt Pavement (RAP). RAP use began in the 1970s and is seen as a cost-effective and more environmentally friendly method to produce hot mix asphalt (HMA) (Mogawer et al., 2012). RAP is typically milled from existing pavements and then crushed and sized at a plant for incorporation into new HMA mixtures. The RAP material contains aggregates coated with asphalt binder that has been aged to some extent during its exposure in the field. The introduction of the aged binder from the RAP into a new mixture with a virgin binder will stiffen the mixture over that produced with only virgin materials. A primary concern is that the inclusion of the RAP materials will make the mixture more brittle and lead to decreased cracking resistance. This has led to hesitancy from state agencies to expand specifications to include higher percentages of RAP (Mogawer et al., 2012). A critical element in evaluating the elevated stiffness and loss of ductility involves the amount of blending that occurs between virgin and RAP binder.

Various researchers (Bonaquist, 2005; Daniel et al., 2010; Daniel et al., 2013; McDaniel et al., 2012; Mogawer et al., 2012; Shah et al., 2007) have been working to evaluate the amount of

blending that occurs in mixtures; the results indicate that some blending occurs, but it is likely dependent upon specific material, mixture, and production characteristics. State agencies have developed different specifications regarding the amount of RAP that can be used based on local experience. Some agencies give full credit for the binder contributed from the RAP while others assign partial credit based on the amount of blending that may be occurring.

In colder climates, thermal cracking is a major type of distress that agencies need to address. As pavement temperatures drop, thermal stresses build and cracking occurs when the thermal stress exceeds the tensile strength of the material. The temperature at which the pavement cracks is called the critical cracking temperature. Thermal stresses that develop, and therefore the critical cracking temperature, will be a function of the rate of cooling and also the temperature at which cooling starts due to the viscoelastic nature of asphalt. Faster cooling rates mean that thermal stresses build up quicker and the material cracks at a warmer temperature because the material does not have time to relax; warmer starting (initial) temperatures will shift the cracking temperature. Therefore, the relaxation characteristics of the asphalt binder and mixture are important in evaluating the thermal cracking potential of the material in the field. There are various test methods and procedures to determine the critical cracking temperature of asphalt mixtures and binders. However, these methods use different starting temperatures and cooling rates, and a direct comparison of results from these different test methods will be impacted by the relaxation properties of the asphalt binder or mixture.

Many researchers have studied the low temperature behavior of binders and mixtures (Buttlar and Roque, 1996; Christensen, 1998; Hiltunen and Roque, 1994; Lytton et al., 1993; Marasteanu et al., 2012) and developed models to predict the low temperature cracking that occurs in the field. Several researchers have conducted studies specifically investigating the low temperature

cracking of RAP mixtures. Zofka et al. (2005) conducted a series of BBR and IDT tests to evaluate RAP mixtures using the modified-Hirsch model to find binder stiffness from mixture stiffness. The study produced mixed results with respect to RAP materials, as some mixtures were able to correlate well over the test range, while others were not. This may indicate that other factors are impacting the performance, possibly production-related. Shah et al. (2007) conducted low temperature creep compliance and indirect tensile (IDT) strength tests on plant-produced materials with 15, 25, and 40% RAP, and estimated critical cracking temperature. A statistical analysis showed no significant differences in strength between 15 and 25% RAP mixtures. The mixtures with 40% RAP included strengths about 20% higher than the other mixtures with similar binder grades. The work also concluded that binder grade did not affect the strength of mixtures with 25 and 40% RAP. Behnia et al. (2011) used mixtures ranging in RAP content from 0 to 50% to conduct acoustic emission and disk-shaped compaction tension testing in an attempt to determine the effect of RAP on low temperature cracking resistance. The results show significant reductions in fracture energy and relaxation capabilities for most mixtures. As expected, general increases in stiffness and warmer embrittlement temperatures were observed with the inclusion of RAP. It was also noted that the softer binder grade material was more sensitive to RAP increases.

This paper presents the results of a study on low temperature properties of RAP mixtures conducted as part of the Transportation Pooled Fund Study (TPF) 5(230): Evaluation of Plant Produced RAP Mixtures in the Northeast. Testing was performed on plant-produced mixtures and binder that was extracted and recovered from these mixtures. The study includes eighteen different mixtures produced with different virgin PG grades and RAP contents. Specifically, the objectives of this paper are to:

1. Evaluate the impact of cooling rate and starting temperature on the critical cracking temperature of mixtures containing RAP;

2. Evaluate the impact of RAP content on the low temperature properties of mixtures;

3. Evaluate the benefit of using softer virgin binder grades to mitigate the impact of the aged RAP binder in the mixture;

4. Compare the low temperature cracking properties determined from the different mixture and binder tests.

3.2 Materials and Production Properties

Materials from a batch plant in Vermont (VT) and drum plants in New Hampshire (NH) and New York (NY) were sampled as part of Phase I of TPF 5-230. Specimens were compacted at the plant (plant-produced, plant-compacted (PMPC)) and loose mix was sampled for reheating and fabrication of specimens in the lab (plant-produced, laboratory-compacted (PMLC)). PMLC samples were reheated and compacted according to the project protocol designed to minimize additional aging of the mixtures. As per the protocol, mixture was heated in five-gallon buckets, with the lid on, for one hour at a temperature 10ºC lower than the plant discharge temperature. Then, the bucket was heated at the same temperature for one hour with the lid off the bucket. After this second hour of heating, the temperature of the mixture was checked to confirm the center of the mixture was at least 75ºC (Mogawer et al., 2012). Virgin asphalt binder was sampled from the tank at the time of production. Asphalt binders were extracted from PMPC specimens and RAP material in accordance with Method A of AASHTO T164 "Quantitative Extraction of Asphalt Binder from Hot Mix Asphalt (HMA)" (AASHTO, 2012d) and then recovered in accordance with AASHTO T170 "Recovery of Asphalt from Solution by Abson Method" (AASHTO, 2012f).

The NH mixtures were produced with one binder grade, while the NY and VT mixtures were produced using two different binder grades. RAP percentages ranging from 0 to 40% by weight of mixture were used throughout the study. Table 3.1 shows the continuous binder grades for the tank binders and the extracted RAP binder. Note the NYb PG 58-28 tank binder actually meets the specifications for a PG 58-34 material. Tables 3.1 and 3.2 display the material and production parameters for the test mixtures. Note that one RAP source was used for the NH mixtures, one source for the NY mixtures, and one source for the VT mixtures. The naming convention for the materials is as follows: NH, NY, or VT denotes the production location, a lowercase letter after the state abbreviation indicates the virgin binder grade, and the number indicates the RAP percentage by weight of mixture. For example, NYb30 is a mixture produced in New York with a PG 58-28 virgin binder and 30% RAP by weight of mixture. Note in Table 3.2, the measured binder percentage is found from the extraction procedure, and the RAP percentage by weight of binder was calculated from the design binder content.

Table 3.1: Continuous PG grades and mixture gradations

Mix	Virgin Continuous PG Grade	Percent Passing									
		19.0	12.5	9.5	#4	#8	#16	#30	#50	#100	#200
NHe00	66.3-29.7	100	99	86	58	43	32	25	16	7	3.6
NHe20		100	99	87	58	42	33	26	16	7	3.6
NHe30		100	99	87	56	42	34	26	16	7	3.6
NHe40		100	99	86	56	41	33	25	15	6	2.7
NH RAP	85.5-13.2	100	100	98	74	56	44	33	22	12	7.4
NYb30	61.0-34.6	100	97.5	91	60	33	21	15	10	6	5.3
NYb40		100	98.1	89	54	32	18	13	9	5	3.2
NYd00	67.0-25.5	100	100	91	68	42	27	19	13	5	3.8
NYd20		100	99	91	59	31	19	12	8	7	3.8
NYd30		100	95	86	54	30	23	17	12	8	6.0
NYd40		100	98	89	53	31	19	14	10	6	4.3
NY RAP	87.2-19.9	100	98	93	66	47	32	22	13	7	4.5
VTa00	56.3-32.5	100	100	99	79	51	31	19	11	6	3.8
VTa20		100	100	98	79	51	31	19	12	7	4.6
VTa30		100	100	99	75	48	30	19	12	7	4.5
VTa40		100	100	98	77	49	29	18	12	8	4.6
VTe00	64.4-30.2	100	100	100	77	49	30	18	10	6	3.3
VTe20		100	100	99	81	54	32	20	12	7	4.3
VTe30		100	100	98	78	49	29	18	11	7	4.3
VTe40		100	100	99	75	47	27	16	9	5	4.5
VT RAP	73.8-25.2	100	99	90	72	52	36	24	16	11	8.3

Table 3.2: Mixture design and production information

Mix	Nominal Maximum Aggregate Size (NMAS) (mm)	% Total Binder (design/ measured)	% RAP by weight of mix/by weight of binder	RAP Binder Content (%)	Voids in Mineral Aggregate (VMA)	Voids Filled with Asphalt (VFA)	Aggregate Temp. (ºC)	Discharge Temp. (ºC)	Compaction Temp. (ºC)	Silo Storage Time (h)
NHe00	12.5	5.7/5.8	0/0	--	14.9	74.8	n/a	165.6	148.9	6.00
NHe20		5.7/5.5	20.0/16.8	4.79	14.5	79.9		157.2	154.4	1.25
NHe30		5.7/5.3	30.0/25.2	4.79	14.4	81.3		168.3	157.2	1.00
NHe40		5.7/6.0	40.0/33.6	4.79	14.5	82.1		168.3	157.2	n/a
NYb30	12.5	5.2/5.0	30.0/28.4	4.93	13.7	81.1	210.0	151.7	135.0	3.50
NYb40		5.2/4.9	40.0/37.7	4.90	12.7	88.4	232.0	165.6	135.0	4.00
NYd00		5.2/5.0	0/0	--	12.6	89.3	191.0	154.4	143.3	2.75
NYd20		5.2/5.2	20.0/19.0	4.95	14.1	79.9	210.0	160.0	143.3	0.75
NYd30		5.2/5.5	30.0/28.4	4.93	13.0	85.1	210.0	151.7	143.3	2.75
NYd40		5.2/5.1	40.0/37.7	4.90	12.5	87.9	232.0	165.6	143.3	3.00
VTa00	9.5	6.7/6.3	0/0	--	20.2	76.3	n/a	171.1	171.1	n/a
VTa20		6.8/6.2	20.0/15.9	5.41	18.8	81.9		162.2	162.2	
VTa30		6.6/6.2	30.0/24.6	5.41	17.7	82.5		160.0	160.0	
VTa40		6.6/6.3	40.0/32.8	5.41	18.0	77.8		148.9	146.1	
VTe00		6.5/6.6	0/0	--	20.3	71.5		165.6	148.9	
VTe20		6.7/6.3	20.0/16.1	5.41	18.7	79.7		148.9	148.9	
VTe30		6.6/6.1	30.0/24.6	5.41	19.1	75.9		161.1	154.4	
VTe40		6.6/6.1	40.0/32.8	5.41	18.2	76.4		146.1	146.1	

3.3 Testing Program

3.3.1 Asphalt Binder Tests

Binders were graded in accordance with AASHTO R29 "Grading or Verifying the Performance Grade of an Asphalt Binder" (AASHTO, 2012e), AASHTO M320 "Standard Specification for Performance-Graded Asphalt Binder" (AASHTO, 2012n), and AASHTO R49 "Determination of Low-Temperature Performance Grade (PG) of Asphalt Binders" (AASHTO, 2012a). The critical cracking temperature of the asphalt binder (ac Tcr) was determined using the TSAR™ software from Abatech Inc., which conforms to AASHTO R49 specifications. The bending beam rheometer (BBR) and direct tension tests (DTT) were performed on binder that was aged in a pressure aging vessel (PAV). Virgin binders sampled from the tank and binders extracted and recovered from the RAP were aged in a rolling thin-film oven (RTFO). The recovered binder from the plant produced mixtures was assumed to be short-term aged, so no RTFO aging was done on these materials prior to dynamic shear rheometer (DSR) testing or PAV aging.

3.3.2 Asphalt Mixture Tests

Mixture testing included the thermal stress restrained specimen test (TSRST), low temperature creep and tensile strength testing in IDT mode, and uniaxial thermal stress and strain testing (UTSST). The TSRST was performed in accordance with AASHTO TP10 "Method for Thermal Stress Restrained Specimen Tensile Strength" on specimens with an air void target of $7\pm1\%$ (AASHTO, 2012b). When material was available, three replicates were tested for each mixture. The TSRST operated at an initial temperature of 4°C and cooled specimens at a rate of 10°C/h. The failure temperature and failure stress were recorded for analysis.

Creep compliance and tensile strength testing was completed according to AASHTO T322 "Determining the Creep Compliance and Strength of HMA Using the Indirect Tensile Test Device" (AASHTO, 2012h) on specimens with an air void target of 6±0.5%, using three replicates. The results from creep compliance and strength testing were used to determine the critical cracking temperature cracking temperature of the mixture (mix Tcr) using the Low Temperature Stress (LTStress) spreadsheet (Christensen, 1998), which uses a simplification of the Thermal Cracking Model (TCModel) (Hiltunen and Roque, 1994) to determine thermal stress and tensile strength.

Additionally, the mixture thermal stress curves were predicted using the principles of linear viscoelasticity (LVE) to find the critical cracking temperature. Using an approach from Christensen (2003), the thermal stress-temperature curve was estimated in the following manner. Dynamic modulus ($|E^*|$), measured using AASHTO TP79 "Standard Method of Test for Determining the Dynamic Modulus and Flow Number for Hot Mix Asphalt (HMA) Using the Asphalt Mixture Performance Tester (AMPT)" (AASHTO, 2012i) was converted to relaxation modulus using the constitutive relationship shown in Equation 3.1:

$$\sigma = \int_0^t E(t-\tau)\frac{\partial\epsilon}{\partial\tau}d\tau \qquad [3.1]$$

where σ is the stress, ϵ is the strain, t is time, E(t) is the relaxation modulus, and τ is the integration variable. When coupled with a cooling rate-dependent strain rate, a thermal stress curve can be developed. Dynamic modulus data for these mixtures can be found in another study (Mogawer et al., 2012). The storage modulus, E′, is then fit to a series of exponentials known as a Prony series using the collocation method (Tschoegl, 1989). The numerical

interconversion from the dynamic storage modulus to relaxation modulus was carried out based on the methodology devised by Park and Schapery (1999) using Prony series coefficients.

The effect of transient temperatures was accounted for by the time-temperature shift factor, aT, as shown in Equation 3.2. In this work, the materials were assumed to remain thermorheologically simple throughout the simulation.

$$\xi(t) = \int_0^t \frac{1}{a_T} d\tau \qquad [3.2]$$

The numerical solution of Equation 3.1 was carried out using Matlab™. The measured IDT strength at -10°C was used as the threshold for determining the end of the computations. Whenever the calculated stresses reach this limit, the program stopped and saved the corresponding temperature at failure.

The NY mixtures were also subjected to the UTSST developed at University of Nevada, Reno (Alavi and Hajj, 2013) for the identification of thermo-viscoelastic properties (air void target of 6±0.5%). The UTSST is a modified-TSRST which accounts for the development of thermal strain through the inclusion of an unrestrained specimen alongside the standard restrained TSRST specimen. The restrained specimen consisted of one 57 mm diameter by 140 mm height specimen that was cored perpendicular to the compaction direction from a long-term aged Superpave gyratory compacted sample (150 mm diameter). The unrestrained specimen was made up of two specimens (57 mm diameter, 140 mm height) glued together by a thin layer of epoxy with a coefficient of thermal contraction similar to that of a typical HMA. The long-term aging of the various compacted mixtures was conducted using a forced-draft oven at 85°C for five days in accordance with AASHTO R30 (AASHTO, 2012c). In order to avoid stress

development before the start of the test, a starting temperature of 20°C was employed, along with a cooling rate of 10°C/h. When material was available, two replicates were tested for each mixture. Figure 3.1 is a schematic of the UTSST setup.
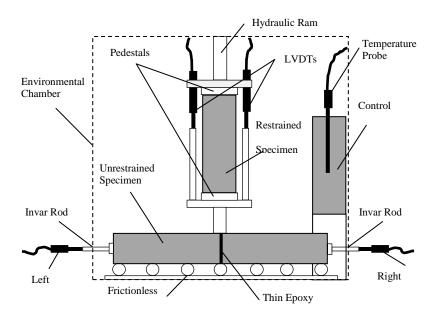
Figure 3.1: UTSST setup showing restrained and unrestrained specimen (Alavi et al., 2013)

By relating thermal stress in the restrained specimen to the thermal strain in the unrestrained specimen through the Boltzmann equation, the relaxation modulus with temperature can be determined. This relation is shown in Equation 3.1.

Modeling of this relation allows for the identification of five distinct stages of material behavior: (1) viscous softening; (2) viscous-glassy transition; (3) glassy hardening; (4) crack initiation; and (5) fracture. At the viscous softening stage, the relaxation modulus of the asphalt mixture increases rapidly, mostly in a linear fashion, with decreasing temperature. Viscous-glassy transition occurs when the glassy properties of the material overcome the viscous properties. The transition stage can be detected as the point at which the second derivative of the relaxation modulus with respect to temperature reaches a maximum value. The glassy hardening stage

behavior of the asphalt material is pure glassy. The glassy hardening stage can be identified as the point at which the second derivative of the relaxation modulus with respect to temperature reaches zero at the colder temperature side. Crack initiation occurs when micro-cracks form in the specimen due to the thermal-induced stress. This stage is identified as the maximum value of the relaxation modulus. Fracture is defined as the point where the asphalt mixture specimen breaks due to the propagation of micro-cracks (Alavi et al., 2013). Sample plots showing measured thermal stress and strain, as well as the resulting relaxation modulus are displayed in Figure 3.2.
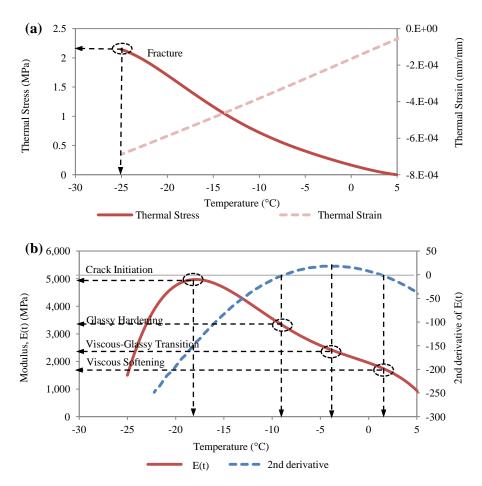
Figure 3.2: Sample UTSST data with (a) measured thermal stress and strain; (b) calculated modulus and identified thermo-viscoelastic stages (Alavi et al., 2013)

3.3.3 Cooling Rates and Starting Temperatures

Each of the standard test methods to evaluate cracking temperature uses a different starting

temperature and cooling rate. These are summarized in Table 3.3. Different cracking

temperatures are expected from these tests simply because of the viscoelastic behavior of the

asphalt. AASHTO R49 and TCModel allow for analytical evaluation of critical cracking

temperature at different starting temperatures and cooling rates for binders and mixtures,

respectively. In order to compare the different test methods at the same rates, analysis was

performed at cooling rates of 1, 2, 4, 5.6, and 10°C/h and starting temperatures of -5, 0, 5, and

10°C. The LVE analysis was also conducted at these cooling rates and temperatures.

Table 3.3: Standard starting temperatures and cooling rates

Method	Starting Temperature (°C)	Cooling Rate (°C/h)
Binder T_{cr} (AASHTO R49)	0	1
IDT Mixture T_{cr}	10	5.6
LVE Approach	10	5.6
TSRST (AASHTO TP10)	5[a]	10
UTSST	20	10

[a] A starting temperature of 4°C was used for the testing in this study

To evaluate the expected performance of the mixtures in place, it is important to know typical

cooling rates and starting temperatures in the field. As part of this study, three locations in the

Northeast United States were investigated to determine typical starting temperatures and cooling

rates for a particular cooling event: Albany, NY; Burlington, VT; and Augusta, ME. Using the

Enhanced Integrated Climatic Model (EICM) from the Mechanistic-Empirical Pavement Design

Guide (M-EPDG) (ARA, Inc., 2004), pavement surface temperatures were found during the

months of November through March. Based on the data, the fastest cooling rate normally takes

place during the afternoon and evening hours. The average cooling event starting temperatures

and corresponding cooling rates were found for each location over the study period. A more

detailed review of cooling rates would involve a procedure to analyze critical cracking temperature based on a two-step cooling event, as evidenced in the data and by another study (Cortez and Hajj, 2011). However, in this paper the initial, more severe cooling rate was used. Figure 3.3 illustrates the two-step cooling event in a sample dataset, with the box signifying the portion of the cooling event used in this paper to establish starting temperature and cooling rate.
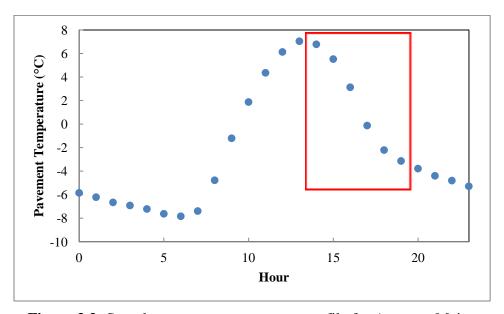
Figure 3.3: Sample pavement temperature profile for Augusta, Maine

The values generated by this investigation are shown in Table 3.4. The observed cooling rates were between 0.87 and 2.00°C/h, with starting temperatures ranging between -0.38 and 14.23°C depending on the time of winter.

Table 3.4: Typical starting temperatures and cooling rates for three locations in the northeastern United States

Month	Albany, NY		Burlington, VT		Augusta, ME	
	Starting Temperature (°C)	Cooling Rate (°C/h)	Starting Temperature (°C)	Cooling Rate (°C/h)	Starting Temperature (°C)	Cooling Rate (°C/h)
January	2.92	1.28	-0.38	0.96	0.77	1.32
February	8.79	1.89	5.71	1.43	6.78	1.98
March	14.23	1.72	11.28	1.56	12.42	2.00
November	13.05	1.40	10.64	1.03	12.31	1.56
December	6.10	1.48	3.96	0.87	4.99	1.23

3.4 Results and Discussion
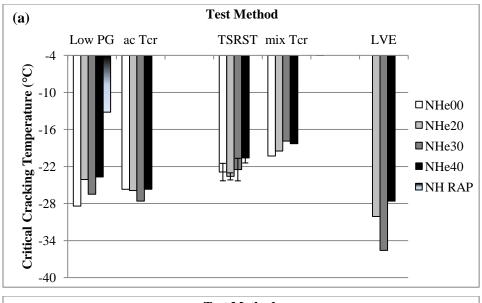
The low temperature cracking properties determined using the standard procedures for the various binder and mixture tests are shown for all four sets of mixtures in Figure 3.4. The error bars in Figure 4 denote a spread of one standard deviation from the mean.

From these plots, the impact of RAP can be discussed across the featured starting temperatures and cooling rates, as well as the effect of softer binder grades at higher RAP contents. In terms of test comparison, the TCModel mixture predictions usually result in warmer cracking temperatures than the binder analysis, with the largest differences at the softer binder grades (PG 52-34 and PG 58-28). The transition to a softer binder grade results in a better low temperature cracking resistance in the extracted and recovered binder, but not necessarily in the mixture. The TSRST-measured results show a colder cracking temperature with the binder grade softening, while the mix Tcr predictions remained about the same in the VT mixtures. The TCModel methodology actually predicted a warmer temperature for the NYb PG 58-28 mixture than the NYd PG 64-22 mixture. Due to the state of the binder after extraction and recovery (fully blended) it is difficult to assess with certainty that the mixture is exhibiting the "black rock" phenomenon. Nonetheless, an interesting finding lies in the discrepancy in impact of binder

51

grade change. Lastly, the UTSST-measured results correlated well with the TSRST for most NY mixtures (<1.0°C), with an exception for the NYd PG 64-22 40% RAP mixture.

The trends observed with the LVE prediction approach are similar to those observed from the TCModel analysis, with the exception of the NH mixtures; however, the temperatures themselves are colder than those observed through other testing procedures (Figure 3.4). Warmer cracking temperatures are observed with faster cooling rates, and as starting temperature increases, a change in the cooling rate is more significant. However, the impact of RAP observed from the LVE predictions is not as large as those observed from the TCModel and AASHTO R49 analyses on the mixtures and binders, respectively. This may be an indication of the differences in the blending of the RAP and virgin binders between the two different approaches.

Figure 3.4 can also be used to examine the impact of blending in the RAP materials. As mentioned, critical cracking temperature for the mixture is almost always warmer than that of the binder. The exact degree of blending is outside the scope of this paper, but further study could utilize stiffness measures between virgin and RAP binders and mixtures as one method to determine the blending in a typical RAP mixture. The subsequent sections discuss the binder results, the mixture results, and a comparison of the binder and mixture results.
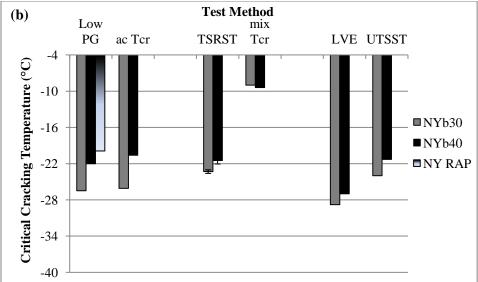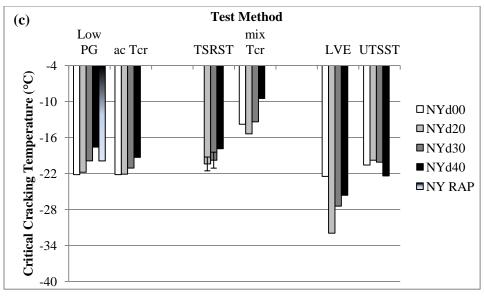
Figure 3.4: Test method comparison of critical cracking temperature (a) NHe PG 64-28 (b) NYb PG 58-28 (c) NYd PG 64-22 (d) VTa PG 52-34 (e) VTe PG 64-28

Figure 3.4 (continued): Test method comparison of critical cracking temperature (a) NHe PG 64-28 (b) NYb PG 58-28 (c) NYd PG 64-22 (d) VTa PG 52-34 (e) VTe PG 64-28
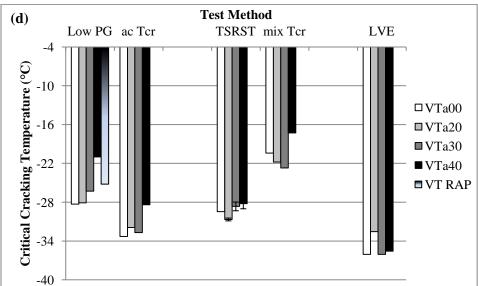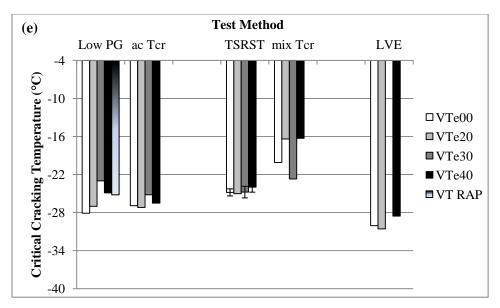
Figure 3.4 (continued): Test method comparison of critical cracking temperature (a) NHe PG 64-28 (b) NYb PG 58-28 (c) NYd PG 64-22 (d) VTa PG 52-34 (e) VTe PG 64-28

3.4.1 Asphalt Binder Characterization

The continuous grade testing is an important measure of the differences between RAP and the virgin materials. An increase in continuous grade with RAP content is expected as more aged material is included. Figure 3.5 presents the continuous low PG grade for each recovered binder determined using both the creep stiffness (S) and m-value from BBR testing. From the data shown, the stiffness-based grade is similar among all recovered binders, other than the increase between VTa PG 52-34 virgin and 20% RAP binders. The m-value-based grade changes with RAP content, and is controlling the low temperature grade for all but one of the recovered binders, indicating that the addition of the RAP changes the relaxation properties of the binder and may correlate to the binder's inability to resist increasing thermal stresses.

For the NY recovered binders, the continuous low PG grade test data increases with RAP content. At the 40% RAP level, the continuous low PG grade is close to a grade stiffer than the designed grade for the NYd PG 64-22 and NHe PG 64-28 binders. For VTa PG 52-34 binders,

the 40% RAP is a full binder grade warmer, but the 30% RAP grade is only 2°C warmer than the virgin material. For the VTa PG 52-34 binder, the 40% RAP material grades two full binder grades warmer than the designed -34°C. However, it appears that the VTa PG 52-34 binder does not meet the specification, as the virgin material grades to a PG xx-28 binder.
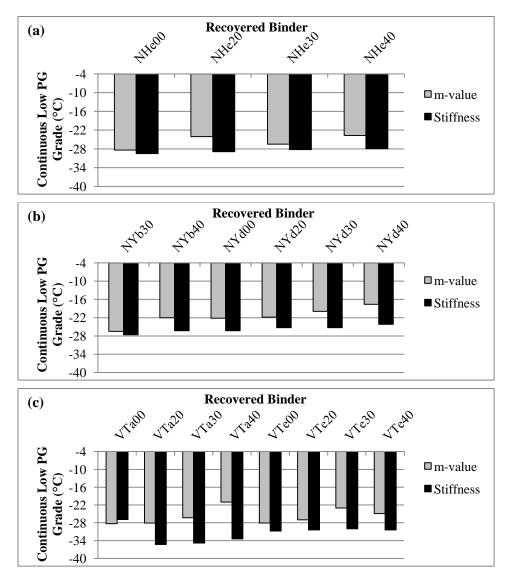
Figure 3.5: Comparison of m-value and stiffness-based continuous low PG grades (a) NHe PG 64-28 (b) NYb PG 58-28 and NYd PG 64-22 (c) VTa PG 52-34 and VTe PG 58-28

The binder critical cracking temperatures, ac Tcr, for the asphalt binders were determined using different cooling rates and starting temperatures to evaluate the impact of both variables on the calculated ac Tcr. Figure 3.6 shows the impact of cooling rate for the five sets of recovered binders at the standard starting temperature of 0°C. Faster cooling rates result in warmer cracking temperatures. The impact of the virgin binder grade on ac Tcr is clear; softer virgin binder grades result in colder cracking temperatures. The presence of RAP in the recovered binder generally results in warmer cracking temperatures; there are clear differences between most virgin and 30 or 40% RAP recovered binders whereas for some sets of recovered binders the virgin and 20% values are similar or the 20 and 30% values are similar. RAP content does not appear to have a large impact on the change in ac Tcr predictions from one cooling rate to another; for example, the difference between the ac Tcr at a cooling rate of 1°C/h and 10°C/h is similar (approximately 5°C) for all binders. The starting temperature influences the impact of cooling rate: at warmer starting temperatures, the impact of cooling rate is greater.

Figure 3.7 shows the impact of starting temperature for the binders at the standard cooling rate of 1°C/h. Colder starting temperatures result in colder critical cracking temperatures, but the impact is not as great as the impact of cooling rate. The starting temperature graphs also show that harder virgin binder grades and higher RAP contents result in warmer critical cracking temperatures. The NH binders appear to soften up to the 30% RAP level, with the expected stiffening (warmer critical cracking temperature) occurring with 40% RAP. The effect of the starting temperature is larger for faster cooling rates. Warmer virgin binder grades and mixtures with higher RAP contents show a larger impact of cooling rate, likely due to the reduced ability of the binders to relax, as indicated by a lower m-value-based low temperature grade.
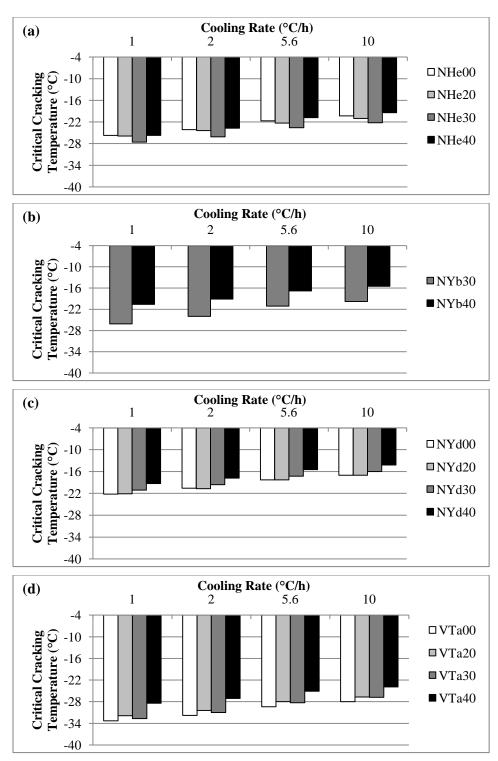
Figure 3.6: Binder critical cracking temperature determined using different cooling rates with various RAP contents (a) NHe PG 64-28 (b) NYb PG 58-28 (c) NYd PG 64-22 (d) VTa PG 52-34 (e) VTe PG 64-28
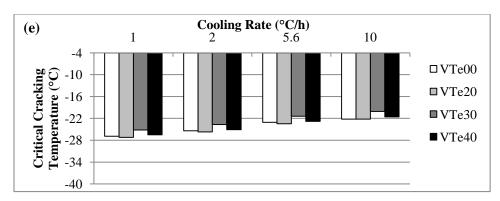
Figure 3.6 (continued): Binder critical cracking temperature determined using different cooling rates with various RAP contents (a) NHe PG 64-28 (b) NYb PG 58-28 (c) NYd PG 64-22 (d) VTa PG 52-34 (e) VTe PG 64-28
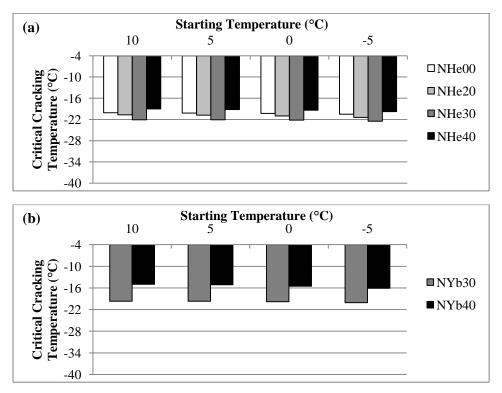
Figure 3.7: Binder critical cracking temperature determined using different starting temperatures with various RAP levels (a) NHe PG 64-28 (b) NYb PG 58-28 (c) NYd PG 64-22 (d) VTa PG 52-34 (e) VTe PG 64-28
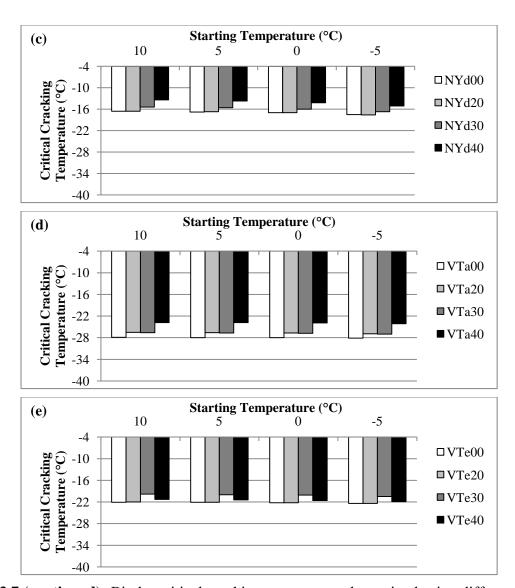
Figure 3.7 (continued): Binder critical cracking temperature determined using different starting temperatures with various RAP levels (a) NHe PG 64-28 (b) NYb PG 58-28 (c) NYd PG 64-22 (d) VTa PG 52-34 (e) VTe PG 64-28

Figure 3.8 below shows a comparison of the continuous low PG grade experimental data and critical cracking temperature predictions for all RAP contents determined at the rates of 1°C/h and 10°C/h at a starting temperature of 0°C. A line of equality is also shown. At the faster cooling rate, the VT materials with the PG 52-34 virgin binder have the best agreement between continuous low PG grade and ac Tcr. The materials with the PG xx-28 and PG xx-22 virgin binders have better agreement at the 1°C/h rate. Figure 3.9 shows the range of ac Tcr that

represent actual cooling rates observed in the field for all RAP contents. These are bracketed by results using a starting temperature of 10°C and cooling rate of 1°C/h (coldest ac Tcr) and results using a starting temperature of 0°C and cooling rate of 2°C/h (warmest ac Tcr). This graph indicates that the continuous low PG grade is a good indication of the binder critical cracking temperature determined using the AASHTO R49 approach for the PG xx-28 and PG xx-22 binders and the conditions in New England.
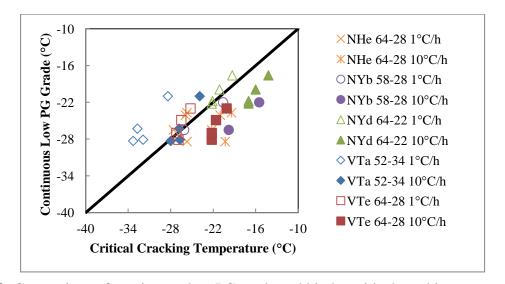
Figure 3.8: Comparison of continuous low PG grade and binder critical cracking temperature at cooling rates of 1°C/h and 10°C/h for extracted and recovered binders
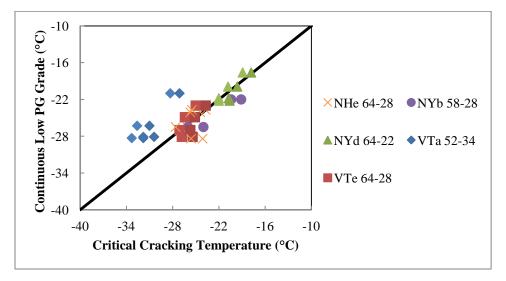
Figure 3.9: Comparison of continuous low PG grade and binder critical cracking temperature at cooling rates and starting temperatures representing actual field conditions

61

3.4.2 Asphalt Mixture Characterization

The average indirect tensile strengths measured at -10°C for all of the mixtures are shown in Figure 3.10. Generally, increases in RAP content increase the strength of the mixtures and stiffer virgin binder grades have higher strengths for the VT mixtures. This can be expected due to the presence of stiffer binder in the mixtures. The NH and VT mixtures generally have lower tensile strength values than the NY mixtures, which may be attributed to differences in the binder grades, gradation, binder content differences, or the fact that NY mixtures were produced at lower temperatures than the NH and VT mixtures. Note that tensile strength is a function of temperature, and trends among the data shown in Figure 3.10 may be different at non-standard temperatures. The error bars shown indicate one standard deviation from the mean in each direction.
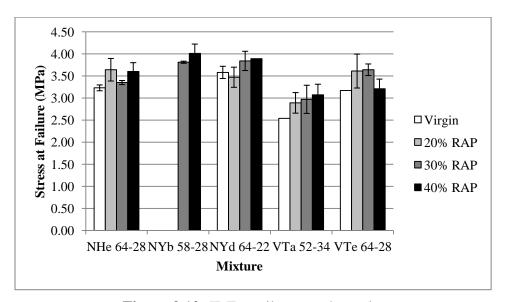
Figure 3.10: IDT tensile strength results

The mixture critical cracking temperatures, mix Tcr, were predicted using the TCModel approach at the different starting temperatures and cooling rates. Figure 3.11 shows that cooling rates can change the mix Tcr up to and beyond a standard binder grade (6°C). The maximum

change over the range of cooling rates was observed in the VTa PG 52-34 mixture with 30% RAP, where the critical cracking temperatures at a 1°C/h and 10°C/h cooling rate are -30 and -20°C, respectively. The smallest change (3°C) was observed for the NYb PG 58-28 mixtures. At faster cooling rates, the thermal stresses at a given temperature are higher, resulting in warmer mix Tcr values. At warmer starting temperatures, the impact of cooling rate on the critical cracking temperature is larger (see Figure 3.12). The anticipated warmer critical cracking temperatures with warmer starting temperatures were observed throughout.

The effect of increasing RAP content on critical cracking temperature is not as clear for the mixtures as it was for the binder results, indicating that additional mixture or production factors (i.e., volumetrics, silo storage, moisture) may be impacting the critical cracking temperature. The compaction temperatures for the VTa PG 52-34 mixtures with 0, 20, and 30% RAP are 10 to 22°C higher than the average compaction temperature of the other VT mixtures. This may influence the cracking performance. With the exception of the NHe PG 64-28 and NYb PG 58-28 mixtures, the 40% RAP mixtures yielded the warmest critical cracking temperatures, leading to the supposition that this RAP level may carry with it reduced thermal cracking resistance. This agrees with analysis done as part of another study by McDaniel et al. (2012). The researchers conducted IDT strength and creep compliance testing and found that 40% RAP mix Tcr values were nearly a full binder grade warmer than the virgin mixture. Additionally, the group observed a half-grade stiffening (about 3°C) when comparing the 25% RAP to the virgin mixtures in the study (McDaniel et al., 2012).
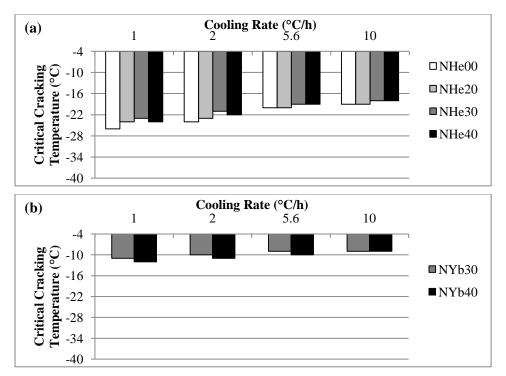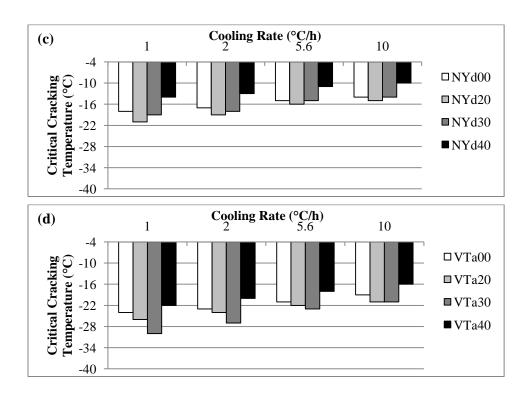
Figure 3.11: TCModel critical cracking temperature determined using different cooling rates for mixtures with various RAP contents at 0°C starting temperature (a) NHe PG 64-28 (b) NYb PG 58-28 (c) NYd PG 64-22 (d) VTa PG 52-34 (e) VTe PG 64-28

(e)
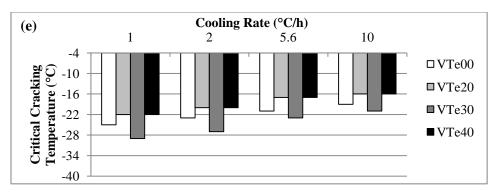
Figure 3.11 (continued): TCModel critical cracking temperature determined using different cooling rates for mixtures with various RAP contents at 0°C starting temperature (a) NHe PG 64-28 (b) NYb PG 58-28 (c) NYd PG 64-22 (d) VTa PG 52-34 (e) VTe PG 64-28

(a)
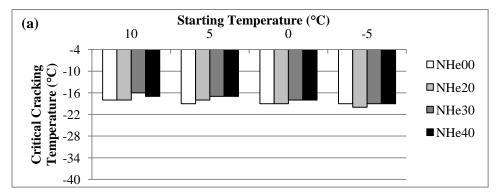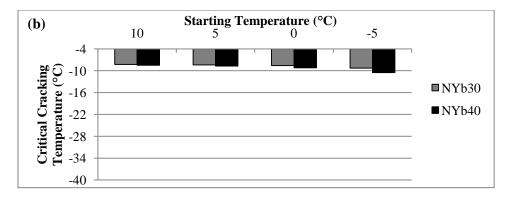
Figure 3.12: TCModel critical cracking temperatures based on varying starting temperature at 10°C/h cooling rate (a) NHe PG 64-28 (b) NYb PG 58-28 (c) NYd PG 64-22 (d) VTa PG 52-34 (e) VTe PG 64-28

(b)
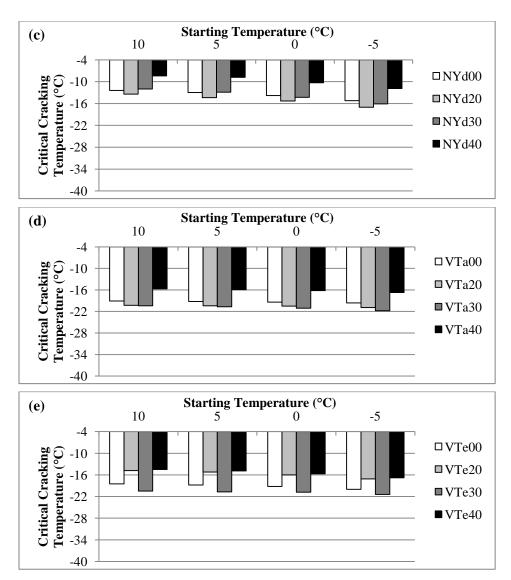
Figure 3.12 (continued): TCModel critical cracking temperatures based on varying starting temperature at 10°C/h cooling rate (a) NHe PG 64-28 (b) NYb PG 58-28 (c) NYd PG 64-22 (d) VTa PG 52-34 (e) VTe PG 64-28

The TSRST experimental results are displayed in Table 3.5. Due to a material shortage, data for the NYd PG 64-22 virgin mixture is not available. The same trends observed with the TCModel and LVE predictions are seen with the TSRST results. The critical cracking temperature is warmest at the 40% RAP condition (except for the NHe PG 64-28 and NYb PG 58-28 mixtures). The VT mixtures seem to be more resistant to changes in critical cracking temperature with increases in RAP. This lack of sensitivity may be tied to asphalt content or production

parameters; the most notable of which is silo storage aging, to which the VT mixtures were not subjected. Additional study is needed to isolate these variables.

Figure 3.13 presents a comparison between the IDT strength measured at -10°C and TSRST stress at failure for all mixtures. The IDT strengths for the PG xx-28 and PG xx-22 mixtures are higher than the TSRST failure stresses, while the VTa PG 52-34 mixture shows results on both sides of the line of equality. This seems to be influencing the LVE analysis results, as the failure criteria for this method is the IDT tensile strength. Since the IDT strength is higher than the TSRST stress at failure, the LVE predicted mix T_{cr} are lower (colder), indicating that perhaps IDT strength is not an appropriate failure criteria for this method.

UTSST provides many details regarding mixture behavior at low temperatures. In the case of the NYd PG 64-22 material, the fracture temperatures were similar and about -20°C for the 0, 20 and 30% RAP mixtures. The addition of 40% RAP resulted in a slight shift to a colder temperature (-22°C). In the case of the NYb PG 58-28 mixture, the addition of 30 and 40% RAP resulted in fracture temperatures of -24 and -21°C, respectively. The NYb PG 58-28 mixture results follow the trend seen in the TSRST data, but contradict the TCModel predictions. A significant decrease in the crack initiation temperature (colder) was observed with the increase of RAP content. In the case of the RAP mixtures, the crack initiation temperature was found to be very close to the fracture temperature. Figure 3.14 shows the calculated difference between the fracture and crack initiation temperatures. The data show that the addition of RAP resulted in a significant loss in the ductility property of the mixture while still maintaining similar or better fracture temperature properties (i.e., fracture temperature and fracture stress). Similarly, the glassy hardening temperatures were colder for the mixtures with RAP material. Figure 3.14 also

shows the calculated difference between the crack initiation and glassy hardening temperatures. This difference was on average around 11°C and relatively similar for all evaluated mixtures.

A decrease in the viscous-glassy transition temperature (i.e., colder temperatures) was observed with the increase in RAP content (see Table 3.6). Except for the NYd PG 64-22 40% RAP mixture, the addition of RAP shifted the viscous-softening temperatures to the warmer side, indicating stiffening of the asphalt mixtures with the addition of RAP. The addition of RAP increased the relaxation modulus of the asphalt mixture at colder temperatures. This was observed with the higher values for the glassy hardening and crack initiation moduli for RAP containing mixtures.

At first a decrease in the viscous-glassy transition and viscous softening moduli values was observed with 20% RAP when compared to the 0% RAP, followed by an increase in the moduli values with the increase in RAP content. The addition of 40% RAP to the PG 64-22 mixture resulted in a higher viscous-glassy transition and viscous softening moduli values than the 0% RAP mixture. The addition of RAP to the mixtures increased the stress at which cracks initiated. Furthermore, the crack initiation and fracture stresses for mixtures containing RAP were relatively close to each other. The viscous softening stresses for all evaluated mixtures were small and very similar regardless of the RAP content and binder type.

Table 3.5: TSRST results

Mix	PG Grade	% RAP	Air Voids (%)	Temperature at Failure (ºC)	Load at Failure (N)
NHe	64-28	0	6.9	-22.9	5183
		20	7.0	-23.6	5609
		30	7.5	-22.5	5277
		40	7.1	-20.6	4627
NYb	58-28	30	7.4	-23.3	7451
		40	7.1	-21.5	7548
NYd	64-22	0	n/a	n/a	n/a
		20	9.2	-20.4	5822
		30	7.6	-19.8	6910
		40	6.7	-17.9	6997
VTa	52-34	0	7.4	-29.5	6088
		20	6.9	-30.7	6938
		30	6.7	-28.6	6721
		40	7.5	-28.2	6438
VTe	64-28	0	7.7	-24.8	5707
		20	6.5	-25.0	7095
		30	6.9	-24.8	6705
		40	7.0	-23.9	6985
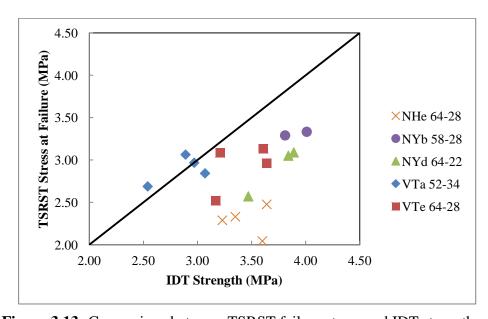
Figure 3.13: Comparison between TSRST failure stress and IDT strength
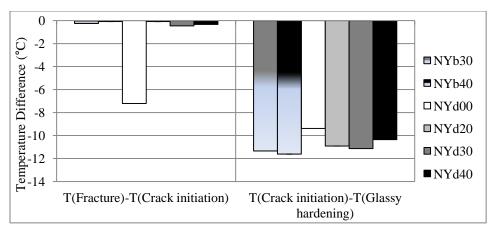
Figure 3.14: UTSST differences between fracture and crack initiation temperatures, as well as crack initiation and glassy hardening temperatures

Table 3.6: UTSST thermo-viscoelastic and fracture results for NY mixtures

Thermo-viscoelastic and Fracture Properties	Mixture					
	NYb30	NYb40	NYd00	NYd20	NYd30	NYd40
Fracture temperature (°C)	-24.0	-21.3	-20.6	-19.8	-20.1	-22.4
Fracture stress (MPa)	3.75	3.90	3.35	3.60	3.95	3.80
Crack initiation temperature (°C)	-23.9	-21.1	-13.4	-19.7	-19.6	-22.1
Crack initiation modulus (MPa)	11,488	11,129	7,632	10,825	12,350	12,154
Crack initiation stress (MPa)	3.75	3.85	2.30	3.60	3.85	3.70
Glassy hardening temperature (°C)	-12.3	-9.7	-4.0	-8.7	-8.5	-11.7
Glassy hardening modulus (MPa)	6,874	6,962	5,037	6,672	7,734	7,798
Glassy hardening stress (MPa)	1.25	1.45	0.95	1.30	1.50	1.50
Viscous-glassy transition temperature (°C)	0.1	2.5	4.5	3.1	3.6	3.6
Viscous-glassy transition modulus (MPa)	1,460	2,033	2,154	1,816	2,247	2,758
Viscous-glassy transition stress (MPa)	0.20	0.30	0.35	0.20	0.30	0.50
Viscous softening temperature (°C)	11.5	13.6	12.3	13.7	14.7	8.6
Viscous softening modulus (MPa)	397	567	1,119	429	512	1,368
Viscous softening stress (MPa)	0.01	0.03	0.09	0.02	0.03	0.09

3.4.3 Comparisons between Binder and Mixture Results

Comparisons between binder and mixture results are useful to better understand the impacts of RAP on the low temperature properties of the mixtures. The goals of the comparison are to evaluate production factors, mixture design (i.e., using a softer binder grade), and internal mechanisms such as blending. A comparison of TSRST actual cracking temperature to the test-measured continuous low PG grade (Figure 3.15) shows that the NH and VT mixtures deviate more from the line of equality than the NY mixtures, with the VTa PG 52-34 mixtures showing a lower cracking temperature than the extracted and recovered binder grade. The NH and NY mixtures were stored in a silo for several hours, which may result in more complete blending between the virgin and RAP binders, which would result in better agreement between mixture and binder results. However, the NH data shown in Figure 14, and the mixture critical cracking temperatures determined from the TCModel (Figure 3.15b) are warmer than the low PG grade, which may indicate a lack of blending between virgin and RAP binders.

A comparison of TSRST results with the AASHTO R49 and TCModel-based predictions, as shown in Figure 3.16, can evaluate the effectiveness of the model in matching to experimental data. The open symbols represent the AASHTO R49 (ac Tcr) and TCModel (mix Tcr) predictions at the standard starting temperatures and rates, while the closed symbols represent the AASHTO R49 and TCModel predictions using the TSRST starting temperature and cooling rate (4°C and 10°C/h, respectively). The binder cracking temperatures agree better with the TSRST data than the mixture cracking temperatures, and the standard starting temperature and cooling rate is better than the predictions using the TSRST starting temperature and rate.

Since the low temperature grade of an asphalt binder is designed to account for the climate of the given region, a comparison between continuous low PG grade and cracking temperatures using a

71

typical field cooling rate is shown in Figure 3.17. TSRST measurements match best with the continuous low PG grade. On average, the TSRST produced a cracking temperature 0.3°C colder than the continuous low PG grade. The calculated variances are similar for the ac Tcr and TSRST differences from the continuous low PG grade, but the average difference for ac Tcr at a typical field condition is 1.6°C colder than the continuous low PG grade.
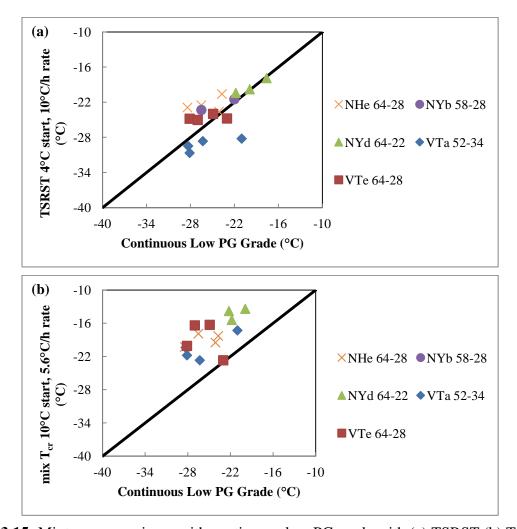
Figure 3.15: Mixture comparisons with continuous low PG grade with (a) TSRST (b) TCModel at standard starting temperature and cooling rate
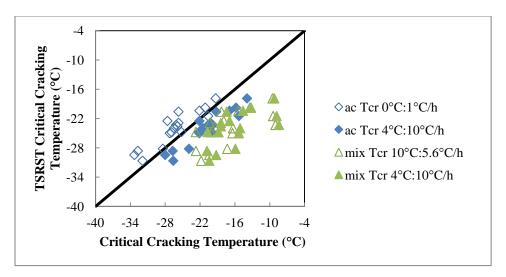
Figure 3.16: TSRST comparison with AASHTO R49 (ac T_{cr}) and TCModel (mix T_{cr}) predictions
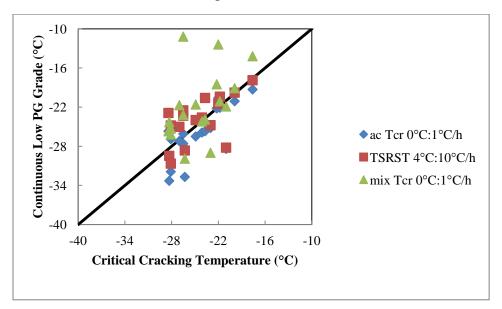
Figure 3.17: Continuous low PG grade comparison with TSRST and typical field cooling rates

3.5 Conclusions

This study sought to evaluate effects of blending, production parameters, RAP percentage, and test method on the low temperature cracking resistance of HMA and asphalt binders. A large range of starting temperatures and cooling rates were used in the analysis in an attempt to

73

identify trends with respect to critical cracking temperatures. The following conclusions are supported by the data:

1. Overall, increases in RAP resulted in warmer critical cracking temperatures, probably due to faster growing thermal stresses, which may be attributed to a decreased ability of the binder to relax. As RAP content increased, the mixtures exhibited higher IDT tensile strengths values. The IDT strength values were higher than the TSRST thermal stress at failure for all but two VTa PG 52-34 mixtures.

2. A possible solution to embrittlement caused by higher RAP contents is to use a softer, or lower, PG grade binder. In this study, the lower PG grade decreased binder and TSRST critical cracking temperatures. However, the TCModel predictions were not significantly impacted by the change in binder grade.

3. The UTSST was used to determine thermo-viscoelastic properties of the NY mixtures. The fracture temperatures from the UTSST correlated well with the TSRST. The addition of RAP shifted the crack initiation and glassy hardening temperatures to colder temperatures along with an increase in the relaxation modulus and thermal stress. Furthermore, the addition of RAP altered the fracture behavior of the evaluated mixtures from ductile failure toward a brittle failure as observed with the close proximity between the crack initiation and fracture temperatures.

4. NY critical cracking temperatures found from the TSRST experimental data match well with the continuous low PG grade on extracted and recovered binders. This result may indicate that significant blending is occurring in these mixtures, potentially from the silo storage aging experienced by the materials. However, the NH TSRST-measured critical cracking temperature and TCModel predictions for all eighteen

mixtures are warmer than the test-measured continuous low PG grade, indicating that perhaps blending is not occurring in silo aged material. It is important to note that available predictive models have inherent shortcomings which may mask actual phenomena or introduce a degree of error.

5. Cooling rates impact critical cracking temperature, especially for mixtures. A warming of 10°C was predicted over an increase in cooling rate from 1°C/h to 10°C/h. The impact of cooling rate appears to be elevated at stiffer PG grades and increased RAP content, possibly due to reduced relaxation capabilities of stiffer materials. For the mixture, as cooling rate became more severe, the critical cracking temperature increased in all cases. The TCModel predictions for the NYb PG 58-28 mixture showed a heightened resistance to critical cracking temperature change with changes to the cooling rate. Generally, the 40% RAP materials produced the warmest critical cracking temperatures. An enhanced study of typical cooling rates is needed in future work, particularly to address a two-step cooling event with a steep initial cooling followed by a gradual second stage of cooling. This would require testing equipment with a programmable temperature setting to monitor variation of low temperature properties when subjected to more realistic cooling conditions. An accurate representation of the cooling curve may lead to changes in critical cracking temperature.

6. The pavement temperature at the onset of a cooling event impacts the critical cracking temperature of RAP materials. For binders and mixtures, the effect of the initial temperature is greater at faster cooling rates. As expected, warmer starting

temperatures resulted in warmer critical cracking temperatures for binder and mixtures.

7. The TSRST values match well with the standard starting temperature and cooling rate for binder critical cracking temperature analysis. On average, the TSRST temperatures were 1.8°C warmer than the standard binder critical cracking temperature predictions. This correlation requires more study to determine if the similarities in critical cracking temperature between TSRST and the binder analysis methods are easily reproducible. If so, this finding could lend itself to blending assessment of RAP mixtures as deviation from the TSRST-binder critical cracking temperature correlation may relate to decreased mobilization of the RAP binder. However, a baseline needs to be established for the mixture mobilization, possibly through chemical analysis methods.

8. The analysis method used, along with its respective parameters, had a large influence on the resultant critical cracking temperature of the asphalt mixtures. The widest differences among analysis methods in the critical cracking temperature study were seen in the TCModel and LVE approaches. TCModel usually predicted warmer temperatures, especially at the default starting temperature and cooling rates of 10°C and 5.6°C/h. The LVE approach resulted in colder predictions, which does not follow the expected trend as it relates to RAP materials. However, the failure criteria used in the LVE calculations was the IDT tensile strength, which was usually higher than the TSRST actual strength. Had the calculations been based on the TRST failure stress instead of the IDT values, the critical temperatures would have been considerably warmer.

The results of this study are important to the community as it relates to low temperature performance of RAP mixtures, which is a concern for northern climates. It must be understood however that these results are based on specific mixtures, and at this point it is not certain if the trends in this study can be applied to all RAP mixtures and binders. If the properties of RAP mixtures are better understood at both the mixture and binder levels, owner agencies can design for higher RAP percentages. The results relate critical cracking temperature to standard and actual cooling rates in the field, which provides insight into the conservative nature of some of the testing protocols.

Future work is needed for a more complete understanding of low temperature cracking of RAP mixtures. A more detailed climate study is needed to better understand the typical cooling event in New England and the associated impacts on virgin and RAP mixtures. Additional work is required to focus on the effects of specific production parameters on cracking resistance of RAP materials, as the data presented in this paper may be influenced by production variations. It is also important to note that with changing RAP contents, gradation changes may be influencing the observed trends. Avoiding gradation changes with increased RAP is difficult in practice, but further work should look to isolate gradation changes to better determine the impacts of a varying distribution. A plan to better evaluate the degree of blending between virgin and RAP binders, especially as it relates to plant production, is also needed. The degree of blending is critical for low temperature cracking performance; if a portion of the RAP binder is not active, the mixture is effectively under-asphalted. The pavement structure will then be more prone to cracking, resulting in increased maintenance costs. Finally, the test method comparisons featured in this paper present the need for refinement of analysis procedures to better mimic the measured binder grade or critical cracking temperature based on the actual cooling rates.

In closing, the findings presented in this study reinforce the need for more accurate representation of RAP behavior as it relates to low temperature cracking performance. Results also show value in using a softer binder grade, particularly at the 40% RAP level for some of the mixtures. This finding is of relevance to agencies in the planning and design of mixture specifications, as a softer binder grade presents the opportunity for increased low temperature cracking resistance.

3.6 Acknowledgements

CHAPTER 4

APPLYING THE GLOVER-ROWE PARAMETER TO EVALUATE LOW TEMPERATURE

PERFORMANCE OF HOT MIX ASPHALT LTPP SECTIONS

4.1 Introduction

In the asphalt materials field, it is well-known that cracking presents challenges to effective design and maintenance of pavements. In cold climates, transverse cracking caused by thermal shrinkage is a major distress mode. As temperatures decrease, thermal stress increases and can eventually exceed the tensile strength of the material. It has been found that the relaxation modulus of asphalt binders controls the ability to alleviate thermal stress build-up and resist thermal cracking (Marasteanu, 2004). The efforts of the Strategic Highway Research Program (SHRP) in the 1990s developed the bending beam rheometer (BBR) and direct tension tests (DTT) to determine low temperature binder grades. The critical values in the specification were based on field observations (Stoffels et al., 1994), but are there alternate, perhaps more efficient methods to correlate cracking performance to the laboratory?

Recently, researchers sought to classify cracking resistance through the use of an index parameter. Using a mechanical-empirical relationship with observed cracking, Glover developed a parameter relating storage shear modulus (G') and dynamic viscosity (η') to ductility at a common temperature-frequency combination (Glover et al., 2005). Critical envelopes were designed to correlate with field measurements of non-load associated cracking (Kandhal, 1977). In addition, Anderson et al. (2011) proposed parameters to relate ductility and binder properties

to non-load associated cracking for airport pavements. The findings of the study identified the Glover parameter $(G'/(\eta'/G'))$ and the difference between the continuous low temperature binder grade measured via the Superpave creep stiffness and m-value (ΔT_c) as parameters to identify changes in cracking susceptibility with aging. Three binders with different aging levels were exposed to dynamic shear rheometer (DSR) and ductility testing, along with the standard BBR and DTT procedures. The authors found that while the Glover parameter and ΔT_c were the best indicators of durability, there also appeared to be value in the rheological index (R), of which each binder has a unique relationship with the Glover parameter. The R-value relates the elastic asymptote of the master curve (glassy modulus, G_g) to the G* measured at the crossover frequency (ω_c), where $\delta = 45°$ (Figure 4.1) (Anderson et al., 1994). The authors observed a flattening complex shear modulus master curve with aging, which can be conveyed through the rheological index. Figure 4.2 displays a sample of the R-value plotted against the crossover frequency for detection of crack susceptible materials at varying depths in the pavement structure (B for bottom layer, T for top layer).

There are several factors which influence cracking resistance, one of the most important being associated with irreversible oxidative aging. Over time, asphalt mixtures are exposed to the environment and undergo embrittlement due to the formation of ketones and other oxidized elements in the binder. Oxidative aging is directly attributed to increases in stiffness and decreases in ductility, which increase susceptibility to cracking. As the plot shows, aging should result in an increase in R-value and a decrease in crossover frequency, while work being done on rejuvenated binders show the opposite trend. It is believed that changes in rheological properties can be directly attributed to changes in cracking resistance of asphalt materials.
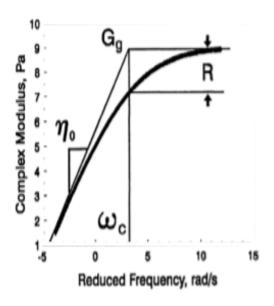
Figure 4.1: Schematic of definition of the rheological index (Anderson, Rowe, and Christensen, 2008)
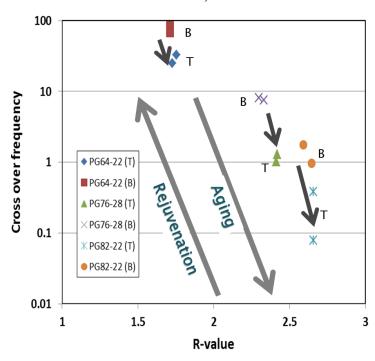
Figure 4.2: Sample crossover frequency-rheological index plot for monitoring of aging and cracking susceptibility (Rowe, 2014)

81

In a prepared discussion to the Anderson et al. (2011) study, Rowe offered an expression of the Glover parameter. The Glover-Rowe parameter (Equation 4.1) features the complex shear modulus (G*) and phase angle (δ) of the asphalt binder at 15°C and a frequency of 0.005 rad/s.

$$\frac{G^*(\cos \delta)^2}{\sin \delta} \qquad [4.1]$$

Because the parameter is calculated at a fixed frequency, Rowe ignored the frequency term of the simplification and expressed the parameter purely in terms of G* and δ, allowing users to plot the ductility-based failure planes in Black Space. Rowe asserts that the use of Black Space encourages clear illustrations of aging impacts. The diagram typically plots complex modulus versus phase angle in a display of stiffness versus relaxation. Black Space plots are particularly useful in viscoelastic analyses because they do not require manipulations using time-temperature superposition. Therefore, experimental values can be plotted among each other without the use of shift factor and sigmoidal fit functions. Airey (2002) found that Black Space diagrams are also helpful in identifying testing inaccuracies and assessing impacts of aging and polymer modification on asphalt.

Figure 4.3 shows sample data plotted with the Glover-Rowe parameter set to the converted ductility limits in Glover et al. (2005) for prediction of the onset of cracking. The materials presented show that as reclaimed asphalt pavement (RAP) is added (NHe00 has no RAP, while NHe40 has 40% RAP by weight of mixture) the location in Black Space shifts from smaller G* and larger δ to larger G* and smaller δ. This is expected as materials age and as more aged material is added to a binder. All of these binders pass the Superpave cracking parameters G*sinδ and G*/sinδ. However, the Glover-Rowe parameter predicts that all of the materials containing RAP will have cracking issues.
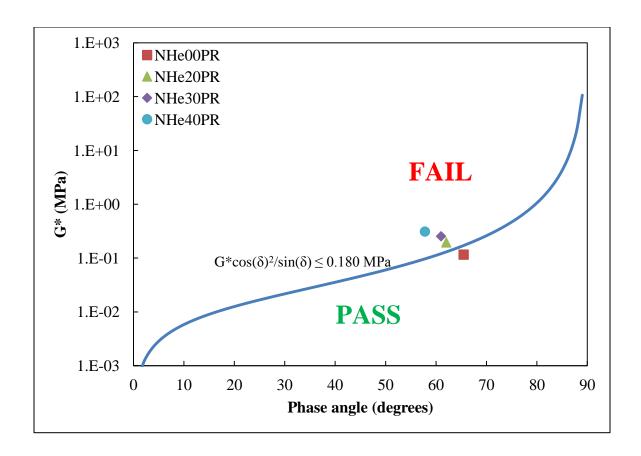
Figure 4.3: Sample Glover-Rowe Black Space diagram

Furthermore, King et al. (2012) confirmed an asphalt binder's location in Black Space as an important performance parameter for age-induced cracking. Using the Glover-Rowe parameter, the authors argue that the standard Superpave fatigue parameter ($G^*\sin\delta$) developed through SHRP is not an adequate damage indicator for cracking. The authors recommend development of a "damage region" in Black Space which combines the DSR outputs (G^* and δ) with the S and m values from the BBR.

Romero and Jones (2013) found value in using a modified Black Space diagram using the S and m values from the BBR. The material plot was used for low temperature performance of the mixture, but the corresponding modified Black Space for binders is used in this paper.

83

4.2 Objectives and Scope

The objectives of this paper are to:

1. Compare methods to combine stiffness and relaxation properties as it relates to transverse cracking performance;

2. Assess the data collection scheme featured in the Long-Term Pavement Performance (LTPP) database;

3. Provide recommendations to allow for more robust indication of materials with poor resistance to low temperature cracking.

The analysis provided is of particular importance to engineers in northern climates, as many asphalt pavements are aged and exposed to frequent low temperature events which can induce thermal cracks. Four LTPP projects from the United States and Canada are discussed as it relates to several rheological properties. For three of the projects, binder was extracted and recovered once during the service life of the pavement, while one project underwent binder extraction, recovery, and material testing at three different points over the service life. Note that in this study only existing data in the LTPP database was analyzed. The opportunity may exist to request additional material through the LTPP Materials Reference Library, but this is outside the current scope of work.

Linear viscoelastic interconversions are used to assess the validity of the Glover-Rowe parameter for field-aged materials exhibiting transverse cracking. A modified Black Space diagram using the S-value and m-value measured from BBR testing (Romero and Jones, 2013) is also displayed, with comments on its viability as an indicator for poor low temperature cracking

performance. The authors also present a crossover frequency-rheological index plot to determine if this measure can identify poor performing materials as well.

Additionally, the importance of these analyses is tied to industry exploring the opportunity to expand usage of RAP. RAP presents benefits to society in the form of increased landfill and material savings, but the ramifications on cracking resistance is the subject of many research endeavors. By undertaking a study that examines field performance and laboratory measurements of field-aged materials, the authors are disseminating information that is of particular importance in today's increasingly cost-conscious infrastructure environment.

4.3 Materials and Methods

General properties of the selected projects are displayed in Table 4.1. All binders were placed as part of a dense-graded HMA, with collected surface layer thicknesses ranging from 55.9 to 73.7 mm. As shown in the table, all materials are field-aged, and feature a range of binder grades that can be encountered in cold climates. These projects were selected because the resulting material master curves were able to provide an interpolated Glover-Rowe value. Other projects or test sets were discarded because of a reduced frequency range that was deemed inadequate to capture the 15°C, 0.005 rad/s temperature-frequency combination in the master curve. Generally, test temperatures that do include a temperature greater than 15°C are indicative of an insufficient dataset for this analysis unless a slow loading rate is applied to capture these areas of the master curve. Projects were selected in cold climatic regions, including the "Wet, Freeze" climate zone classification for Michigan, Ontario, and Quebec, and the "Dry, Freeze" classification for Saskatchewan. Note the Saskatchewan binders are all from the same project, but were sampled in three different years, corresponding to three levels of field aging.

Table 4.1: Selected project information and binder properties

Project Information						
State	**Michigan**	**Ontario**	**Quebec**	**Saskatchewan**		
SHRP ID	0901	0901	0901	0901	0901	0901
Aging Type	Field	Field	Field	Field	Field	Field
Test Date	1/1998	6/1998	4/2001	2/1998	2/1999	3/2001
Traffic Properties						
Traffic Open Date	12/1/1973	6/1/1997	12/1/1996	10/1/1996		
AADTT (Test Year)	1893	450	585	437	436	494
Functional Class	Rural Principal Arterial-Interstate	Rural Principal Arterial-Other	Rural Principal Arterial-Other	Urban Principal Arterial-Other		
Binder Properties						
PG Grade	PG 64-22	PG 58-40	PG 52-34	PG 58-28		
Penetration Grade	N/A	85/100	N/A	150/200		
Viscosity (60° C)	N/A	N/A	601	699		
Viscosity (135° C)	N/A	N/A	218	232		
Penetration (25° C)	N/A	N/A	185	171		
Volumetric Properties						
Mix Design Method	Superpave	Marshall	Superpave	Superpave		
Pb	6.5	5.5	N/A	5.1		
VMA	16	16	N/A	14		
Gmm	N/A	2.446	N/A	2.439		

To satisfy the study objectives, an approach to calculating distress is needed, so that the analysis methods can provide more accurate insight into the material behavior over the service life. The LTPP data included transverse cracking data for the various projects. When analyzing the Glover-Rowe parameter as an indicator for cracking in the field, it is important to document the service life of each pavement section before experiencing cracking, along with the increase in cracking as the pavement ages. Transverse cracking deduct values calculated using a simple exponential relationship at the low, medium, and high severity levels (Bennert and Maher, 2013) are presented in Figure 4.4.
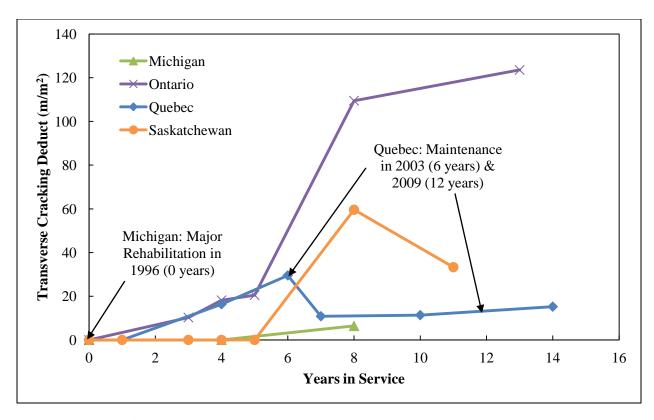
Figure 4.4: Transverse cracking measurements for each project

The Ontario pavement section opened to traffic in 1997 and experienced some transverse cracking within the first three years. Also, as the pavement aged, the transverse cracking increased much more than the cracking in other sections. The Ontario project is an ideal pavement section to compare due to the abundant cracking that occurred in the field. It is important to note that this section also shows increased levels of longitudinal cracking, which may indicate an overall construction issue which is exacerbating the poor condition of the pavement. The Quebec pavement section experienced cracking shortly after the traffic open date (approximately one to four years after). Furthermore, cracking first appeared between five and eight years of service for the Saskatchewan pavement section.

It is important to note the dates of the rehabilitation efforts for each of the pavement sections, as shown in Figure 4.4. The Michigan pavement section was originally constructed in 1973. In

1996, the year that the LTPP study was started on this section, the structure underwent major rehabilitation including a 218 mm asphalt concrete overlay and fracture treatment of the Portland cement concrete (PCC) pavement as a base for the new asphalt surface layer. The first year of service for the Michigan section is considered 1996 because of the major rehabilitation. In 2003 (6 years in service), the Quebec pavement section was rehabilitated with a 25 mm asphalt concrete overlay. A decrease in the transverse cracking of the Quebec pavement section at that time can be attributed to this maintenance. In 2009 (12 years in service), maintenance was again performed on the Quebec section including milling off the asphalt concrete and applying a 51 mm overlay. No rehabilitation efforts have been reported for the Ontario or Saskatchewan projects. It is also important to note that distress surveys and materials were not obtained every year, creating gaps in the timing of crack development in these sections.

In order to conduct analysis using the Glover-Rowe parameter, G* and δ master curves are required. The data acquired from the LTPP database on the recovered field-aged binder includes BBR data measured at 8, 15, 30, 60, 120, and 240 s, as well as DSR data measured at particular temperatures with a fixed frequency of 10 rad/s to correspond to the Superpave specification. The test method specifications for BBR and DSR testing followed AASHTO T313 and AASHTO T315, respectively (AASHTO, 2012j; 2012m).

According to AASHTO M320 (AASHTO, 2012n), the Superpave failure criteria for creep stiffness (S) corresponds to a maximum allowable value of 300 MPa for adequate low temperature performance. Also, a minimum m-value of 0.300 is specified because a greater rate of change for asphalt binder stiffness over time is desired for low temperature cracking. These values are reported at 60 s from the start of the test. In most cases, LTPP data for multiple replicates and temperatures were measured using the BBR. The test temperatures correspond to

the anticipated low temperature performance grade plus 10°C. The anticipated low temperature grades are determined based on the minimum low pavement temperature expected in a particular location.

DSR testing for Superpave grading involves a sinusoidal oscillatory load measured at the standard frequency. DSR testing is performed at both intermediate (i.e., 13, 16, 19° C) and high temperatures (i.e., 52, 58, 64° C). The test temperature varies for each project and is related to the pavement temperatures experienced at the location of interest. During testing, the test strain amplitude and torque are measured to determine the complex shear modulus and phase angle of the specimen.

As it relates to analysis, the authors assume measurements were taken in the linear viscoelastic region of behavior, which allow for interconversions to merge creep stiffness from the BBR with $G*$ from the DSR into one master curve that will span an appropriate range of temperature-loading rate combinations. The assumption of linear viscoelasticity is commonplace in the asphalt materials testing protocols, as the material behavior is easier to predict and is assured to adhere to the time-temperature superposition principle.

A critical element in master curve construction involves the shift factor functions, which allows for isothermal curves to be shifted along a time or frequency axis to form a smooth master curve. In theory, the shift factors should be equal at a particular temperature for any viscoelastic material property. For a thermorheologically simple material, as asphalt is in the linear viscoelastic region, a master curve constructed at one reference temperature can represent properties at many other temperatures through its location on the reduced frequency or reduced time axis.

To conduct the interconversion, the authors utilized Abatech, Inc.'s RHEA™ software package. The first step in the procedure was to compile the creep stiffness isotherms from the BBR data. The process explained here is expressed in further detail in Rowe (2014). The software fits the data with the Christensen-Anderson (CA), Christensen-Anderson-Sharrock (CAS), and Christensen-Anderson-Marasteanu (CAM) rheological models to determine the preliminary creep stiffness (S(t)), master curve with the best fit. At this stage, the Hopkins and Hamming method is used to convert the S(t) master curve to relaxation modulus (G(t)). Then, the time domain values from the S(t) data are altered and placed into the G(t) function to provide an estimation of the binder storage and loss moduli. Lastly, a density correction is applied to obtain the corresponding dynamic (oscillatory) isotherms.

With the conversion of BBR data to the dynamic realm, G* and δ master curves can be constructed. The RHEA™ package utilizes shifts of the data using the G', G", and G* shift factor curves to assess the quality of the data. As mentioned previously, these shift factor curves should be the same for each modulus. The single point isotherms obtained from the LTPP database DSR tests enable the user to a) construct a more complete master curve that carries low temperature and some high temperature functionality and b) allow for the Glover-Rowe parameter to be calculated using the functional form of the G* and δ master curves. The use of these functions also enable for calculation of the crossover frequency and rheological index.

4.4 Results and Discussion

Upon completion of the data analysis, some concerning observations were noted. Several times, the isotherms corresponding to intermediate DSR temperatures (i.e., 13°C, 16°C) had to be removed in order to proceed with an optimal fit given the available data. This leaves a wide gap

between the BBR temperature isotherms (i.e., -24°C) and high temperature DSR isotherms (i.e., 58°C) along the reduced frequency axis. Also, the Glover-Rowe parameter is taken at a temperature of 15°C, so it would be ideal to have measured points around that temperature. The functional fit root mean square (RMS) error percentages for the chosen projects ranged from 7.59% to 16.97%, which are high for this type of data. This is likely attributed to single frequency isotherms and the large gaps between isotherms along the reduced frequency axis.

After sorting and compiling all the data, limitations were evident when attempting to convert to a G* master curve. Few projects had enough replicates to pursue with data analysis. Furthermore, some projects were removed due to extrapolation in the master curve of the Glover-Rowe specification of 15°C and 0.005 rad/s. These limitations must be considered in the following discussion of results.

4.4.1 Superpave Low Temperature Specification Indicator

The first analysis approach uses the standard Superpave criteria for low temperature performance grading. In Figure 4.5, the continuous low temperature binder grades determined from BBR tests are plotted against the design low temperature grade, or the grade that it should be for the given location. The Ontario binder, which experienced significant thermal cracking in the field, was specified as a PG xx-40 binder, but the field extractions show an m-controlled binder grade of -25.5°C, over two grades (12°C) stiffer (warmer) than design at a test date of 1998 (1 year in service). Meanwhile, the extracted Michigan and Saskatchewan samples are about two full grades softer than the design grade, which may explain the limited distress readings during the first five years of service for each pavement.

91

Generally, it is thought that as binders age, the continuous low temperature binder grade becomes more m-controlled (or smaller difference between S-value and m-value) due to reduced relaxation capabilities. Looking at the Saskatchewan samples, the results are inconclusive as the binders are S-controlled and do not experience significant changes in continuous grade between 1998 and 2001 (2-5 years of service). The discrepancies between the field binders and the design binder may be a result of poor reporting in the LTPP database, leniency in specification enforcement, or inconsistent quality assurance/control (QA/QC) practices. All of these factors may impact the performance of the pavement.
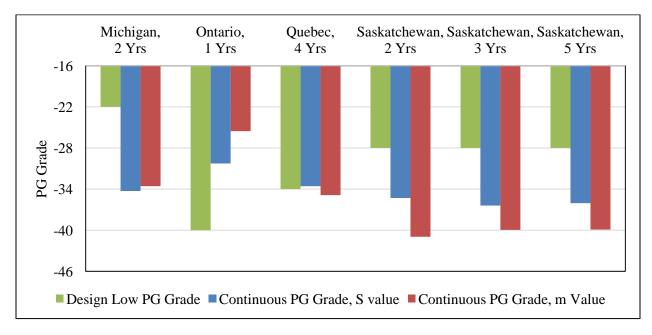
Figure 4.5: Continuous low temperature binder grades

The Superpave pass/fail values, along with the measured data from the LTPP database, are shown in Figure 4.6. Each point in the figure shows the BBR results at a certain test temperature. The test temperature is compared to the low temperature binder grade by use of dashed/solid lines and open/filled circles so that it can be seen whether the S and m values should have failed based on the as-designed low temperature binder grade.

Based on the BBR results, the Ontario and Quebec field-aged binders should be prone to low temperature cracking at the given aging times, as both of the binders fail the S(60) and m-value criteria. The Ontario binder is specified as a PG 58-40, but fails the Superpave criteria for a PG xx-28 binder after one year of field aging. The binder likely has reduced relaxation capabilities which inhibit the material's ability to resist cracking due to low m-values. This would suggest that significant embrittlement of the binder has occurred or shortcomings in QA/QC during construction. The Quebec material fails marginally due to high stiffness and no longer passes the PG xx-34 criteria after four years of field aging. However, the Michigan binder is specified as a PG 64-22 but passes the Superpave criteria at temperatures colder than PG xx-22. The Saskatchewan binder is specified as a PG 58-28, but passes the criteria for a PG xx-34 after five years of field aging. The reader should realize the limitations of the data, as the facility cracked by the next distress survey, but no laboratory data was available in the LTPP database.
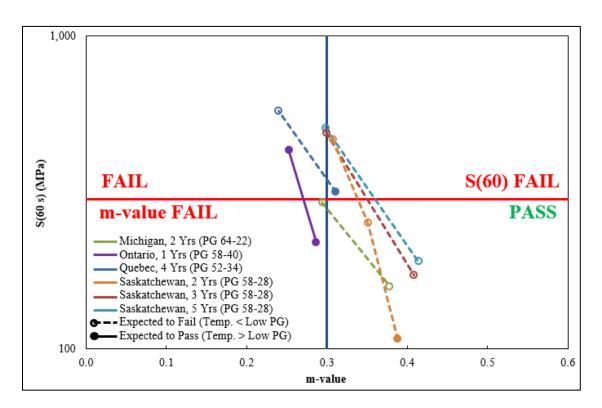
Figure 4.6: Creep stiffness and m-value measurements at 60 s

4.4.2 Glover-Rowe Parameter

The second approach undertaken involves a more traditional Black Space plot using modulus and phase angle. Figure 4.7 shows the interpolated G* master curves for the evaluated binders. The G* master curves exhibit some noteworthy trends among the analyzed binders. At high frequencies, the Quebec and Saskatchewan 1998 (2 Yrs) data shows the stiffest properties, while the Michigan binder is the softest. At low frequencies, the projects are quite different. Ontario pavement sections are stiffer at the lower frequencies, but become less stiff than other projects at higher frequencies. Another key trend to note is the stiffness of the Saskatchewan binder as it ages. At most frequencies, the Saskatchewan project seems to become less stiff as it ages, which is contrary to expected trends. The G* test measurements indicate that the Saskatchewan 1999 (3 Yrs) sample is less stiff than the 1998 sample. However, the Saskatchewan 2001 (5 Yrs) sample seems to be slightly stiffer than the 1999 sample. These inconsistencies may be a result of limited data points for master curve creation, testing/sampling variability, or lot-to-lot variation within the project.

Using the master curve, the complex modulus and phase angle were calculated and plotted in Black Space, as shown in Figure 4.8. Low temperature cracking is often associated with low phase angles (i.e., 10-20°) and high stiffness (G*) areas of the Black Space plot. In the figure, the projects in the high stiffness-low phase angle area are very similar and no distinctions can be made between the projects. However, above the crossover frequency the curves start to separate. In the 60-80° phase angle range, the Ontario binder displays much more elastic properties and is softer than the other materials at a given phase angle. The Glover-Rowe measurement of 15°C and 0.005 rad/s corresponds to higher phase angles and lower modulus values, due to the slow loading rate. Recall the Ontario section experienced low temperature cracking very early in its

pavement life. This shows that in this instance, the Glover-Rowe parameter (Figure 4.9) was able to identify the pavement sections that would experience low temperature cracking. This is due to its location at the Glover-Rowe failure line for the field aged binder obtained in 1998.
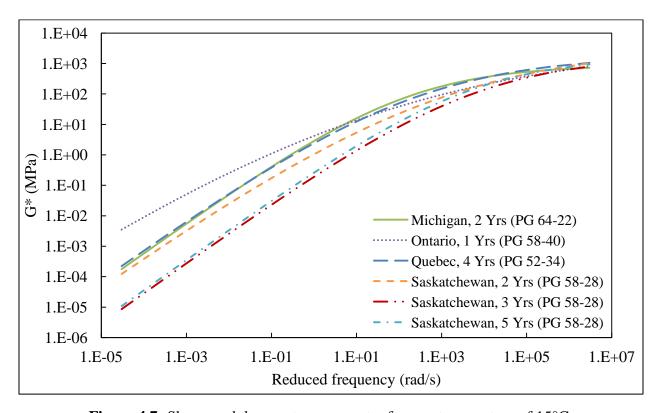
Figure 4.7: Shear modulus master curves at reference temperature of 15°C

However, the other cracked sections (Quebec and Saskatchewan at 5 years service) are not at risk according to the 15°C, 0.005 rad/s configuration. Perhaps the temperature-frequency combination is insufficient to detect cracking in these materials. As discussed earlier, low temperature cracking would occur at lower phase angles, but the Glover-Rowe methodology requires a slow loading rate condition where phase angles are likely higher. This leads the authors to hypothesize that the location on the master curve or the failure plane value is insufficient for proper detection of the other cracked sections. Note that the Saskatchewan materials do not follow the expected trend with age (increased stiffness, decreased phase angle).

95
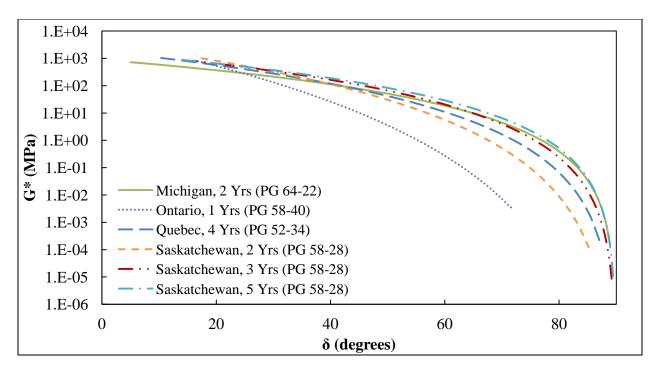
Figure 4.8: Black Space diagrams for the featured binders at 15°C reference temperature
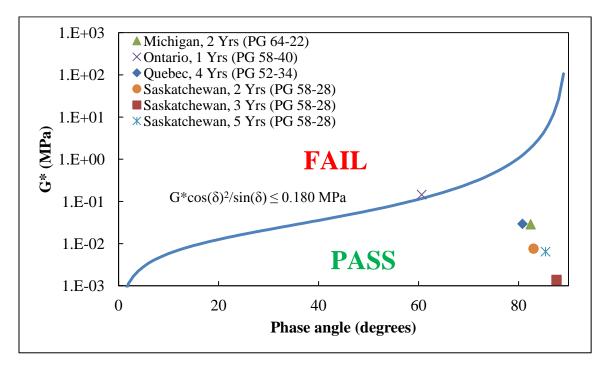
Figure 4.9: Black Space with Glover-Rowe measurements (15°C, 0.005 rad/s) presented

96

4.4.3 Crossover Frequency and Rheological Index Approach

A final approach that holds promise as it relates to cracking indication is to use the crossover frequency and rheological index to describe the shear dependency and viscoelastic behavior of the binder (Anderson et al., 2011; Rowe et al., 2013). As materials age, the rheological index should increase while the crossover frequency decreases. Materials which are more susceptible to cracking should have a lower crossover frequency (elastic region covers more of the reduced frequency axis) and higher rheological indices (larger difference between glassy modulus and crossover modulus).

Figure 4.10 shows a crossover frequency-rheological index space. The Ontario binder is easily distinguished from the others, as the R-value is much higher than the other materials. The crossover frequency is also at least an order of magnitude smaller than the other binders. The Michigan binder, which had experienced lower levels of thermal cracking, shows the lowest R-value, but the second lowest crossover frequency. The Quebec binder has a larger R-value, but similar crossover frequency to that of the Ontario material.

There may be a data discrepancy among the Saskatchewan binder samples, as the sample at 2 years life is stiffer and is located in a position in Figure 4.10 which corresponds to a lower cracking resistance when compared to the 3 and 5 year samples. The amount of aging between the samples is not expected to be severe from 2 to 5 years of service and the master curves should be similar in shape and magnitude or slightly stiffer and more elastic with time. The data in this plot seems to be governed by the shape of the master curve and given the degree of interpolation required due to data limitations, caution should be exercised when coming to conclusions regarding the Saskatchewan samples. It is also possible there are recording and testing errors, but it is postulated that the primary mechanism behind the disagreement with the

expected trend is due to the interpolation influencing the master curve shape (also an issue in Figure 4.9).
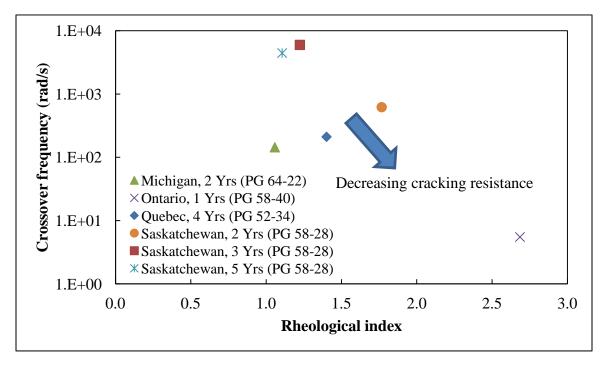
Figure 4.10: Crossover frequency-rheological index space for LTPP binders

4.5 Conclusions

In closing, three rheological parameters that engineers can consider in the evaluation of low temperature cracking resistance for hot mix asphalt sections were investigated. This study focused on six field-aged binder samples from four pavement sections, paired with field cracking measurements from the LTPP database. The four sections were compared against three material spaces – a BBR-based S(60) and m-value space, a Black Space (G* and δ) diagram, and a crossover frequency-rheological index diagram. Each approach was able to detect the worst performing section (Ontario), while the S(60) versus m-value space was able to detect two of the three cracked sections.

Despite some data limitations, the authors were able to deem the chosen projects as appropriate for analysis of the Glover-Rowe parameter as an indicator for pavement cracking performance in the field. Using only LTPP data caused several problems with selecting projects for analysis due to the inconsistency in data availability. Few projects had data available in all categories required to characterize the full project, which can lead to errors when interpolating the shape of the master curve. The Saskatchewan materials do not follow the expected trend with age, potentially due to this issue. In order for successful evaluation of the Glover-Rowe parameter, data at lower and higher temperatures than the evaluation point (15°C) are needed, preferably at multiple frequencies for each isotherm. This will create a master curve which can eliminate concerns with extrapolation and have sufficient test data for trustworthy interpolation.

Based on the results of this study, the authors recommend the BBR S and m-value diagram as an indicator for field cracking of aged binders when a typical LTPP dataset is available. However, the rheological index and Glover-Rowe parameter show promise for low temperature crack indication as well. The authors propose a more robust dataset be used to allow for a wider range of reduced frequencies to be captured in the G* and δ master curves, as some projects had many replicates at one temperature, while others may have had only one replicate for several temperatures, neither of which is ideal for the analysis approach. Research in this area is progressing towards Black Space-based indicators, and a well-conducted frequency sweep using the DSR or BBR may have profound benefits as it relates to binder performance. Future work would expand the available data, possibly through use of the LTPP Materials Reference Library, to provide more field validation sites. It may also be possible to include reclaimed asphalt pavement (RAP) materials into this type of analysis with the use of a shift factor to relate to mixture properties where complete mobilization is not present as it is with extracted and

recovered binder. It must also be stated that asphalt-aggregate interactions during construction of asphalt pavements influences performance (Tabatabaee et al. 2012, Alavi et al. 2013). Explorations into mixture-based Black Space parameters are ongoing (Romero and Jones 2013, Mensching et al. 2015) and it is anticipated that these methods will best capture aggregate interaction effects on field performance moving forward.

4.6 Acknowledgements

CHAPTER 5

EXPLORING LOW TEMPERATURE PERFORMANCE IN BLACK SPACE

5.1 Introduction

It is well known that cracking presents major challenges to the effective design and maintenance of asphalt concrete pavements. In colder climates, transverse cracking caused by thermal loading is a major distress mode. As temperatures decrease, thermal stress increases and can eventually exceed the tensile strength of the material. The relaxation modulus of asphalt binders controls the ability of the mixture to alleviate thermal stress build-up and resist thermal cracking. Although relaxation modulus is difficult to obtain experimentally, the principles of linear viscoelasticity can be applied to convert from other, more easily-measured material properties (i.e., complex modulus and creep compliance).

Researchers have sought to classify non-load associated cracking resistance through the use of an index parameter. Field studies have shown that ductility, measured at an intermediate temperature, correlates well with observed cracking (Clark, 1958; Doyle, 1958; Kandhal, 1977). Using a mechanical-empirical relationship with observed cracking, Glover developed a parameter that relates storage shear modulus (G') and dynamic viscosity (η') of the binder to ductility at a common temperature-frequency combination. The rationale stems from the ease associated with a typical complex shear modulus (G*) test, as opposed to binder ductility testing (Glover et al., 2005). Critical envelopes were designed to correlate with field measurements of non-load associated cracking (Kandhal, 1977). In a study by Anderson et al. (2011), researchers

identified parameters to relate ductility and binder properties to non-load associated cracking for airport pavements. The findings of the study identified the Glover parameter (G'/(η'/G')) and the difference between the continuous low temperature binder grade found via creep stiffness (S(t)) and the log-log slope (m-value) of the creep curve (ΔTc = Tc,m(60) − Tc,S(60)) as parameters to identify changes in relaxation properties with aging. Three binders with different anticipated aging levels were exposed to dynamic shear rheometer (DSR) and ductility testing, along with the standard procedures for determining continuous low temperature performance grade. The authors found that while the Glover parameter and ΔTc were the best indicators of durability, there appeared to be value in using the rheological index (R), of which each binder has a unique relationship with the Glover parameter. The authors also observed a flattening complex shear modulus master curve with aging, which can be conveyed through the rheological index.

In a prepared discussion to the Anderson et al. (2011) study, Rowe offered a simplification of the Glover parameter. This Glover-Rowe (G-R) parameter (Equation 5.1) uses the G* and phase angle (δ) of the asphalt binder at 15°C and a frequency of 0.005 rad/s.

$$\frac{G^*(\cos \delta)^2}{\sin \delta} \qquad [5.1]$$

Since the parameter is calculated at a fixed frequency, Rowe expressed the parameter purely in terms of G* and δ, allowing users to plot the ductility-based failure planes in Black Space. Rowe asserts that the use of Black Space encourages clear illustrations of aging impacts. Figure 5.1 shows a sample dataset plotted with the G-R parameter (referred to as the G-R intermediate temperature measure) set to the converted ductility limits featured in Glover et al. (2005). A value of 180 kPa corresponds to the onset of non-load associated cracking, while a value of 450

kPa or larger relates to significant cracking issues. The sample data in Figure 5.1 is from a study evaluating different binder aging levels (pressure aging vessel and rolling thin-film oven). The diagram shows that as the materials are exposed to additional aging, their location in Black Space shifts to a stiffer, more elastic condition. There are several factors that influence cracking resistance, one of the most important being associated with irreversible oxidative aging. Oxidative aging is directly attributed to increases in stiffness and decreases in ductility, which decrease cracking resistance. The Superpave fatigue parameters are also plotted, showing that all binders pass the criteria, even after 60 hours of pressure aging (PAV). However, the G-R parameter predicts that most of these materials will have cracking issues (Bennert, 2014).

King et al. (2012) further reinforced the importance of an asphalt binder's location in Black Space as a performance parameter for age-induced cracking. Using the G-R parameter, they argue that the standard Superpave parameter ($G^*\sin\delta$) developed in the Strategic Highway Research Program (SHRP) is not an adequate damage indicator for cracking. The authors recommend development of a "damage region" in Black Space which combines the DSR outputs (G^* and δ) with the creep stiffness and slope values from the bending beam rheometer (BBR). This is a concept currently being explored by Rowe (2014).
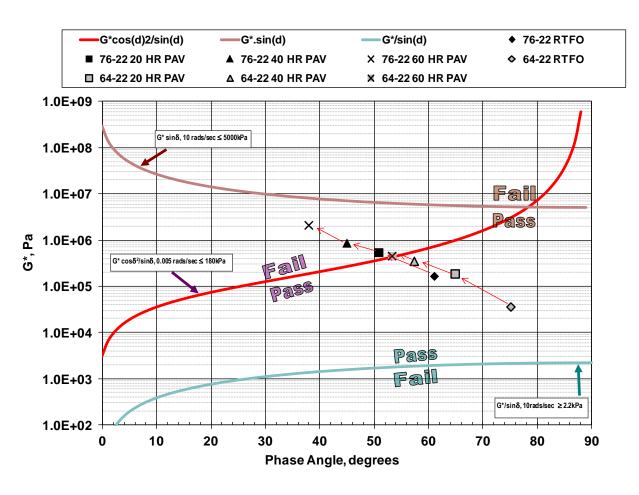
Figure 5.1: Sample Glover-Rowe Black Space diagram (Bennert, 2014)

But are these binder characterizations enough to fully explain the field behavior of asphalt mixtures? The research presents a need for a mixture-specific parameter due to impacts of aggregate-asphalt interactions on performance. Recently, Tabatabaee et al. (2012) found that the number of aggregate contact points influences the coefficient of thermal contraction for the mixture. This relationship causes a change in the accumulation of thermal strain, which impacts viscoelastic properties at low temperatures. Also, Alavi et al. (2013) found that aggregate source had a significant effect on the evolution of thermal stress and strain measured during low temperature evaluation of asphalt mixtures in the laboratory.

But are there other elements which factor into cracking resistance, specifically low temperature cracking? Do binder-mixture conversion techniques (i.e. Hirsch and Christensen-Anderson-Marasteanu (CAM) models) translate to the easy-to-understand Black Space diagram (Christensen, Pellinen, and Bonaquist, 2003; Marasteanu and Anderson, 1999)?

Throughout industry, contractors and owner agencies strive for a balance between robust and cost-effective acceptance and quality control procedures to predict performance, usually on a subjective level. While the G-R parameter appears to be a powerful tool for cracking indication, the approach was derived for asphalt binders. While some mixture properties can be predicted through manipulation of material properties of the binder, the authors believe a more direct method can be derived. This method would build upon premises of the G-R formulation, but be applied to mixture variables. The increased scrutiny of the mixture properties is critical as the community moves towards increased levels of reclaimed asphalt pavement (RAP) in field sections. Typically, binders which include RAP are extracted and recovered using chemical solvents, which result in a fully-blended condition. The literature suggests that complete mobilization of the RAP binder does not normally occur at the time of mixing, and that in reality a partially-blended condition dependent on production parameters is likely (McDaniel et al., 2000; Soleymani et al., 2000; Oliver, 2001; Mogawer et al., 2012; Mensching et al., 2014).

To this point, little study has been done to formulate this type of parameter for mixture performance. Kim and Wen (2002) found that fracture energy at 20°C exhibited high correlations with field performance of WesTrack sections. The researchers used indirect tension (IDT) loading to evaluate several mixture parameters with respect to fatigue cracking. Researchers in the Midwestern United States have also used disk-shaped compact tension test (DCT) data to recommend a threshold performance specification value based on fracture energy (Marasteanu et

al., 2012). Recently, Romero and Jones (2013) utilized BBR mixture testing to develop a surrogate Black Space using the creep stiffness and m-value obtained from the test as opposed to the traditional modulus and phase angle space. The authors postulate that a thermal stress failure envelope can be displayed in this space, but the envelopes have not yet been identified. These works aid in the rationalization of a mixture-based Black Space parameter which can serve as an adequate indicator of non-load associated cracking performance.

The paper focuses specifically on thermal cracking, as the structural considerations surrounding fatigue performance are vastly more complex and require extensive analysis to characterize. With this in mind, the objectives of this paper are to:

1. Validate the G-R approach for materials with laboratory and field performance measurements;
2. Develop an indicator parameter for low temperature cracking of mixtures using a combination of relevant material properties;
3. Develop an alternate approach to study mixture performance in Black Space.

It is believed that the theory and application described herein will provide users with a simple cracking indicator robust enough to capture measured trends in conventional and RAP materials. Several mixtures from Alberta, Indiana, New Hampshire, New Jersey, New York, and Vermont are utilized, as well as the SHRP core binders. Laboratory and field cracking information is presented to aid in the correlation and evaluation of failure envelopes.

5.2 Theoretical Approach

In order to satisfy the objectives outlined above, knowledge of viscoelastic behavior and rheological modeling is needed. Furthermore, any developed mixture parameter must have a

sound, fundamental backing. The premise circulates around the principle that a traditional Black Space diagram for mixture, comprised of dynamic modulus ($|E^*|$) and δ, is a valuable tool in representing two critical properties for determination of thermal cracking resistance: stiffness and stress relaxation. It is expected that as temperature decreases, an asphalt mixture becomes stiffer and more elastic, resulting in reduced relaxation capabilities (decreased slope of relaxation modulus master curve). The increasing prevalence and ease of using $|E^*|$ and δ for mixture performance is also a major reason for development of a parameter that requires nothing more than a cracking measure and a master curve in the linear viscoelastic region. In this section, the underlying theory and assumptions behind the binder parameter evaluations and the proposed mixture parameter are explained. Later, the theory described here will be applied to laboratory and field-measured cracking data to establish critical envelopes for low temperature performance indication.

5.2.1 Interconversions and Master Curve Construction

In developing the Black Space diagram, material master curves are required. It is well-known that when measurements are taken in the linear viscoelastic region, material properties (i.e., $|E^*|$ and creep compliance) can be converted among each other to gain a more complete understanding of the mechanical behavior. In this study, the RHEA™ software (Rowe and Sharrock, 2000) has been used extensively for the analysis of the rheology data, which is based upon the methods developed by Gordon and Shaw (1994). Shift factors move the position of an isothermal curve with reference to a specific temperature (T_R) to another location on the time or frequency axis. In the linear viscoelastic region, the same shift factor shall apply for all the viscoelastic parameters.

The amount of shift applied to two adjacent isotherms depends upon a numerical optimization that results in the two isotherms being represented by a single curve with the closest possible representation by a single function. Two types of shift are considered for asphalt materials; 1) adjustment for density considerations and 2) adjustment for loading time and frequency.

The adjustment for density results in a slight vertical shift to each isotherm. The rationale for this alteration is that to correctly describe the frequency response of a material, the behavior can be related in the manner described by Rouse (1953). The assumption is that when the stiffness at a given temperature is shifted to another temperature, the response at that new temperature will be associated with a material that would have a different density. Consequently, to correctly account for this the stiffness is adjusted according the expression in Equation 5.2:

$$S(T_R, t) = \frac{T_R}{T} \frac{\rho(T_R)}{\rho(T)} S\left(T, \frac{t}{a_T}\right)$$ [5.2]

   where:

   $S(T_R, t)$ = Stiffness at reference temperature (T_R) and loading time (t);

   T   = temperature;

   ρ = density; and

   t/a_T = shifted time.

If density shifts are not implemented, significant errors can result when interpreting master curve data over a large range of temperatures (Rowe et al., 2011). Equation 5.2 is shown in the format applied to BBR data. For a shift to DSR data, as an example, the parameters G*, G' or shear loss modulus (G") are substituted for the bending stiffness.

The adjustment for loading time results in a horizontal shift to the isotherm in relation to the reference isotherm. The method adopted follows the traditional approach of shifting the modulus values (either relaxation shear modulus (G(t)) or G' and G")) along the horizontal axis to form smooth curves of modulus. The shift procedures for producing a master curve have been developed by various researchers. Gordon and Shaw (1994) defined various methods that can be applied for the characterization of viscoelastic materials. These methods have formed the basis of the techniques employed in the RHEA™ software. For the production of master curves, the following general steps are executed:

1. Determine an initial estimate of the shift for each pair of isotherms using a linear fit and checking against a modified Williams-Landel-Ferry (WLF) calculation using Ferry's original "universal" constants (Williams et al., 1955).

2. Iteratively refine the pairwise shifts using weighted least squares polynomial fits.

3. Allow the order of the polynomial to be an empirical function of the number of data points and the decades of time/frequency covered by the pair of isotherms.

4. Sum the optimized shift factors for each successive pair from zero at the lowest temperature to obtain a distribution of shifts with temperature above the lowest.

5. The shift at TR is interpolated and subtracted from every temperature's shift factor, causing TR to become the origin of the shift factors.

In the software implementation of Gordon and Shaw's (1994) methods, a cubic spline fit has been used for the final shift to the reference temperature. Importantly, the implementation of the Gordon and Shaw method for producing shift factors makes no assumptions regarding the final shape of the master curve (relationship between stiffness and time or frequency) or the relationship between shift factor and temperature. Thus both loading rate dependency and

temperature dependency are calculated independently. These methods, implemented in Rowe and Sharrock (2000) also allow for gaps in isothermal data to be captured through the use of a "wild" shift factor.

The relaxation (generalized Maxwell model) and retardation (generalized Kelvin-Voigt model) spectra analysis (Baumgaertel and Winter, 1989) can also be applied to data from the BBR enabling the interconversion to dynamic data. The procedure adopted to perform this interconversion is explained below:

1. The BBR data is fitted with the Christensen-Anderson (CA), Christensen-Anderson-Sharrock (CAS) and Christensen-Anderson-Marasteanu (CAM) models (Rowe et al., 2001) to identify the fit with the lowest error. This master-curve is adopted.

2. The Hopkins and Hamming (1957) method to convert to relaxation modulus (E(t)) is used.

3. The E(t) data is then fitted with a CAM model using the glassy modulus determined from the initial fit. This gives a function which describes the E(t) data.

4. The discrete spectra is calculated for the E(t) fitted function.

5. The reciprocal of the observed times are then substituted into the function to estimate the E', E" data points.

6. The data points are shifted using the original shift values obtained along with a reverse density correction to obtain dynamic isotherms corresponding to the original data.

7. Extensional data is then output, converting to G', G" (or G*).

The use of BBR data converted to dynamic data assists with the generation of mater curves to a) define the properties in a stiffness range were rheometers have problems with strain resolution and b) produce reliable data using the 8 mm geometry (typically used for the lower temperatures and higher stiffness range in DSR testing). Using converted BBR data generally assists in better defining the time-temperature properties over a greater range than would be otherwise possible. If data is being combined from the two measurement types it is important to ensure that comparable data is being combined (e.g., aging condition). Researchers are aware that differences exist in the isothermal storage times between the BBR and DSR test methods, but these are anticipated to be minimal since the maximum times used in both tests for storage and conditioning are similar.

In the analysis of data it is imperative to consider the quality of the master curves produced and when and how to should exclude data from the analysis. In previous work (Rowe and Sharrock, 2000), the root mean square (rms%) fit has been used as a statistic to assess the quality of fit to the data. The error at any point between the calculated modulus and a model fit to that frequency or time has been calculated on a log basis and expressed as a percentage error and averaged for the data set. For BBR data sets and master curve generation, the error produced with a three parameter model, such as with the CAM model, the rms% error should be 2.25% or less (Rowe et al., 2001). If only 2 isotherms are used the error should be less than 1.25% as indicated in the standard ASTM D6816 (2002). The goodness of fit relies upon the ability of a binder to exhibit those properties throughout the range considered. The CAM model, which lends itself to the BBR data, is shown in Equation 5.3:

$$S(T,t) = S_g \left[1 + \left(\frac{t}{\lambda} \right)^{\beta} \right]^{\frac{-\kappa}{\beta}} \qquad [5.3]$$

111

where:

$S(T, t)$ = bending stiffness at a temperature (T) and reduced time (t);

S_g = glassy bending stiffness modulus;

λ = reduced time at maximum curvature;

t = loading time of interest;

β, κ = fitting parameters.

In terms of complex shear modulus, typically obtained from the DSR, the expression for the CAM equation is presented in Equation 5.4:

$$G^*(T, \omega_r) = G_g \left[1 + \left(\frac{\omega_0}{\omega_r} \right)^\beta \right]^{\frac{-\kappa}{\beta}}$$

[5.4]

where:

$G^*(T, \omega_r)$ = complex shear modulus at temperature (T) and reduced frequency (ω_r);

G_g = glassy modulus;

ω_0 = crossover frequency;

β, κ = fitting parameters.

In most master curve analyses, the value of κ is equal to unity. This parameter is related to the slope of the viscous asymptote. The relationship for phase angle can be obtained from the differential of the modulus with respect to the frequency (Christensen, 1992; Rowe, 2009) and is represented by Equation 5.5:

$$\delta = \frac{90}{1 + (\frac{\omega}{\omega_0})^\beta}$$

[5.5]

where:

$\delta(T, \omega) = p$hase angle at temperature (T) and reduced frequency (ω_r).

In the original SHRP research, Anderson et al. (1994) proposed a parameter that is defined as the rheological index (R). Equation 5.6 gives the relationship between R and the master curve at the crossover frequency (ω_0):

$$R = \log G_g - \log G^*(\omega_0) \tag{5.6}$$

A modified Kaelble shift factor function is used in this method to develop expressions since it is more inclusive of data types (Rowe and Sharrock, 2011). The shift factor can then be multiplied by a particular isothermal frequency to find the corresponding reduced frequency. The modified Kaelble function is defined in Equation 5.7:

$$\log a_T = -C_1 \left(\frac{T - T_d}{C_2 + |T - T_d|} - \frac{T_R - T_d}{C_2 + |T_R - T_d|} \right) \tag{5.7}$$

where:

   a_T = time-temperature shift factor;

   T_d = defining temperature for inflection point;

   T_r = reference temperature;

   C_1 and C_2 = fitting constants.

For the mixture analysis, many of the same manipulations involving the |E*|, δ, and aT formulations are similar. In this study, the generalized logistic, or Richards curve, is used to fit the master curve (Richards, 1959). The differential method described by Rowe (2009) is utilized to determine the phase angle at a particular temperature-frequency combination. Equations 5.8 and 5.9 detail the Richards curve, with its appropriate differential form. Note that particular manipulations of the Richards shape parameters describe asymptotic and inflection point characteristics of the master curve (Rowe et al., 2011).

$$\log |E*| = \delta + \frac{\alpha}{[1+\lambda e^{\beta+\gamma \log(\omega)}]^{1/\lambda}} \qquad\qquad [5.8]$$

$$\delta(\omega) = -90\alpha\gamma \frac{\alpha}{[1+\lambda e^{\beta+\gamma \log(\omega)}]^{(1+\frac{1}{\lambda})}} \qquad\qquad [5.9]$$

where:

    $\alpha, \beta, \gamma, \lambda$ = shape parameters;

    δ = lower asymptote of modulus master curve.

5.2.2 Considerations for Black Space Diagram

The Black Space diagram, a plot of complex stiffness modulus versus phase angle, is a valuable rheological tool because it enables users to assess how stiffness and elasticity of a material are related with or without using the time temperature superposition principle (TTSP) to convert to the reduced frequency or time domain (Airey, 2002). Since the phase angle describes the relaxation (King et al., 2012; Rowe, 2014), the use of a Black Space diagram can lend itself to low temperature considerations in a similar manner to that used by Leahy et al. (1994) for results from the BBR. In Glover et al. (2005), the parameter formulated was based upon a relationship between G', η', and ductility to determine an appropriate temperature-frequency combination. As it relates to mixture Black Space and low temperature cracking indication, a particular temperature-frequency combination will allow for the most comprehensive assessment of the performance.

Since the G-R cracking parameter as defined by Anderson et al. (2011) is measured at a condition of 15°C and 0.005 rad/s to capture the performance associated with non-load associated cracking (King et al., 2012; Rowe et al., 2013), the authors first used the same combination for the mixture. Recently, Rowe (2014) converted the Superpave low temperature

specification (S ≤ 300 MPa, m ≥ 0.300 at 60 s) to corresponding G* and δ values for a Black Space-based alternative to the standard criteria (referred to as the G-R low temperature thresholds).

Due to the interaction of the asphalt binder with aggregate the Black space plot that occurs with a mixture is that associated with a sigmoidal model behavior with the phase angle tending to zero at both very high and low values of |E*|, as shown in Figure 5.2. The aggregate structure begins to dominate behavior at high temperatures, due to the low stiffness and viscous flow of the asphalt binder whereas at lower temperatures the mixture volumetrics and binder stiffness control the behavior. The highest value of phase angle in this plot is associated with the inflection point in the master curve as described by Equation 5.8. It can be seen in this example that this occurs around a stiffness of 1,000 MPa.
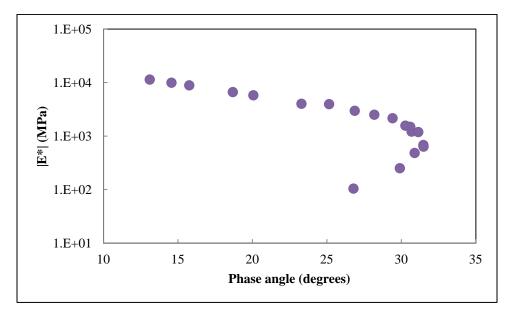
Figure 5.2: Sample Black Space diagram for asphalt mixture

Naturally, the next question becomes: what is the representative temperature-frequency combination? As a preliminary exercise, this paper chooses three arbitrary frequencies, all measured at a reference temperature of 15°C: 0.005 rad/s, 5 rad/s, and 500 rad/s.

In a previous paper (Mensching et al., 2014), typical cooling rates for New England sections were evaluated. A low temperature event, no matter how severe of a cooling rate, results in stiffening of the asphalt binder which in turn requires the need to evaluate properties at a faster loading rate to obtain information at an appropriate stiffness for assessment in the Black Space diagram. Additional evidence of the importance of frequency selection for a low temperature mixture parameter exists in the reality of varying relaxation response with loading rate/time. In other words, during a cooling event the relaxation modulus of the mixture is changing as the temperature changes. This complicates the issue if, for performance evaluation, a single temperature and frequency is being considered for use within the Black Space. Significant care must be taken to ensure that the temperature-frequency combination is actually relevant to field performance.

5.3 Materials and Methods

In order to establish a well-rounded exploration of low temperature performance, laboratory and field-measured cracking measurements are desired. With this in mind, materials from a variety of locations were used in the analysis. The first dataset comes from the New Jersey Long-Term Pavement Performance (LTPP) SPS-5 sections. As part of the LTPP SPS-5 sections, a 0% RAP mixture and a 30% RAP mixture were overlaid at different thicknesses (50 and 125 mm) using two different surface preparation conditions (milled and unmilled surface). Pavement distress was measured yearly during the service life of the sections. Prior to the end of service life,

116

Bennert and Maher (2014) procured field cores from the 15 year old pavement, as well as sampled loose mix that was stored at the LTPP Materials Reference Library in Sparks, Nevada. Intermediate and low temperature asphalt binder and mixture testing were conducted on the procured materials. As part of the study, asphalt binder was extracted and recovered from the loose mix and field cores. The test results from the G* master curves (American Association of State Highway and Transportation Officials (AASHTO) T315) are described in the following section. Cracking data from the overlay tester (OT) (Texas DOT Tex-248-F) is also included in this study (AASHTO, 2012m; Texas DOT, 2014).

The second set of materials was part of a study for Indiana DOT, where three national highway sites at different ages were monitored and subjected to performance grading, DSR frequency sweeps (AASHTO T315), AASHTO R49 critical cracking temperature (CCT) characterization via direct tension testing (DTT) (AASHTO T314), and the Superpave Shear Tester (SST) (AASHTO T320), among other tests (AASHTO, 2012m; 2012a; 2012k; 2012l). Each of these pavements had surface cracking and the results from this study are described in detail in a report prepared by Pellinen et al. (2004).

The third set of materials are from a report prepared for the Federal Highway Administration (FHWA) Binder Expert Task Group (ETG), based on results from the Lamont Test Road in Alberta (Bouldin et al., 1999; Bouldin et al., 2000). Seven binders were used in the study with varying material properties, crude sources, and binder grades. This analysis has been extended with results obtained from retesting the SHRP core asphalts (Anderson et al., 2013).

The Lamont binders were graded according to the Superpave criteria (AASHTO M320), which specifies the use of the DSR, BBR (AASHTO T313), and DTT to identify high and low

temperature performance grade, respectively (AASHTO, 2012n; 2012j). The G* master curve for the binder was developed from a frequency sweep (0.1 rad/s to 10 rad/s) at 6°C increments from 10°C to 64°C. However, to improve the CAM model fit, data with stiffness values lower than 100,000 Pa were generally excluded from the analysis in accordance with the recommendations developed by Rowe (2014) which resulted in exclusion of temperatures generally above 30°C.

In order to evaluate the relationship between laboratory cracking and the Black Space outputs, mixture data from Transportation Pooled Fund Study (TPF) 5(230) are also included. Material information from the eighteen Phase I mixtures are outlined elsewhere (Mensching et al., 2014). For all of the Pooled Fund mixtures, the master curves ($|E^*|$ and δ) (AASHTO T342), thermal stress restrained specimen test (TSRST) (AASHTO TP10), OT, and the IDT low temperature strength (AASHTO T322) results were utilized when available (AASHTO, 2012g; 2012b; 2012h). As done in Mensching et al. (2014), CCT of the mixtures were predicted according to a variation of TCModel (Hiltunen and Roque, 1994) by Christensen (1998). The materials from TPF-5(230) are all plant-produced, laboratory-compacted materials.

5.4 Results and Application

The details provided below are separated into binder and mixture sections for ease of reference. The G-R binder parameters are evaluated and compared between field and laboratory cracking data. The mixture section provides preliminary findings as it relates to the formation of a mixture-based Black Space parameter. Throughout the explanation of results and Black Space applications, various failure parameters will be used. Readers are asked to consult other works for listings of all field and laboratory test values used in this study (Bennert and Maher, 2014;

118

Pellinen et al., 2004; Bouldin et al., 1999; Bouldin et al., 2000; Daniel et al., 2014; Mensching et al., 2014).

5.4.1 Binder Comparisons

The first subsection below presents the comparison of the G-R intermediate temperature based parameter with laboratory and field cracking measurements for each set of data. These comparisons are done in Black Space. The second subsection compares a low temperature critical cracking value determined using the G-R approach with other CCT values.

5.4.1.1 Glover-Rowe Intermediate Temperature-Based Parameter

In this section, the G-R intermediate parameter is evaluated against transverse/thermal cracking measurements from the NJ, Indiana, and Lamont sections. Overlay test results are correlated with Black Space location for the NJ and Pooled Fund materials. It is likely that the intermediate temperature parameter will have mixed agreement with low temperature cracking data, as the stiffness-relaxation combination to best describe this type of distress is at high modulus, low phase angle locations in Black Space. The authors believe that in order to detect performance in the most accurate fashion possible, every distress type will correspond to a different zone in Black Space.

New Jersey SPS-5 Sections

Figure 5.3 shows the transverse cracking results for the NJ 50 mm overlay sections in terms of a transverse cracking deduct. Deduct values are a more-standardized way of converting distress measurements separated by severity levels into a composite value. The field performance results indicate that the 30% RAP mixture shows a larger degree of transverse cracking than the virgin mixture. As the service life of the pavement increases, the amount of transverse cracking in both

the virgin and 30% RAP sections increase until the transverse cracking progresses into block cracking for the 30% RAP sections.
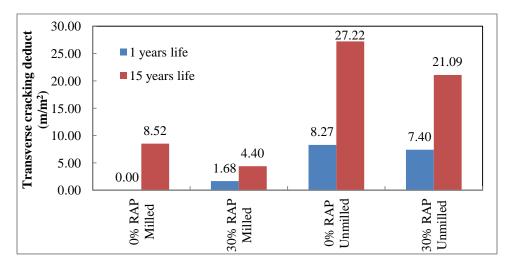
Figure 5.3: Transverse cracking for New Jersey's SPS-5 50 mm overlay sections (after Bennert and Maher, 2014)

The G* master curve data from the NJ LTPP SPS-5 sections plotted in Black Space are shown in Figure 5.4. For the analysis, it was assumed that the stored loose mix had aged properties of a 1 year old pavement, while the field cores were taken at the end of the service life of the pavement (about 15 years old). The progression of transverse field cracking can be tracked in the Black Space diagram by combining the transverse cracking noted in Figure 5.3 with the Black Space information shown in Figure 5.4 for the milled surface condition. The data label next to the Black Space data point is the transverse cracking deduct value measured and calculated from the visual distress survey conducted. As shown in Figure 5.4, the Black Space diagram was capable of tracking the transverse cracking distress, and matches quite well to the G-R intermediate temperature cracking thresholds at the end of the pavement life. It is noted that the 30% RAP field core transverse cracking deduct should theoretically be much higher as this section migrated into block cracking. Although the Black Space diagram is not able to differentiate the progression of transverse cracking to block cracking, the migration of the Black Space data into a

120

more severe area of cracking clearly follows the pavement distress observed in the test sections. The same trend is found when evaluating the unmilled surface pavement section. However, the magnitude of the actual transverse cracking deduct is higher, which appears to be directly related to the surface treatment. Refer to Figure 5.3 for the cracking deduct values of the unmilled sections.

As shown Figure 5.4, the virgin binder is firmly in the pass region, indicating that at approximately 1 year, there should not be any non-load associated cracking. Meanwhile, the 30% RAP mixture (1 year) is close to the "onset of cracking" zone, indicating that cracks could initiate shortly. This represents a slight discrepancy as thermal cracks were observed at this time, but the G-R intermediate temperature parameter does not detect it. The test data for the field cores show that both mixtures should be exhibiting cracking.

Based on the data presented using the NJ LTPP SPS-5 test sections, it appears that the Black Space diagram analysis is able to track the accumulation of transverse cracking magnitudes in the milled and unmilled pavement sections. The actual magnitude of the transverse cracking deduct values appears to be influenced by the surface condition prior to paving (i.e., milled or unmilled). And to some degree, the test data was also able to validate the proposed thresholds recommended by Rowe (2011). Recall the thresholds are best suited for intermediate temperature conditions, such as the conditions possible during age-induced cracking events.

The G-R intermediate parameter was also measured against OT results on the NJ binders (Figure 5.5). As expected, cycles to failure decrease with pavement age and increase in RAP content. The 0% RAP mixture experienced a larger change in field performance and cycles to failure with age than the 30% RAP material. The binder location in Black Space relates well to the OT

results, indicating again that the Black Space concept is related to the cracking performance of asphalt mixtures.
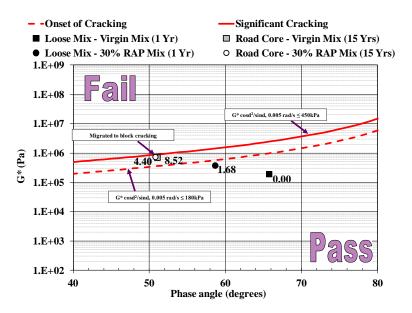
Figure 5.4: Black Space diagram for New Jersey's LTPP SPS-5 binders superimposed with transverse cracking field measurements for milled pavement
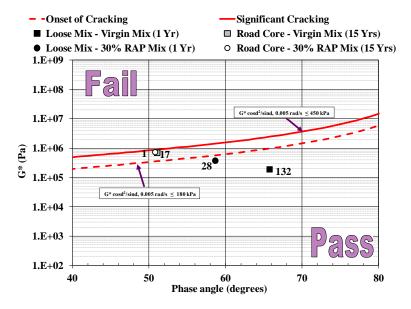
Figure 5.5: Black Space diagram for New Jersey's LTPP SPS-5 binders superimposed with overlay tester fatigue life

Indiana Sections

The primary distress mode for the Indiana sites was surface cracking, and all sites showed some degree of surface cracking. Only one site had transverse cracking which may have been related to thermal effects. However, it is possible that this may also have been influenced by the larger overall degree of cracking on this site compared to the other locations. As shown in Figure 5.6, the data clearly shows that Site 1 is the poorer performing mixture. Although not shown for the sake of brevity, the AASHTO R49 CCTs do not match with the Indiana sites as well. The AASHTO R49 temperature ranks Site 1 as the poorest, but Sites 2 and 3 are ranked incorrectly. Overall the analysis of this study suggests that this approach may have some use in the assessment of load associated surface and/or transverse cracking on these types of sites.
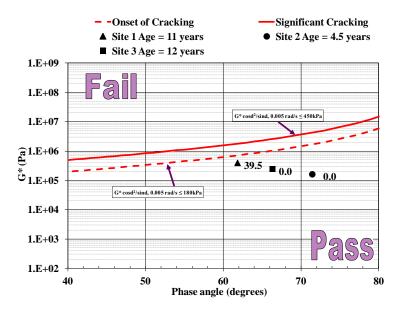
Figure 5.6: Black Space diagram with transverse cracking deduct values for Indiana sections

Lamont Sections

In Figure 5.7, the Lamont binders are plotted at the intermediate G-R condition. The binders are named L1 through L7 to follow the scheme by Bouldin et al. (1999; 2000). Also shown are the

cracks recorded for each section (number of cracks per kilometer). The Black Space location at 15°C and 0.005 rad/s does not appear to track well with observed cracking for these binders, confirming that the G-R parameter does not relate to low temperature performance when evaluated at a frequency of 0.005 rad/s at 15°C.
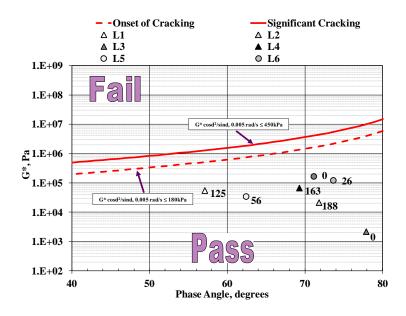
Figure 5.7: Black Space diagram with transverse cracking frequency for Lamont sections

5.4.1.2 Glover-Rowe Low Temperature-Based Parameter

With consideration to low temperature cracking it is not expected that the G-R parameter as developed by Anderson et al. (2011) and Rowe (2011) to be applicable. For a differing distress type, involving different temperatures and rates of loading some adjustments would be anticipated. Rowe (2014) suggested that the G-R parameter can be applied to the cold temperature cracking specification when the value is set at 184 MPa (at a frequency consistent with the 60 seconds of loading in a BBR) and temperature is made to be the dependent variable. The G-R low temperature binder grade refers to the CCT (the temperature at which G-R = 184 MPa) minus 10°C.

Lamont Sections and SHRP Asphalts

In this analysis the CCT was obtained for the seven Lamont sections (Bouldin et al., 2000) and the SHRP core asphalts which have been recently retested by the Asphalt Institute (Anderson et al., 2013).

The Lamont binder data available for reanalysis was largely obtained on RTFO samples with some minimal data collected over PAV conditions which was suitable for production of master curves and the evaluation of the G-R low temperature parameter. In the development of the critical cracking method with the Lamont data, no PAV aging was performed. The RTFO aging condition was used because the cracking in the field occurred within 2 years of construction (Bouldin et al., 1999).

In the determination of the CCT using the G-R low temperature parameter, master curves were developed using both BBR and DSR data. Data below the stiffness of 100,000 Pa was generally excluded from the data sets as recommended by Rowe (2014). However, since several of these data sets were older, particularly for the Lamont data, this requirement was relaxed in a few cases. In addition, for data sets for Lamont sections 6 and 7 only BBR data was available and consequently the calculations were based only on this data.

The results from this analysis are plotted in (Figure 5.8). It can be seen that a fairly good agreement exists between the predictions from both methods. For the SHRP core asphalts, an S or m has been placed by the data point to indicate which parameter was controlling the AASHTO M320 test parameter. The largest deviation from the line of equity was binder AAM which had the largest difference in the failure temperature as determined by S and m (7.2°C). Since the AASHTO M320 defines the failure area by two straight lines whereas the G-R low temperature

parameter uses a line which passes through the apex created by the M320 straight lines, the expectation is that those binders with highly divergent grades from S and m would be graded somewhat differently. It is also anticipated that the G-R low temperature representation of the failure space might be more consistent with performance since a 90° corner is typically unrepresentative of field behavior and rather the transitions are more gradual.
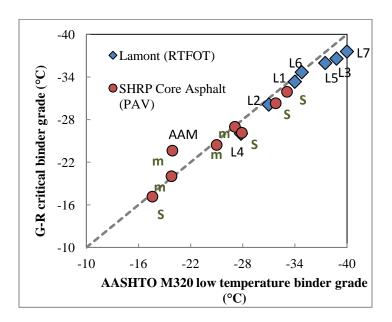
Figure 5.8: Correlation between Glover-Rowe low temperature binder grade and AASHTO M320 continuous binder grade

Table 5.1 compares the field cracking of the Lamont sections against the G-R critical temperature. Ideally, the warmest temperature would correspond with the poorest performing sections. While not an exact match, the G-R CCT agrees very well with the observed cracking at the Lamont Test Road.

Table 5.1: Comparison of Glover-Rowe low temperature criteria with Lamont binders

Binder	L1	L2	L3	L4	L5	L6	L7
G-R CCT (°C)	-23.3	-20.1	-26.6	-16.0	-26.0	-24.7	-27.6
Number of transverse cracks per km	125	188	0	163	56	26	0
G-R rank/field rank	5/5	6/7	2/1	7/6	3/4	4/3	1/1

In the determination of the G-R low temperature parameter for a binder purchase specification for cold temperature cracking, several approaches exist. These include the testing scheme developed by Anderson et al. (2011) in which three isotherms of are collected from the DSR and uses to construct a partial master curve from which parameters may be determined or alternately methods as proposed by Rowe (2014) could be considered including the use of a 4 mm plate in the DSR.

5.4.2 Mixture Comparisons

In comparing a mixture-based Black Space to field performance, the authors used field and laboratory parameters from several projects. In this section, comparisons between mixture Black Space, field cracking, and available laboratory tests are presented for the Indiana and New Jersey sections. Comparisons between mixture Black Space and laboratory testing are also presented for the Pooled Fund mixtures.

5.4.2.1 Indiana and New Jersey Mixture Black Space

In Figure 5.9, field performance (measured as the transverse cracking deduct value) is compared against the Black Space values for the NJ SPS-5 and Indiana materials, measured at a temperature of 15°C and frequencies of 500, 5, and 0.005 rad/s. Looking at the entire Black Space curve of these mixtures confirms that the 30% RAP mixture has a notably lower phase

angle than the virgin mixture closer to the region of the inflection point frequency (or maximum phase angle as shown in Figure 5.2). When comparing the NJ Black Space points with the field cracking (Figure 5.9), DCT, and OT measurements (Figure 5.10), the modified G-R value ($E^*\cos^2(\delta)/\sin(\delta)$) detects the poorer performing 30% RAP mixture as phase angle moves towards it maximum. The OT results follow the trend seen in the DCT and field measurements.
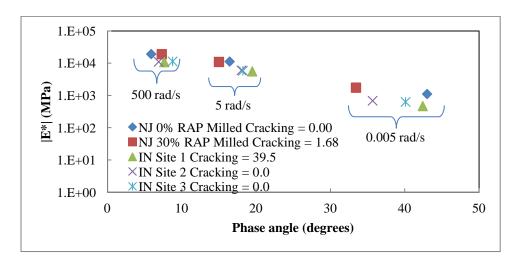
Figure 5.9: Mixture Black Space diagram with transverse cracking deduct values for New Jersey 50 mm milled sections at reference temperature of 15°C and frequencies of 500 rad/s, 5 rad/s, and 0.005 rad/s
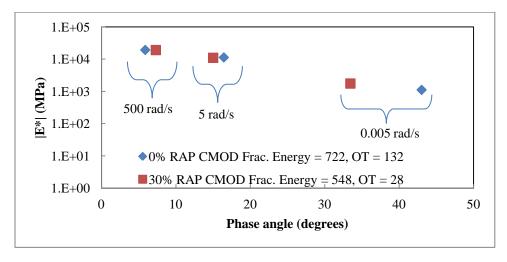
Figure 5.10: Mixture Black Space diagram with crack mouth opening displacement fracture energy values (J/m^2) and overlay test cycles to failure for New Jersey mixtures at 15°C and frequencies of 500, 5, and 5 rad/s

The Indiana mixtures in Figure 5.9 also show the greatest differences in Black Space at 0.005 rad/s. The overall Black Space curves confirm that as the measurements proceed down the reduced frequency axis (towards higher temperatures), the phase angle readings are have greater differences among the three mixtures, which should allow for better detection of differences in performance. The modified G-R value would dictate that Site 2 is the poorest performing material, but the field measurements show Site 1 is the worst performer. However, recall that while Site 1 experienced transverse cracks, all three sections show surface cracking distress. It is also worth noting that the Indiana $|E^*|$ and δ master curves produced higher rms% values than the NJ mixtures, which reinforces the caution needed in developing master curves and executing the test protocols.

5.4.2.2 Exploration of Mixture-Based Black Space Parameter

For the Pooled Fund mixtures, the authors took the approach of using the data as an exploratory exercise towards a mixture-based Black Space parameter for low temperature cracking detection. Since no field data is available at this time, laboratory tests with a critical temperature output were used. The first step in the process was to fit the $|E^*|$ and δ master curves. Each low temperature critical temperature was shifted to a $|E^*|$ and δ corresponding to a 15°C reference temperature at frequencies of 500, 5, and 0.005 rad/s. Figure 5.11 displays the Black Space plots corresponding to the TSRST and the TCModel simulation at 10°C starting temperature and 5.6°C/h cooling rate.
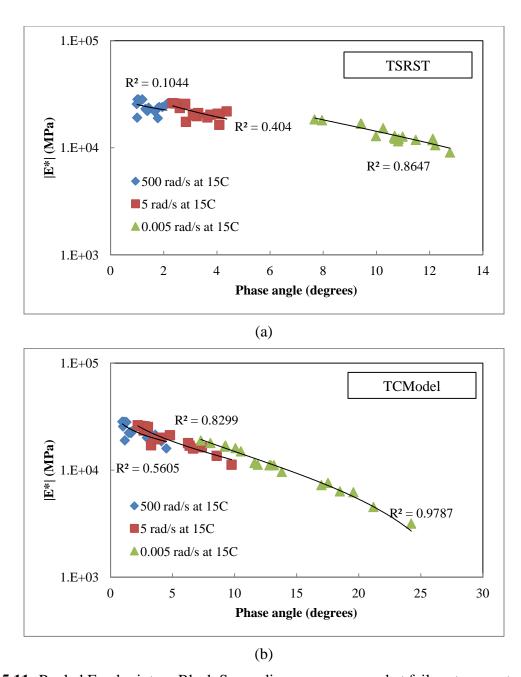
Figure 5.11: Pooled Fund mixture Black Space diagrams, measured at failure temperature for (a) TSRST and (b) standard TCModel setup

Perhaps the most obvious finding is that the R^2 value of the logarithmic trendline increases as the

frequency decreases. This is likely due to the location on the $|E*|$ and δ master curves. At the

higher frequencies, the part of the master curve being used is closer to the glassy modulus and

the glassy plateau. Thus the total range in stiffness being obtained when analyzed on a log scale

is smaller. Based on previous discussion in this paper, it is possible that the optimum frequency for a mixture-based parameter may lie closer to the inflection frequency (or maximum phase angle).

Once an appropriate frequency is found, the development of the failure bands with respect to a cracking measure (laboratory or field) would be initiated. In this paper, the authors chose the shifted 0.005 rad/s frequency at 15°C and calculated the modified G-R value for each mixture for each laboratory test (Figure 5.12). This frequency was chosen due to the enhanced ability to detect Black Space differences as the curve progresses towards the maximum phase angle. The idea is that particular laboratory (or field) tests may be captured by the mixture G-R parameter better than others. This would aid in the definition of the failure bands for a mixture-based G-R parameter. The figure below shows that performance groupings may exist, and there may be useful commonalities shown by the mixture G-R parameter (e.g., the PG 52-34 binder possibly performing better).

In Figure 5.13, the |E*| and δ at the CCT equivalent of the 15°C, 0.005 rad/s is shown for the Pooled Fund mixtures. The failure bands would be plotted in Black Space to identify the poorly performing mixtures based perhaps on a degree of separation in the diagram. However, some kind of field validation for any failure band definition is required regardless of whether or not a laboratory test is chosen for parameter development.
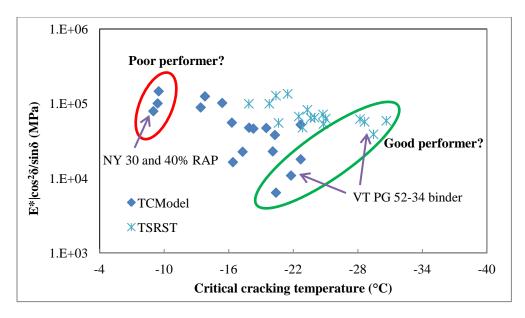
Figure 5.12: Modified mixture Glover-Rowe values against critical cracking temperature for Pooled Fund mixtures

(a)
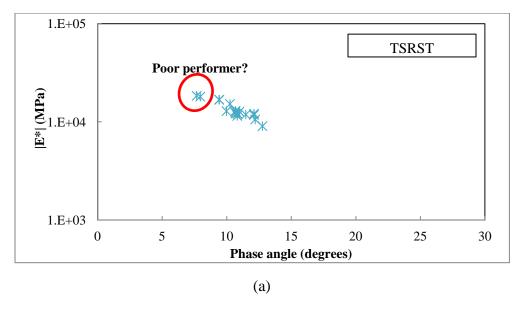
Figure 5.13: Mixture Black Space diagrams for Pooled Fund materials, with hypothetical failure band definition scheme for (a) TSRST and (b) TCModel at the CCT and shifted 0.005 rad/s frequency

(b)
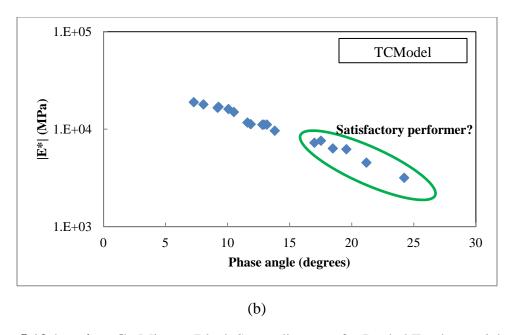
Figure 5.13 (continued): Mixture Black Space diagrams for Pooled Fund materials, with hypothetical failure band definition scheme for (a) TSRST and (b) TCModel at the CCT and shifted 0.005 rad/s frequency

5.5 Conclusions and Recommendations

This study serves two purposes to the asphalt materials community: 1) to evaluate an emerging method to examine non-load associated cracking, and 2) to introduce the concept of a mixture-based parameter for low temperature performance that will simplify testing requirements. The paper applies over 15 materials to the G-R parameter at low and intermediate temperature conditions, with the idea being to compare the Black Space to a cracking measure. Also, over 20 mixtures are used in a preliminary discussion of a mixture-based Black Space parameter. Based on the results and discussion above, the following conclusions and recommendations have been drawn:

1. The G-R intermediate parameter, measured at 15°C and 0.005 rad/s, possesses the ability to match performance from the OT quite well. The OT holds the potential to test non-load associated cracking in the form of reflective cracks. The results

presented here may introduce a method to use the DSR and OT in tandem to assess thermal reflective cracking resistance.

2. The NJ sections seemed to track well in Black Space between start and end of life measurements when the binders were compared to the G-R intermediate parameter. The virgin and 30% RAP binders started at different locations in Black Space, but ended virtually at the same location. This agreed with the laboratory and field measurements that showed the virgin mixture undergoing more damage over the course of its life than the 30% RAP material. This is an interesting finding worth exploring for other RAP mixtures – perhaps a relationship exists regarding a predetermined level of additional damage RAP materials can absorb. Potential candidates for this type of investigation are HMA test strips where a virgin mixture is laid next or in very close proximity to a RAP mixture to monitor distress with similar traffic levels and, presumably, similar mixture designs without the influence of climate.

3. The Indiana mixtures did not line up in Black Space as hoped. Possible reasons include higher variability in mixture testing, and the influence of overall pavement condition on the formation of thermal cracks.

4. All Lamont binders passed the intermediate temperature thresholds, but all but two of the seven sections cracked in the field. The intermediate temperature condition was able to distinguish one of the uncracked sections in Black Space, while the other uncracked section was not separated in the space from the cracked sections. This finding is likely tied to the notion that for every distress type, a particular Black Space region will best detect changes in performance. The Lamont binders exhibited

thermal cracks in the field, which is better tied to the G-R low temperature thresholds. Climate differences between the Lamont location (Alberta) and the location of the original mixtures used in the G-R intermediate temperature calibration (Pennsylvania) may also influence the results. The G-R low temperature CCT predicted the ranks of the field performance with little error, demonstrating its effectiveness with observed thermal cracking measures.

5. The G-R CCT calculation holds potential for virgin materials. Both the Lamont and SHRP core asphalts agree with the AASHTO M320 continuous low binder grade very well. Next steps would be to look into reclaimed asphalt pavement (RAP) binders to establish the effectiveness of the parameter when alternate materials are introduced. The G-R CCT calculation could also lend insight into the mobilization that occurs in RAP mixture when compared to the completely blended baseline provided by extracted and recovered binders.

6. An exploration into a mixture-based Black Space parameter is presented. The results show that measuring the $|E^*|$ and δ at frequencies closer to the inflection point (peak of mixture phase angle master curve) may hold more promise when it comes to performance prediction at low temperatures. The authors postulate that an exceedingly low temperature coupled with a very fast loading rate may in fact result in a stiffness-elasticity condition that is essentially at the glassy asymptote. At this location, variability within the data may climb substantially with small changes in phase angle, causing a negative impact to the effectiveness of the analyzed portion of the Black Space diagram.

In closing, the G-R parameter at the intermediate condition shows an inconsistent ability to monitor low temperature performance in Black Space. However, the low temperature condition of the G-R parameter (which centers on a conversion of the Superpave low temperature criteria) holds promise for low temperature performance detection.

Future work is needed to assess the effectiveness of the parameter with varying amounts of recycled materials. This paper presents preliminary data in the development of a mixture-based Black Space parameter, which would utilize the increasingly prevalent $|E^*|$ and δ master curves. Once this analysis tool is in place, the influence of each length scale (e.g., mixture, mastic, fine aggregate matrix, and binder) on cracking performance can be explored in Black Space through additional research efforts. The authors believe the relationship between stiffness and relaxation can not only be applied to low temperature performance in Black Space, but also to structural distresses, such as classical fatigue cracking. Delving into a fatigue cracking parameter would require incorporation of structural elements, and could hold the potential to significantly reduce testing frameworks across the industry. The authors recommend future work be explored by a team of researchers with access to a wide varying set of data, such as in an ETG setting, to identify the Black Space regions where the G-R parameter will be most effective per distress type.

5.6 Acknowledgements

136

study for their involvement and contributions: Dr. Geoffrey M. Rowe of Abatech, Inc., Dr. Jo Sias Daniel of University of New Hampshire, and Dr. Thomas Bennert of Rutgers University. Acknowledgements are given to Callanan and Pike Industries for supplying the mixtures. Gratitude is also expressed towards Dr. Walaa Mogawer for conducting the TSRST on the TPF 5(230) mixtures.

CHAPTER 6

A MIXTURE-BASED BLACK SPACE PARAMETER FOR LOW TEMPERATURE

PERFORMANCE OF HOT MIX ASPHALT SECTIONS

6.1 Introduction

Low temperature cracking is a major distress type in asphalt pavements that costs agencies and taxpayers countless dollars annually. The cracking itself is governed by the relaxation and strength (fracture energy and ductility) capabilities of the composite, which is inherently tied to the stiffness through principles of viscoelasticity. As the pavement cools, thermal (tensile) stress builds due to the restrained state of the mixture particles. Eventually, either due to thermal cycling or a single, more severe cooling event, the thermal stress exceeds the strength of the material and a crack forms. The crack decreases ride quality, allows for intrusion of water, which causes rapid deterioration of the pavement system, and impacts fuel economy and transportation budgets on a large-scale.

Given the generally poor state of the aging infrastructure in the United States (ASCE, 2013), there is increased scrutiny on decisions made by pavement and materials engineers to produce the longest lasting, most resourceful (i.e., environmentally friendly) pavement systems possible. To achieve these goals, a shift in paradigm is required from volumetric acceptance to performance-based acceptance, where mechanical properties of the materials lend insight into the durability of the structure. This shift is being prioritized by the Federal Highway Administration

(FHWA) as part of the Moving Ahead Progress for the 21st Century Act (MAP-21) funding initiative. An example of a performance-based approach for low temperature cracking uses the disk-shaped compact tension test (DC(T)). A team of researchers developed a draft specification for design of mixtures based on field correlations with the DC(T) test-measured fracture energy, which is being implemented in Minnesota and Iowa (Marasteanu et al., 2012). A recent update mentioned Wisconsin is exploring a similar specification using the DC(T) for low temperature cracking (Dukatz, Hanz, and Reinke, 2015). However, the overwhelming majority of states and owner agencies rely on volumetric based (i.e., density) design and acceptance during production.

Researchers have sought to classify thermal cracking resistance through the use of an index parameter. Field studies have shown that ductility, measured at an intermediate temperature, correlates well with observed cracking (Clark, 1958; Doyle, 1958; Kandhal, 1977). Using a mechanical-empirical relationship with observed cracking, Glover developed a parameter that relates storage shear modulus (G') and dynamic viscosity (η') of the binder to ductility at a common temperature-frequency combination. The rationale stems from the ease associated with a typical complex shear modulus (G*) test, as opposed to binder ductility testing (Glover et al., 2005). Critical envelopes were designed to correlate with field measurements of non-load associated cracking (Kandhal, 1977).

Anderson et al. (2011) identified the Glover parameter and the difference between the S-based and m-based low temperature binder grades as potential indicators for low temperature performance of airfield pavements. In a prepared discussion to this study, Rowe offered an alternate expression of the Glover parameter. This Glover-Rowe (G-R) parameter (Equation 6.1) uses the G* and phase angle (δ) of the asphalt binder at 15°C and a frequency of 0.005 rad/s.

$$\frac{G^*(\cos\delta)^2}{\sin\delta}$$

[6.1]

Since the parameter is calculated at a fixed frequency, Rowe expressed the parameter purely in terms of G* and δ, allowing users to plot the ductility-based failure planes in Black Space. Rowe asserts that the use of Black Space encourages clear illustrations of aging impacts. Figure 6.1 shows a sample dataset plotted with the G-R parameter (referred to as the G-R intermediate temperature measure) set to the converted ductility limits featured in Glover et al. (2005). A value of 180 kPa corresponds to the onset of non-load associated cracking, while a value of 450 kPa or larger relates to significant cracking issues. In this figure, G* and δ are measured at the appropriate temperature-frequency combination, with the two 15 year-old field samples falling between the Glover-Rowe failure bands. The data labels indicate the amount of transverse cracking recorded at each site after 1 and 15 years of service. The distress values shown coincide with the location in Black Space, as the pavements clearly have cracking concerns which are captured by the Glover-Rowe intermediate parameter.

In an attempt to make the Black Space-based methodology more robust, Rowe later converted the Superpave low temperature grade thresholds (S(60 s) ≤ 300 MPa and m(60 s) ≥ 0.300) to G* and δ. The new Black Space limits correspond to a Glover-Rowe value of 184 MPa, which is now referred to as the Glover-Rowe low temperature parameter (Rowe, 2014). The thresholds developed as part of the prepared discussion in 2011 are now part of the Glover-Rowe intermediate parameter. The usefulness of the low temperature parameter is evident when back-calculating the low temperature binder grade, which corresponds well to the Superpave criteria. This method simplifies testing requirements by only using a G* testing sweep in a dynamic shear rheometer (DSR) on pressure-aging vessel (PAV) binders as opposed to the DSR

characterization for intermediate temperatures and the separate bending beam rheometer (BBR)

protocol for the low temperature specification (Rowe, 2014; Mensching et al., 2015).
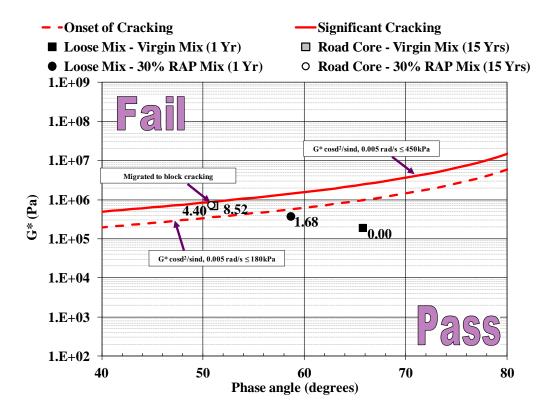
Figure 6.1: Sample Glover-Rowe diagram at the recommended 15°C-0.005 rad/s temperature and frequency combination (Mensching et al., 2015)

With this information in mind, the natural progression of indicator parameters would move

towards mixture characterization. Given the heterogeneity of hot mix asphalt (HMA), there

should be differences in material properties, and hence performance, from the binder. This is

likely due to aggregate interactions, production, or mobilization of additives (e.g., reclaimed

asphalt pavement (RAP), modifiers, and crumb tire rubber) in the mixture (Tabatabaee et al.,

2012; Alavi et al., 2013). In a study by Romero and Jones (2013), preliminary efforts have been

undertaken to identify a mixture-based parameter which featured stiffness and relaxation

properties using the BBR device for mixture. Mensching et al. (2015) began outlining the

process for a Black Space-based mixture parameter, which will be carried through further in this work. The researchers decided that Black Space analysis for low temperature cracking of the mixture will need to be done closer to the inflection point of the Black Space curve. This work is a continuation of that preliminary analysis.

6.2 Objectives

The primary objectives of this paper are to:

1. Assess the value of a parameter which can describe low temperature performance by using dynamic modulus ($|E^*|$) and δ of the mixture using field and laboratory-measured performance;

2. Define failure lines in Black Space which correspond with sites from the Long-Term Pavement Performance (LTPP) database;

3. Provide agencies with a tool to aid in the movement towards a performance-based mixture design, acceptance, or rehabilitation decision-making.

The underlying emphasis of this study is to provide a tool for performance-based decision making for transportation agencies. Ideally, a practitioner would be able to measure the $|E^*|$ and δ at a standard temperature and frequency, such as those in AASHTO T342, during mixture design and plot the point in Black Space, evaluating the position relative to the critical value to determine whether the mixture is prone to low temperature cracking before it is produced (AASHTO, 2012g). The practitioner could then monitor the parameter during production to ensure the location in Black Space does not change due to acceptable construction variation. Furthermore, agencies can refine the methodology by monitoring the shift in Black Space with service life, allowing for modifications and observations to be made based on field-measured

data. The vision for the parameter would for it to become a widespread performance-based specification which can be applied to a pay factor specification to provide contractor's incentive or disincentive based on an easily-measured material property.

6.3 Materials and Methods

The materials used in this study come from two primary sources. Seventeen plant-produced mixtures are used from Phase I of Transportation Pooled Fund Study TPF5-230: Evaluation of Plant-Produced High-Percentage RAP Mixtures in the Northeast. These mixtures underwent a variety of laboratory tests, including dynamic modulus (AASHTO TP79) at 4, 20, and 35°C using frequencies of 25, 10, 5, 1, 0.5, 0.1, and 0.01 (at 35°C only) Hz, low temperature indirect tensile creep and strength testing (AASHTO T322), and thermal stress restrained specimen test (TSRST) (AASHTO TP10) (AASHTO, 2012i; 2012h; 2012b). Tables 6.1 and 6.2 detail the mixture properties of the Pooled Fund materials used in this study. Note that one RAP source was used for the NH mixtures, one source for the NY mixtures, and one source for the VT mixtures. The naming convention for the materials is as follows: NH, NY, or VT denotes the production location, a lowercase letter after the state abbreviation indicates the virgin binder grade, and the number indicates the RAP percentage by weight of mixture. For example, NYb30 is a mixture produced in New York with a PG 58-28 virgin binder and 30% RAP by weight of mixture. Note in Table 6.2, the measured binder percentage is found from the extraction procedure, and the RAP percentage by weight of binder was calculated from the design binder content.

In order to capture field performance, sections from the LTPP database were selected from the Northeastern United States, with the pavement locations shown in Figure 6.2. At this stage,

projects from the Northeast were used to closely match the climate data to be used later on in the analysis. Eight sections were selected to establish details on the properties of a pavement with satisfactory thermal cracking performance in comparison with poor performers. These projects were randomly selected from available sites with test information that can produce a master curve analysis of dynamic modulus and phase angle data. Table 6.3 provides details of the pavement structure and distress values for the analysis dates. Table 6.4 presents available mixture details. The Maine mixture has 30% RAP incorporated (by weight of mix), while the New Jersey mixture has an unreported amount of RAP included. The Maine materials were sampled at two points during service: at 105 days service and 3,334 days service.

The naming scheme uses the state's common abbreviation accompanied by its LTPP project code. It is important to note that not all test dates will correspond exactly with pavement condition survey dates, though an effort is made to compare data taken in close proximity to the distress survey. It is also important to consider that all sections are not the same age and are not exposed to controlled aging conditions.

Figure 6.2: Location of selected LTPP sites (driverlayer.com)

Table 6.1: Continuous PG grades and mixture gradations

Mix	Virgin Continuous PG Grade	Percent Passing									
		19.0	12.5	9.5	#4	#8	#16	#30	#50	#100	#200
NHe00		100	99	86	58	43	32	25	16	7	3.6
NHe20	66.3-29.7	100	99	87	58	42	33	26	16	7	3.6
NHe30		100	99	87	56	42	34	26	16	7	3.6
NHe40		100	99	86	56	41	33	25	15	6	2.7
NH RAP	85.5-13.2	100	100	98	74	56	44	33	22	12	7.4
NYb30	61.0-34.6	100	97.5	91	60	33	21	15	10	6	5.3
NYd00		100	100	91	68	42	27	19	13	5	3.8
NYd20	67.0-25.5	100	99	91	59	31	19	12	8	7	3.8
NYd30		100	95	86	54	30	23	17	12	8	6.0
NYd40		100	98	89	53	31	19	14	10	6	4.3
NY RAP	87.2-19.9	100	98	93	66	47	32	22	13	7	4.5
VTa00		100	100	99	79	51	31	19	11	6	3.8
VTa20	56.3-32.5	100	100	98	79	51	31	19	12	7	4.6
VTa30		100	100	99	75	48	30	19	12	7	4.5
VTa40		100	100	98	77	49	29	18	12	8	4.6
VTe00		100	100	100	77	49	30	18	10	6	3.3
VTe20	64.4-30.2	100	100	99	81	54	32	20	12	7	4.3
VTe30		100	100	98	78	49	29	18	11	7	4.3
VTe40		100	100	99	75	47	27	16	9	5	4.5
VT RAP	73.8-25.2	100	99	90	72	52	36	24	16	11	8.3

Table 6.2: Mixture design and production information

Mix	Nominal Maximum Aggregate Size (NMAS) (mm)	% Total Binder (design/ measured)	% RAP by weight of mix/by weight of binder	RAP Binder Content (%)	Voids in Mineral Aggregate (VMA)	Voids Filled with Asphalt (VFA)	Aggregate Temp. (ºC)	Discharge Temp. (ºC)	Compaction Temp. (ºC)	Silo Storage Time (h)
NHe00	12.5	5.7/5.8	0/0	--	14.9	74.8	n/a	165.6	148.9	6.00
NHe20		5.7/5.5	20.0/16.8	4.79	14.5	79.9		157.2	154.4	1.25
NHe30		5.7/5.3	30.0/25.2	4.79	14.4	81.3		168.3	157.2	1.00
NHe40		5.7/6.0	40.0/33.6	4.79	14.5	82.1		168.3	157.2	n/a
NYb30	12.5	5.2/5.0	30.0/28.4	4.93	13.7	81.1	210.0	151.7	135.0	3.50
NYd00		5.2/5.0	0/0	--	12.6	89.3	191.0	154.4	143.3	2.75
NYd20		5.2/5.2	20.0/19.0	4.95	14.1	79.9	210.0	160.0	143.3	0.75
NYd30		5.2/5.5	30.0/28.4	4.93	13.0	85.1	210.0	151.7	143.3	2.75
NYd40		5.2/5.1	40.0/37.7	4.90	12.5	87.9	232.0	165.6	143.3	3.00
VTa00	9.5	6.7/6.3	0/0	--	20.2	76.3	n/a	171.1	171.1	n/a
VTa20		6.8/6.2	20.0/15.9	5.41	18.8	81.9		162.2	162.2	
VTa30		6.6/6.2	30.0/24.6	5.41	17.7	82.5		160.0	160.0	
VTa40		6.6/6.3	40.0/32.8	5.41	18.0	77.8		148.9	146.1	
VTe00		6.5/6.6	0/0	--	20.3	71.5		165.6	148.9	
VTe20		6.7/6.3	20.0/16.1	5.41	18.7	79.7		148.9	148.9	
VTe30		6.6/6.1	30.0/24.6	5.41	19.1	75.9		161.1	154.4	
VTe40		6.6/6.1	40.0/32.8	5.41	18.2	76.4		146.1	146.1	

Table 6.3: LTPP thermal cracking readings (with years in service in parentheses for particular survey)

Project	CT 0902	CT 5001	MA 1004	ME0503_105 ME0503_3334		NH 1001	NJ 1033	VT 1004
Construction Year	1997	1996	2001	1995		1981	1997	2001
Sample Year	1997	1996	2002	1995	2004	1998	1997	2001
Survey 1	2.4 (4)	0 (3)	0 (7)	0 (2)		10.6 (13)	54.3 (3)	17.7 (3)
Survey 2	3.2 (5)	0 (5)	0 (9)	0 (4)		16.3 (14)	33.9 (6)	44.1 (6)
Survey 3	29.2 (8)	21.6 (8)		0 (5)		25.0 (15)	53.3 (7)	63.4 (8)
Survey 4	27.8 (10)			0 (6)		34.9 (16)	60.1 (10)	
Survey 5	32.8 (12)			0 (7)			78.2 (12)	
Survey 6				0 (8)			51.8 (14)	
Survey 7				0 (9)				

* Deduct values calculated from Bennert and Maher (2013). Maine project sampled after 105 and 3334 days service.

Table 6.4: LTPP mixture design and gradation information

Mix	Design Binder Grade	Binder content (% by weight of mix)	Voids in mineral aggregate (VMA)	Percent Passing									
				19.0	12.5	9.5	#4	#8	#16	#30	#50	#100	#200
CT0902[a]	PG 64-28	5.3	14.4	--	--	--	--	--	--	--	--	--	--
CT5001[a]	AC-20	5.7	14.0[c]	100	94	75	55	42	32	26	14	6	3.5
MA1004[a]	AC-20	4.5	14.9	100	100	87	57	--	26	--	--	--	4.0
ME0503[b]	AC-10	6.4	15.0[c]	100	90	78	49	37	28	18	11	7	5.0
NH1001[a]	AC-10	6.3	17.7	--	--	--	--	--	--	--	--	--	--
NJ1033[a]	AC-20	5.0	14.4	100	94	87	55	37	27	19	12	7	4.0
VT1004[a]	Pen 85-100	6.2	15.4	100	92	78	58	44	32	23	15	--	3.0

[a] Measurements are from as-placed material

[b] Measurements from as-design material

[c] Assumed based on Superpave requirements

6.4 Identifying the Black Space Evaluation Point

In order for the parameter to be more comprehensive and likely to be adopted by agencies, a single evaluation point is needed in Black Space. The point should be measured at a commonly tested temperature-frequency combination and should be tied to the material behavior of mixture.

In a previous work, Mensching and others (2015) plotted |E*| and δ at laboratory-measured critical cracking temperatures corresponding to a very fast loading rate (500 rad/s), an intermediate loading rate (5 rad/s), and a very slow loading rate (0.005 rad/s) at the reference temperature of 15°C (see Figure 6.3).
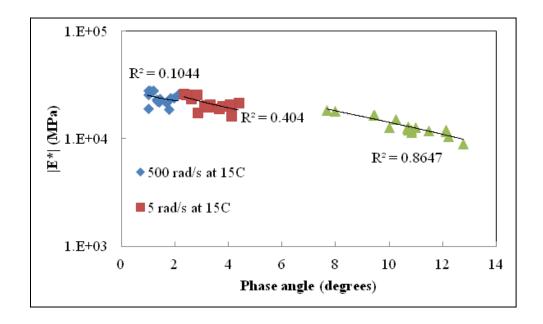
Figure 6.3: Pooled Fund mixture Black Space, measured at TSRST failure temperature (Mensching et al., 2015)

The results showed that separation in Black Space is more prevalent as the reduced frequency approaches the inflection frequency, where aggregate properties begin to have a larger influence over the response due to viscous flow of the binder. Figure 6.4 shows the inflection point for a typical mixture.
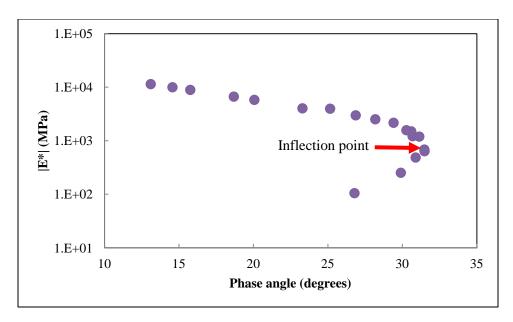
Figure 6.4: Typical Black Space curve with inflection frequency highlighted

In this section, a frequency range is chosen based on analysis of thermal stress and relaxation modulus (E(t)) development in the time domain during typical field cooling events (Mensching et al., 2014). The reference temperature of the material master curves was held at 15°C, which allows for easier manipulation of the data through use of the time-temperature superposition principle (TTSP). The TTSP can be used to shift data along a reduced time (or frequency) axis through use of a shift factor function. The modeled response is assumed to be in the linear viscoelastic region to allow the TTSP to be valid for the analysis. This allows for either the temperature or frequency to be arbitrarily chosen, as a researcher can shift the response along the reduced frequency axis to obtain the properties at any temperature. This was important for the determination of the Glover-Rowe binder parameter as the optimum temperature-frequency combination could then be shifted to points that are easily measured experimentally.

In obtaining the dynamic modulus master curve for the Pooled Fund materials, the test data was fit to the modified Kaelble shift factor function and the Richards sigmoidal function to predict dynamic modulus along the reduced frequency axis. Recall reduced frequency is simply the

actual frequency (i.e., 10 Hz) multiplied by the time-temperature shift factor (a_T) to convert to the reference temperature. Equations 6.2-6.4 display the modified Kaelble, the Richards curve function and its differential (to obtain phase angle), respectively, which were executed by Abatech, Inc.'s RHEA software (Kaelble, 1985; Richards, 1959; Rowe, 2009).

$$\log a_T = -C_1 \left(\frac{T-T_d}{C_2 + |T-T_d|} - \frac{T_R-T_d}{C_2 + |T_R-T_d|} \right) \qquad [6.2]$$

$$\log |E^*| = \delta + \frac{\alpha}{[1+\lambda e^{\beta + \gamma \log(\omega)}]^{1/\lambda}} \qquad [6.3]$$

$$\delta(\omega) = 90\alpha\gamma \frac{\alpha}{[1+\lambda e^{\beta + \gamma \log(\omega)}]^{(1+\frac{1}{\lambda})}} \qquad [6.4]$$

where,

a_T	=	time-temperature shift factor;
C_1, C_2	=	Kaelble fit parameters;
T	=	temperature;
T_d	=	defining temperature;
T_R	=	reference temperature (15°C);
$|E^*|$	=	dynamic modulus;
$\delta, \alpha, \beta, \lambda, \gamma$	=	fit coefficients;
ω	=	angular frequency;
$\delta(\omega)$	=	phase angle.

For the LTPP materials, the mixtures were tested using a resilient modulus protocol at 4, 25, and 40°C and converted to the Verhulst (or standard logistic) function to estimate |E*| using an artificial neural network. The shift factor function was originally described using the polynomial

150

method (Kim et al., 2011). Equations 6.5 and 6.6 provide the form of the Verhulst and shift factor functions. However, for ease in analysis, the predicted |E*| for the LTPP sections were fit to the Richards and modified-Kaelble equations to attain consistency throughout the manipulations.

$$\log|E^*| = \delta + \frac{\alpha}{1+e^{\beta+\gamma\log(\xi)}} \qquad [6.5]$$

$$loga_T = a_1 T^2 + a_2 T + a_3 \qquad [6.6]$$

where,

$|E^*|$ = dynamic modulus;

$\delta, \alpha, \beta, \gamma$ = fit coefficients;

ξ = reduced time $= \dfrac{t}{a_T}$;

a_T = time-temperature shift factor;

a_1, a_2, a_3 = shift factor coefficients;

T = temperature.

To model the thermal stress in the mixture, the Boltzmann superposition principle is utilized over the duration of the event. Equation 6.7 presents the convolution integral form of this principle.

$$\sigma = \int_0^t E(t-\tau)\frac{\partial\epsilon}{\partial\tau}d\tau \qquad [6.7]$$

where,

σ = stress;

t   =   time;

$E(t - \tau)$ =   relaxation modulus;

$\dfrac{\partial \epsilon}{\partial \tau}$ =   change in strain over time step;

$d\tau$ =   integration variable.

To obtain the relaxation modulus, one of several techniques for the interconversion can be executed. In this work, the Prony (or Dirichlet) series of decaying exponentials is used for its robustness and general simplicity in calculation. It has also been found that the Prony series applies to a wide range of linear viscoelastic conditions and has a physical meaning in terms of the generalized Voigt (for creep compliance) and generalized Maxwell or Wiechert (for relaxation modulus) mechanical models (Kim, 2009). Equation 6.8 represents the generalized Maxwell formulation of the Prony series.

$$E(t) = E_\infty + \sum_{i=1}^{m} E_i e^{\frac{t}{\rho_i}} \qquad\qquad [6.8]$$

where,

$E(t)$ =   relaxation modulus;

E_∞ =   equilibrium (long-time) modulus;

E_i =   relaxation strength;

ρ_i =   relaxation time;

t =   time.

While several methods to fit the Prony coefficients exist, the data presented in this work are fit by the method outlined by Baumgaertel and Winter (1989). The method centers on nonlinear regression where not only the Prony coefficients, but also the number of elements in the generalized Maxwell model, are optimized. The accuracy of the method depends on the quality of the mechanical data being input. For the mixtures in this work, the number of relaxation times (and strengths) varies from 9 to 19 modes.

In terms of the strain development, a one-dimensional, linear thermal strain is assumed which is based on the coefficient of thermal contraction (CTC). To calculate the CTC, an equation developed initially by Jones et al. (1968) is utilized (Equation 6.9). Thus, the thermal strain simply becomes the product of the CTC, cooling rate, and the physical time.

$$CTC = \frac{VMA*B_{ac}+V_{agg}*B_{agg}}{3V_{tot}} \quad\quad\quad [6.9]$$

where,

CTC = coefficient of thermal contraction (1/°C);

VMA = percent voids in mineral aggregate;

B_{ac} = volumetric coefficient of thermal contraction of asphalt cement in solid state = 3.45E-04/°C;

V_{agg} = percent aggregate by volume of mixture;

B_{agg} = volumetric coefficient of thermal contraction of aggregate = 1E-06/°C;

V_{tot} = percent of total volume = 100.

In a simplification of the Boltzmann superposition principle, the finite difference put forth by Soules et al. (1987) is used and shown in Equation 6.10. Due to the time-varying temperature observed during a cooling event, the shift factor function (modified-Kaelble) must be integrated with respect to time (Equation 6.11). This is used to describe the change in reduced time in the thermal stress derivation (Alavi, 2014).

$$\sigma_{TH}(t) = \sum_{i=1}^{m} e^{\frac{-\Delta\xi}{\rho_i}} \sigma_i(t - \Delta t) + \Delta\varepsilon E_i \frac{\rho_i}{\Delta\xi}(1 - e^{\frac{-\Delta\xi}{\rho_i}}) \qquad [6.10]$$

$$\xi = \int_0^t \frac{1}{a_T} d\tau \qquad [6.11]$$

where,

$\sigma_{TH}(t)$ = thermal stress at time t;

$\Delta\xi$ = change in reduced time from time $(t - \Delta t)$ to t;

Δt = time step;

$\sigma_i(t - \Delta t)$ = thermal stress component at time $(t - \Delta t)$;

$\Delta\varepsilon$ = change in thermal strain from time $(t - \Delta t)$ to t;

E_i = relaxation strength from Prony series fit;

ρ_i = relaxation time from Prony series fit;

a_T = time-temperature shift factor;

$d\tau$ = integration variable.

6.4.1 Thermal Stress Development and Separation of Relaxation Moduli

Once the relaxation spectra and strain development approach is known, the thermal stress and E(t) curves can be found. Using the pavement temperature data from Mensching et al. (2014), three cooling event scenarios were generated. The details are presented graphically in Figure 6.5 and Table 6.5 as an inset. The cooling events relate to the most drastic average event from the three New England locations, the most drastic scenario using data one standard deviation (stdev) from the mean, and the most drastic scenario using data two standard deviations from the mean. Cooling continued for 7 hours at the constant rate, which is consistent with the duration of the more severe daily cooling found in pavements during a New England winter.

Table 6.5: Cooling event details

Cooling Event Type	Starting Temperature (°C)	Cooling Rate (°C/h)
Normal (mean)	0.0	2.0
Serious (mean + 1 stdev)	-6.0	3.8
Extreme (mean + 2 stdev)	-11.7	5.5
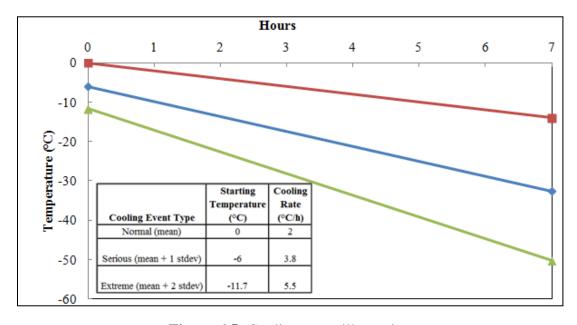
Figure 6.5: Cooling event illustration

6.4.1.1 Pooled Fund Mixtures

The first indicators of the potential for decreased crack susceptibility are the magnitude of the thermal stress and its rate of increase. From the thermal stress curves, the New York PG 64-22 mixtures exhibit the four highest stress values, with the 40% RAP material showing the highest stress overall. Consistent with expectation, the virgin Vermont PG 52-34 mixture produces the lowest thermal stresses due to a soft binder grade that is supposed to supply additional relaxation capabilities. However, it is interesting to see that the virgin NH PG 64-28 mixture experiences similar thermal stresses to the virgin Vermont PG 52-34 material at the "normal" cooling event.

The curves also show that as RAP content increases, the thermal stress increases which is expected due to the notion that as materials age the relaxation capabilities decrease. Therefore, when mixtures have higher percentages of RAP (an aged material) present, the E(t) should be higher than for a material with less aged material.

Note that the rank of the mixtures (i.e., from highest stress/modulus to lowest at a given temperature/reduced time) are not the same – this could be attributed to the strain development scheme or the rate of change (in log-log space) of the E(t) master curve, which is commonly referred to as the m-value. Table 6.6 presents the CTC for each mixture, with Figure 6.6 displaying the m-value at the beginning, middle, and end of thermal loading. These details should give insight into ranking discrepancies between Figures 6.7 and 6.8, which show the thermal stress and relaxation modulus curves, respectively. A lower m-value indicates a smaller change in the relaxation modulus with time (or temperature). At the "Severe" and "Extreme" cooling event, the m-value appears to experience little change from the mid-point to the end of loading. This could be attributed to a response that approaches glassy conditions at very low

temperatures. If the relaxation modulus is not decreasing at a sufficient rate based on the characteristics of the cooling event, the material will be prone to cracking due to rapidly increasing thermal stress. This may also be the reason for the small changes in m-value at the more extreme cooling rates and not for the "Normal" condition.

Table 6.6: Listing of coefficients of thermal contraction for Pooled Fund mixtures

Mix	CTC (1/°C)
NHe00	1.74E-05
NHe20	1.70E-05
NHe30	1.68E-05
NHe40	1.70E-05
NYb30	1.60E-05
NYd00	1.48E-05
NYd20	1.65E-05
NYd30	1.52E-05
NYd40	1.47E-05
VTa00	2.35E-05
VTa20	2.19E-05
VTa30	2.06E-05
VTa40	2.10E-05
VTe00	2.36E-05
VTe20	2.18E-05
VTe30	2.22E-05
VTe40	2.12E-05

After identifying the portion of the relaxation modulus master curve associated with the three cooling events, the targeted reduced time range can be selected to convert to |E*|. These |E*| values will then be adjusted to allow for a common temperature-frequency test combination to be chosen for Black Space analysis. The approach for selecting the |E*| evaluation point involves assessing the range (separation) of relaxation modulus with respect to time over the 17 mixtures. It is believed that the range of relaxation modulus values will lend insight into performance of the materials. For instance, the stiffest mixture (highest relaxation modulus) may mean that the

stress buildup cannot be resisted fast enough and will crack sooner or more often. The opposite could be true for the softest (lowest relaxation modulus) mixture. Figure 6.9 provides a schematic of the E(t) separation concept.
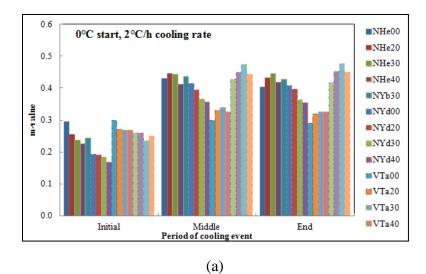
For each temperature point during the thermal event, the difference in log-log space between the stiffest (NYd40) and softest (VTa00) material was monitored. Three criteria were chosen for further investigation: the reduced time where the change in log-log difference of E(t) separation (Equation 6.12) equals 1E-03 MPa, 1E-04 MPa, and the point of maximum E(t) separation.

$$\Delta E(t) \, separation = \left(logE(t)_{stiff} - logE(t)_{soft}\right)_{t} - \left(logE(t)_{stiff} - logE(t)_{soft}\right)_{t-1} \quad [6.12]$$

where,

$E(t)_{stiff}$ = relaxation modulus at time t for stiffest mixture in evaluation group;

$E(t)_{soft}$ = relaxation modulus at time t for softest mixture in evaluation group.

Since the reduced time for each mixture is different at a particular temperature (due to the shift factor function), the reduced time associated with the VTa00 and NYd40 responses were averaged and are displayed in Table 6.7. As the cooling condition becomes more extreme, reduced time values are smaller (corresponding to colder temperatures). This causes a shift down the reduced time axis for the three criteria.

(a)

(b)

(c)
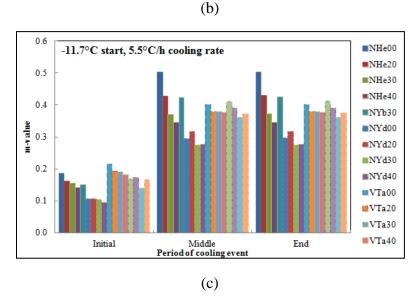
Figure 6.6: Plot of m-values for Pooled Fund mixtures for (a) normal, (b) serious, and (c) extreme New England cooling event
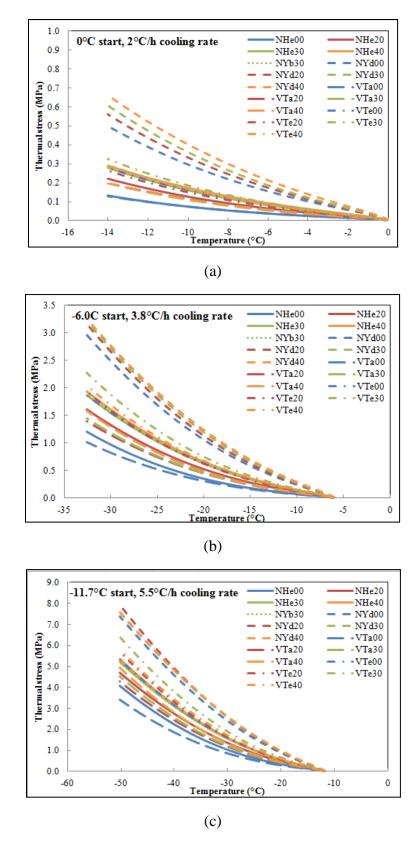
Figure 6.7: Thermal stress curves for Pooled Fund mixtures for (a) normal, (b) serious, and (c) extreme New England cooling event

160

(a)

(b)

(c)
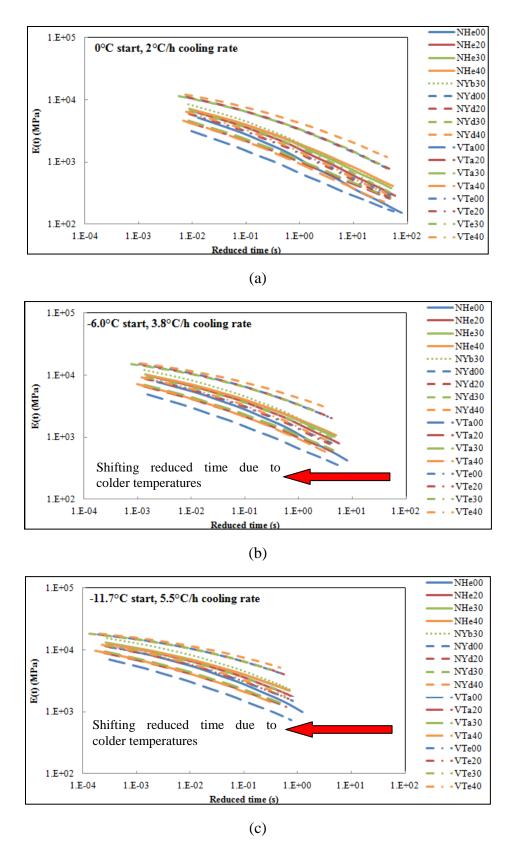
Figure 6.8: Relaxation modulus master curve (at reference temperature of 15°C) for (a) normal, (b) serious, and (c) extreme New England cooling event

161
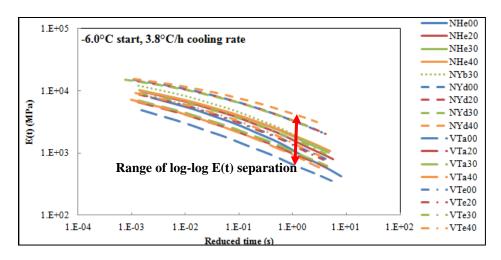
Figure 6.9: Schematic of log-log E(t) separation concept

Table 6.7: Reduced time evaluation points for Pooled Fund mixtures

Cooling event type	Change in log-log separation of 1E-03 MPa (s)	Change in log-log separation of 1E-04 MPa (s)	Maximum separation (s)
Normal	1	5	9
Serious	0.2	1	5
Extreme	0.04	0.2	0.5

For each of the reduced time targets, the angular frequency (Equation 6.13) is found using the approximate conversion used in several studies (Christensen, 2003; Schapery and Park, 1999; Underwood, Sakhaei Far, and Kim, 2010). The corresponding frequency was used to calculate the storage and loss moduli, with |E*| simply being the magnitude in vector space. The Prony representations for the storage and loss moduli are shown in Equations 6.14 and 6.15, respectively. The phase angle is found using Equation 6.4.

$$\omega_R = \frac{2}{\pi \xi} \qquad [6.13]$$

$$E'(\omega) = E_\infty + \sum_{i=1}^{m} \frac{\omega_i^2 \rho_i^2 E_i}{\omega_i^2 \rho_i^2 + 1} \qquad [6.14]$$

$$E''(\omega) = \sum_{i=1}^{m} \frac{E_i \omega_i \rho_i}{\omega_i^2 \rho_i^2 + 1} \qquad [6.15]$$

where,

162

ω_R = reduced angular frequency (rad/s);

ξ = reduced time (s);

$E'(\omega)$ = storage modulus;

$E''(\omega)$ = loss modulus;

E_∞ = equilibrium (long-time) modulus;

E_i = relaxation strength;

ρ_i = relaxation time;

ω_i = angular frequency (rad/s).

The |E*| converted from the E(t)-reduced time combination in Table 6.7 is brought to a measured temperature-frequency combination by calculating the distance in vector space between the converted point and the measured test point. This concept is illustrated in Figure 6.10.

In determining the optimum evaluation point, a decision hierarchy was utilized. Due to the very high thermal stresses generated from the "Extreme" event, the data was not analyzed further since every mixture failed compared to available performance data. Therefore, it is impossible to distinguish satisfactory performance from poor performance. For the "Serious" event, the most desirable separation rule is the maximum separation, which corresponds to approximately 5 seconds reduced time. This reduced time is most consistently captured by the 20°C-1 Hz |E*| point.
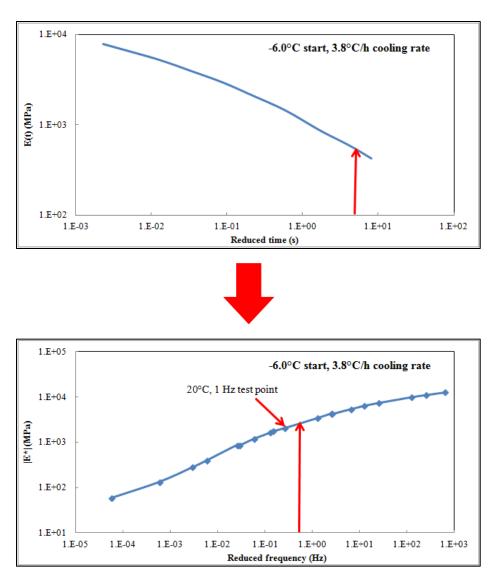
Figure 6.10: Schematic of approach to define target |E*| temperature-frequency combination

Table 6.8 provides the converted |E*| and phase angle point with the corresponding measured |E*| and phase angle for the 20°C-1 Hz condition. By inspection, the desired point (converted) Black Space locations are close in proximity to the available measured data points.

Table 6.8: Dynamic modulus and phase angle data for the 20°C-1 Hz evaluation condition

Mix	Converted |E*| (MPa)	Converted phase angle (degrees)	Measured |E*| (MPa)	Measured phase angle (degrees)	Distance in Black Space
NHe00	2590.4	30.09	2067.7	31.07	522.7
NHe20	3365.5	26.94	2720.1	28.80	645.3
NHe30	3674.5	25.30	2929.7	28.18	744.8
NHe40	3710.7	24.99	2922.5	27.93	788.2
NYb30	4232.2	26.98	3360.4	29.26	871.8
NYd00	6003.4	23.03	4725.3	26.56	1278.1
NYd20	6063.5	23.07	4890.2	25.76	1173.3
NYd30	5916.3	22.07	4735.8	25.92	1180.5
NYd40	7028.7	20.47	5790.0	23.19	1238.7
VTa00	1405.9	29.67	1063.3	31.03	342.6
VTa20	2014.6	27.63	1548.3	29.52	466.3
VTa30	2170.7	27.49	1668.3	29.55	502.4
VTa40	1943.6	29.22	1493.4	30.61	450.3
VTe00	2889.6	27.00	2287.3	29.78	602.3
VTe20	2831.5	27.08	2244.5	30.08	587.0
VTe30	3331.8	26.59	2618.2	28.25	713.6
VTe40	3021.6	27.00	2334.8	30.04	686.8

6.4.1.2 LTPP sites

Using the LTPP sites, the same graphs can be generated to describe the thermal stress development and relaxation modulus throughout the specified cooling events. Table 6.9 shows the CTC values for the LTPP mixtures, with Figure 6.11 showing the m-values at the beginning, middle, and end of the cooling events. NH1001 and CT5001 having the lowest m-values among the LTPP sites, which is an indicator of a material's inability to relax under increasing stress. The same general trends (i.e., small changes from middle to end of the event) observed in the Pooled Fund mixtures are consistent with the LTPP mixtures.
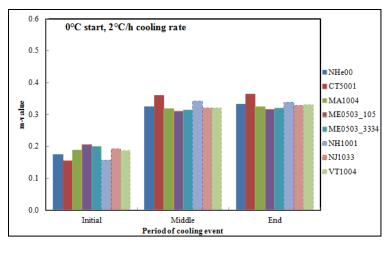
As confirmed by Figures 6.12 and 6.13, the NH1001 and CT5001 projects generate the most thermal stress and largest E(t) values throughout the cooling event. The other six projects do not show the same degree of separation from each other as these two projects. For the NH1001

project, the pavement sampling was conducted after 17 years in service, so a stiffer condition is expected due to aging influences. However, the degree of stiffening due to aging cannot be assessed since data for the newly constructed condition is not available.
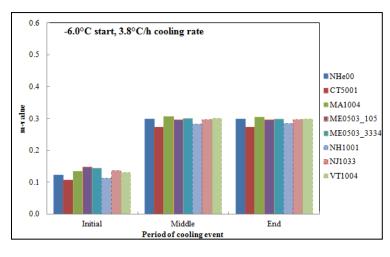
Table 6.9: Listing of coefficients of thermal contraction for LTPP mixtures

Mix	CTC (1/°C)
CT0902	1.68E-05
CT5001	1.64E-05
MA1004	1.64E-05
ME0503_105	1.75E-05
ME0503_3334	1.75E-05
NH1001	2.06E-05
NJ1033	1.68E-05
VT1004	1.73E-05

As was done for the Pooled Fund mixtures, three rules were specified for determining the Black Space evaluation point. As Table 6.10 shows, the more extreme the cooling event, the lower critical reduced time values which correspond to the E(t) separation criteria. The most consistently occurring temperature-frequency combination with the smallest distance from the reduced time target was the 20°C-0.5 Hz measurement, which most closely corresponds to the 1 second reduced time location. It also corresponds to the maximum E(t) separation for the "Serious" event, which is most desirable for analysis. Recall the separation and change in relaxation modulus with time is thought to have performance ramifications and help distinguish the differences between satisfactory and poor performing mixtures. Table 6.11 provides the converted |E*| and phase angle point with the corresponding measured |E*| and phase angle for the 20°C-0.5 Hz condition.

(a)

(b)

(c)
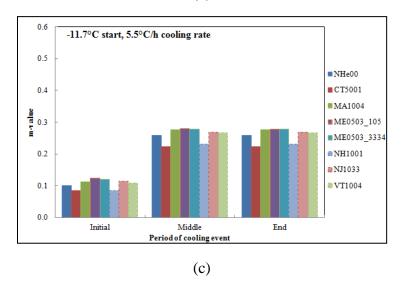
Figure 6.11: Plot of m-values for LTPP mixtures for (a) normal, (b) serious, and (c) extreme New England cooling event

167

(a)

(b)

(c)
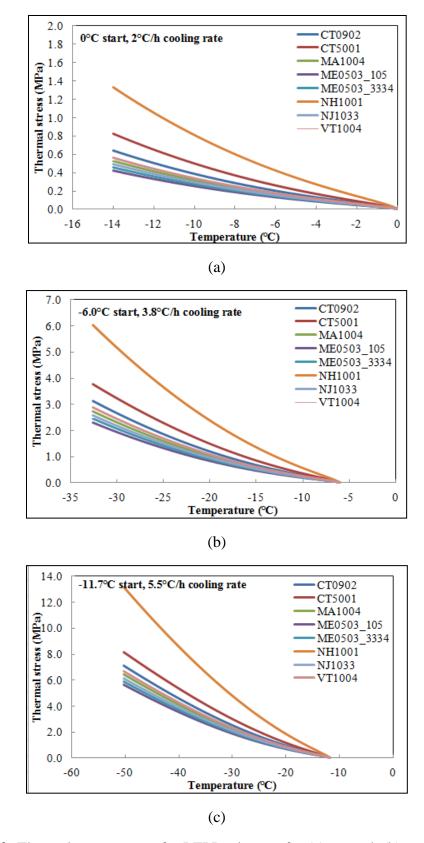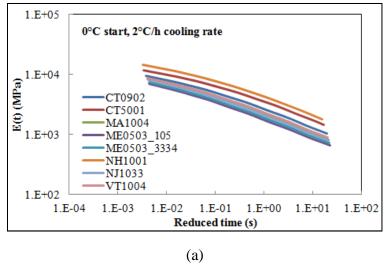
Figure 6.12: Thermal stress curves for LTPP mixtures for (a) normal, (b) serious, and (c) extreme New England cooling event

168

(a)

(b)

(c)
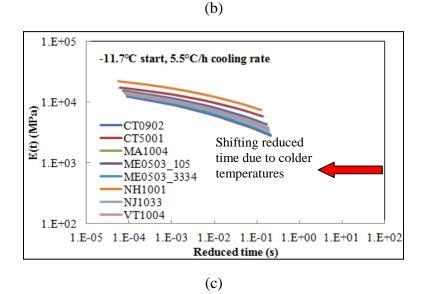
Figure 6.13: LTPP relaxation modulus master curves (at reference temperature of 15°C for (a) normal, (b) serious, and (c) extreme New England cooling event

169

Table 6.10: Reduced time evaluation points for LTPP mixtures

Cooling event type	Change in log-log separation of 1E-03 MPa (s)	Change in log-log separation of 1E-04 MPa (s)	Maximum separation (s)
Normal	0.2	1	7
Serious	0.03	0.2	1
Extreme	0.04	0.03	0.2

Table 6.11: Dynamic modulus and phase angle data for the 20°C-0.5 Hz evaluation condition

Mix	Converted |E*| (MPa)	Converted phase angle (degrees)	Measured |E*| (MPa)	Measured phase angle (degrees)	Distance in Black Space
CT0902	3000.0	25.25	2992.5	23.81	7.6
CT5001	3965.1	24.64	3977.4	22.03	12.6
MA1004	2470.0	25.89	2453.9	24.87	16.2
ME0503_105	2012.3	26.20	1978.9	25.82	33.5
ME0503_3334	2151.0	26.14	2123.0	25.53	27.9
NH1001	4751.6	24.58	4713.1	20.84	38.7
NJ1033	2403.3	25.92	2371.8	25.06	31.5
VT1004	2634.6	25.69	2612.5	24.58	22.1

6.5 Using Black Space for Performance Indication

In the previous section, a process was described to determine a Black Space evaluation point. Ideally, this |E*| and δ combination at 20°C-1 Hz for the Pooled Fund materials and 20°C-0.5 Hz for the LTPP mixtures will provide enough separation to distinguish poor performers from satisfactory performers. In the case of the Pooled Fund materials, the materials are plant-produced, laboratory-reheated with a set protocol as published in Mogawer et al. (2012) and Mensching et al. (2014) to reduce effects on performance and material properties. However, the LTPP materials are field samples and are exposed not only to short-term aging throughout production, but also to field aging of varying degrees (see Table 6.3). The reader should keep this in mind when comparing the effectiveness of the Pooled Fund and LTPP mixtures in Black Space.

Figures 6.14 and 6.15 show the Black Space plots for the Pooled Fund and LTPP materials with the range of |E*| and δ at 20°C-1 Hz and 20°C-0.5 Hz highlighted. The stiffness range is about 1063-5790 MPa and 1978-4713 MPa for Pooled Fund and LTPP mixtures, respectively. The phase angle ranges from 23-31° for the Pooled Fund mixtures and 20-26° for LTPP mixtures.

The range in Black Space alone cannot provide sufficient details for agencies without some performance variable to compare with the stiffness-relaxation (|E*|-δ). For the Pooled Fund mixtures, the thermal stress at the end of the "Normal" and "Serious" cooling events are compared with the IDT low temperature strength and TSRST in Figures 6.16 and 6.17, respectively.

Recall the "Extreme" condition is not shown since every mixture failed. In the "Serious" event, the NYd20, NYd30, and NYd40 materials fail when compared to the TSRST strength (end stress greater than strength). The NYd00 mixture was not tested in TSRST due to a lack of available material, but it can be inferred that the mixture is probably at risk of failing due to the TSRST strengths of the other NYd materials. The NHe40 mixture appears to be at risk for failing when comparing the end stress during the "Serious" event and the TSRST strength. No mixture is at risk of failure during the "Normal" cooling event, which is defined by typical New England conditions. It is important to consider that there is a distribution of temperatures, cooling rates, and cooling times that ultimately cause cracks. It is thought that observed field cracking that may occur in these mixtures is related to periods where the cooling conditions do not follow the assumptions made in this paper.

Using the performance information below, the separation in Black Space can be assessed with respect to poor performers and satisfactory performers. In Figure 6.18, there is clear separation

171

among the NYd mixtures, all of which have failed or are considered at-risk during the "Serious" event. It is promising that the point next-closest to the failure line, but ultimately bundled with the satisfactory performers, is the NHe40 mixture. Previously, this material was identified as at-risk due to the small difference between the TSRST strength and the end stress value. There is also a considerable amount of separation between the NYd40 and NYd20 materials in Black Space (distance of 900), although the stress-strength comparisons do not correlate with the large difference. It is also worth noting that this temperature-frequency combination is near the inflection point frequency for the NH and VT mixtures especially (Figure 6.14).

From the Figure 6.18, a failure line region could be identified. A parameter would be needed to define the line throughout a range of |E*| and δ values, similar to the Glover-Rowe failure line. One approach is to use a measure that can help to quantify a material's ability to dissipate energy, which is considered by many to be related to crack susceptibility of asphalt materials. Four parameters were evaluated briefly with the TSRST strength in an attempt to identify a failure line: storage and loss moduli, |E*|tan δ, and a modified Glover-Rowe parameter (replacing the G* and binder δ with |E*| and mixture δ). If there is a high degree of correlation among two parameters, this could aid in the determination of a failure line, similar to the role the binder ductility test played in the development of the Glover parameter (Glover et al., 2005). There was no clear relationship between TSRST strength and these parameters. While there was no clear trend in the available data compared to the four |E*|-δ related parameters, the proposed failure line should ultimately move in a pattern that generally goes from bottom-left corner of the Black Space plot to top-right to follow the expectation that as |E*| increases and δ decreases, the material is more prone to cracking.

(a)

(b)

(c)
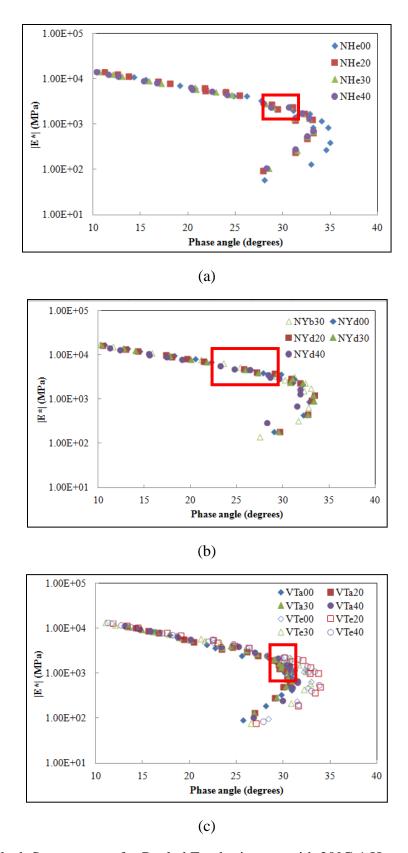
Figure 6.14: Black Space curves for Pooled Fund mixtures with 20°C-1 Hz region highlighted

173
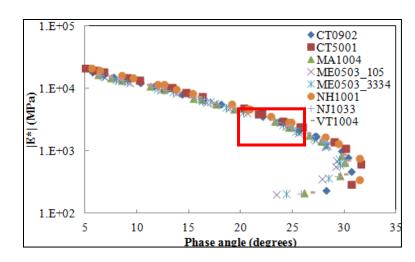
Figure 6.15: Black Space curves for LTPP mixtures with 20°C-0.5 Hz region highlighted
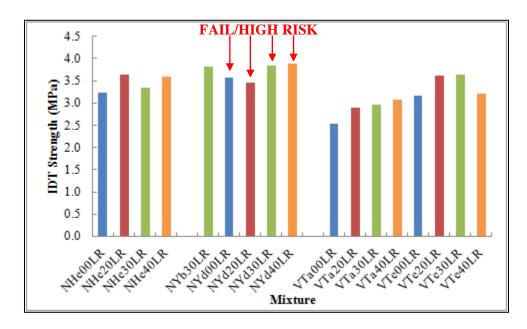
Figure 6.16: Pooled Fund strength values measured in IDT mode

174
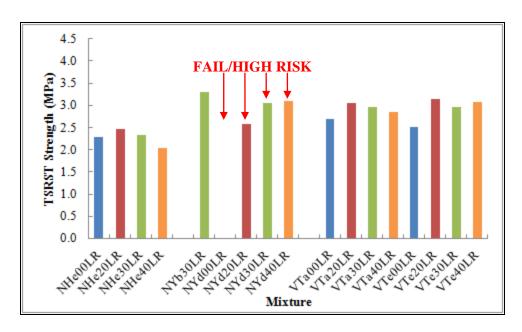
Figure 6.17: Pooled Fund strength values measured in TSRST mode
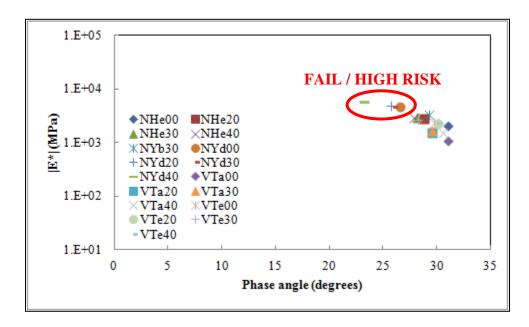
Figure 6.18: Black Space for Pooled Fund mixtures at 20°C-1 Hz condition

Based on the information from Table 6.3, the NJ1033 and VT1004 projects are the poorest performing pavements, while the ME0503 and MA1004 pavements did not crack over the 9 years of data available. Figure 6.19 shows the Black Space points at the 20°C-0.5 Hz test measurement. The NH1001 material produces the largest |E*| and lowest phase angle, but is also

175

the most aged mixture (17 years of service). Field survey data shows that the NH1001 section has experienced significant cracking by year 16 of service. The CT5001 is closest to the NH1001 material, but the survey and sample dates are taken at Year 0 of service with no observed cracking. The Black Space curve is able to capture the expected trend with the ME0503 materials (no field cracking) at the 105 day (Year 0) and 3,334 day (Year 9) conditions. The NJ1033 section is the worst performing mixture, but there is little separation in Black Space from it and the ME0503 and MA1004 mixtures, which did not crack. These differences could be attributed to climate differences (i.e., increased snowfall, coastal effects), testing and sampling variability, production and aging variables, or the influence of additives or recycled materials.
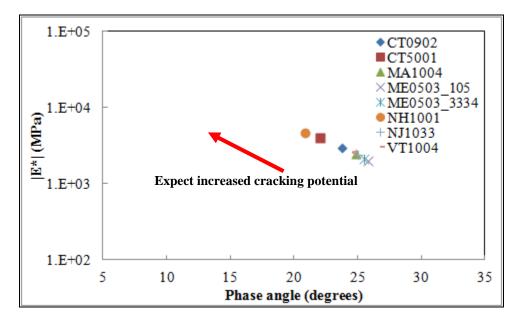
Figure 6.19: Black Space for LTPP mixtures at 20°C-0.5 Hz condition

6.6 Conclusions

In this study, a framework is provided to establish a low temperature analysis method for mixtures in Black Space. Twenty-five mixtures are used, with 17 being from plant-produced, laboratory-reheated specimens and 8 field mixtures from the LTPP database. The framework is

expected to bring value to practice by providing a tool for performance-based mixture design and acceptance of asphalt mixtures. The work done here holds the potential to be the first specification parameter to use strictly Black Space location of the mixture to assess low temperature performance. Based on the results, the following conclusions and recommendations are given:

1. By using a technique centered on separation of relaxation modulus master curves in the reduced time domain, a common temperature-frequency combination can be found to use in Black Space. The point of maximum log-log separation was used to identify 20°C-1 Hz as the optimal temperature-frequency combination for the Pooled Fund mixtures when subjected to a -6.8°C starting temperature and 3.8°C/h cooling rate, which corresponds to a typical New England cooling event which is one standard deviation more extreme than the mean condition. For the LTPP materials, the 20°C-0.5 Hz combination is used, which also corresponds most closely to the point of maximum separation during the same cooling event and happens to occur near the end of the simulation. At this point, the separation rules include a degree of subjectivity in their assignment and physical significance. Future work is needed to analyze the shape of the relaxation modulus master curve to determine more objective decision rules for the temperature-frequency test point selection, perhaps based on sigmoidal coefficient effects on the master curve (Bhattacharjee, Swamy, and Daniel, 2011). It is expected that this approach will work best when using a set of mixtures where stiffness and phase angle differences are not extreme, perhaps on a state-to-state or region-to-region basis. It is recommended that agencies develop a materials

177

catalog and apply the approach to typical mixture designs to determine the optimal test temperature-frequency combination for localized Black Space analysis.

2. The temperature-frequency combination confirms the expectation from an earlier study that phase angle and stiffness values closer to the glassy region do not represent material behavior over the course of a low temperature event, as relaxation modulus decreases resulting in an increase in thermal stress and phase angle and a decrease in $|E^*|$.

3. Of the four Pooled Fund mixtures which definitively failed one of the laboratory tests, there was clear separation in Black Space from the satisfactory performers. The one mixture that was deemed to be at-risk of failure is closer to the anticipated failure line than the other satisfactory performers. For the LTPP mixtures, there is considerable spread and no obvious trend between Black Space location and performance. This could be attributed to discrepancies in sample and survey dates, as well as the spread of aging present over the eight mixtures (0 to 17 years service). The differences in pavement age would make any direct comparisons challenging.

4. Four parameters were considered for definition of a failure line in Black Space: storage modulus, loss modulus, $|E^*|\tan \delta$ and a modified Glover-Rowe expression for mixture. Neither parameter correlated well with the TSRST strength and more data is needed to determine a practical failure line to differentiate poor performing mixtures from satisfactory performance. The parameter should utilize both $|E^*|$ and δ and have the ability to relate to energy dissipation (i.e., $\tan \delta$), as experts in the field deem this property relevant to assessing crack susceptibility. There may be value in calculating fracture energy in future work, which would require some form of thermal strain and

stress measurement, such as the uniaxial thermal stress strain test (UTSST) or the DC(T). Mixtures would be subjected to |E*| testing and a variety of low temperature tests to identify surrogate parameters which could then be related back to Black Space locations through interconversions (preferred) or correlations among available data. The failure line may also rely on the materials catalog to shift in Black Space to best represent the conditions of the construction area. This would require a calibration effort of some kind to ensure the best possible pass/fail indicator.

5. Black Space can be used to capture separation in plant-produced, laboratory-reheated mixtures which were subjected to equal levels of aging. The variation in field aging of LTPP mixtures and the corresponding inability to capture poor performers in Black Space is likely a result of field survey variations or insufficient failure line definition which may be influenced by material type and aging level. It is recommended that multiple sets of material (plant-produced, laboratory-reheated, plant-compacted, field cores) are assessed at varying aging levels, but are compared at similar conditions to help define the failure line and track the materials through Black Space for enhanced understanding of the material behavior. The results of NCHRP 9-58 could especially be of use to this work, as the project focuses on long-term field aging of mixtures. The quantification of field aging on material properties could prove critical in the field implementation of this Black Space parameter. Ongoing field projects can also be used to compare performance to Black Space location, such as those at FHWA's Turner-Fairbank Highway Research Center or Minnesota Department of Transportation's MNROAD facility. At these facilities, a controlled construction is possible, which can alleviate the impact of variability in production and testing on the

material properties. The controlled production being used in Phase III of the TPF 5-230 Pooled Fund Study also lends itself to the future work being recommended. Similar field studies may come about as a result of NCHRP 9-57's findings, as the project team will be developing an experimental design to evaluate low temperature cracking tests. The results of these studies could be of use in determining or refining the failure thresholds in the Black Space-based method.

6. It is recommended the study is also expanded to capture the impact of volumetric variation on Black Space location and performance. By varying mixture design and production variables (i.e., gradation, asphalt content, discharge temperature), conclusions can be drawn that will aid practitioners in the development of a performance-based mixture design and acceptance procedure. Work being done at the Turner-Fairbank Highway Research Center as part of the performance-based mixture design initiative should relate quite well to this recommendation, as voids in mineral aggregate and air voids are being varied for materials produced at the Accelerated Loading Facility (Lee, Gibson, and Kim, 2015).

6.7 Acknowledgements

Massachusetts – Dartmouth for conducting the |E*| and TSRST on the TPF 5(230) mixtures, respectively.

CHAPTER 7

DEVELOPING AN INDICATOR FOR FATIGUE CRACKING IN HOT MIX ASPHALT

PAVEMENTS USING VISCOELASTIC CONTINUUM DAMAGE PRINCIPLES

7.1 Introduction

In the 21st century world, pavement engineers face challenges stemming from increasingly tight budgets and stress from increased congestion and traffic. In most states, the most critical form of asphalt distress comes due to fatigue or repeated loading in bottom-up or top-down states. Fatigue cracking in asphalt pavements result in decreased ride quality, decreased fuel economy, and provides an avenue for intrusion of water, which rapidly deteriorates a pavement system. Federal legislation under the Moving Ahead Progress for the 21st Century Act (MAP-21) places additional emphasis on improving longevity of transportation systems through the need for performance-based design.

In asphalt pavements, design of the mixture is predominantly focused on volumetric optimization – using the best balance between air, asphalt, and aggregate amounts to address permanent deformation (rutting), fatigue, and thermal cracking distress modes. The natural progression then is to design mixtures through material properties and correlations to field performance as opposed to proportioned masses and volumes. The performance-based methodology can then be applied to design as well as production and acceptance, which reinforces its ability to act as a pay factor specification for agencies. This approach to design and acceptance will also be easy to

validate over the course of a pavement's service life and holds potential for increased flexibility from a contractor perspective, as producers can focus on meeting the thresholds set by material property-performance relationships as opposed to many volumetric boundary conditions. This is particularly promising when considering the opportunity to add more recycled and "environmentally friendly" materials to mixture as long as the performance thresholds are met.

In terms of fatigue performance, many models and testing procedures have come about in an attempt to describe the behavior more comprensively. As it relates to performance-based specifications, the semi-circular bending (SCB) test is being used at intermediate temperatures as a tool to establish these performance thresholds in select states (Al-Qadi et al., 2015; Kim et al., 2015; Dukatz, Hanz, and Reinke, 2015). In Louisiana and Wisconsin, a critical fracture energy value from the SCB analysis is being experimented with as a specification, while researchers in Illinois are exploring a flexibility index as a ways to characterize mixture performance for fatigue.

An alternate testing and analysis scheme that shows potential for a performance-based application is the Simplified-Viscoelastic Continuum Damage (S-VECD) model. This constitutive model relates material integrity to an internal state variable of damage and is built upon three primary principles: the elastic-viscoelastic correspondence principle, Schapery's work potential theory to define damage accumulation, and the time-temperature superposition principle (TTSP) with growing damage (Kim and Little, 1990). The primary output is the damage characteristic curve (DCC), which relates pseudostiffness or material integrity (C) and damage (S). Studies have shown that the DCC is a material property independent of loading type, temperature, and frequency (Lee and Kim, 1998a; Daniel and Kim, 2002; Chehab et al., 2003). Recently, the model and testing procedure has been adjusted for use as a direct tension

cyclic test in the Asphalt Mixture Performance Tester (AMPT) (Underwood et al., 2010). The AMPT has been identified as a potential Standard Performance Tester for hot mix asphalt (HMA) and there should be value in coupling this piece of equipment with performance-based methodologies for other major distresses, such as the approach being developed by Mensching et al. (2015) (Witczak, 2005).

Recently, researchers have formulated several parameters to aid in the comparison of performance of asphalt mixtures being subjected to S-VECD analysis through the use of a failure criterion. A failure criterion is required to bring a more objective approach to assessing fatigue resistance of mixtures. Initial attempts relied on a reduction in stiffness by a given percentage, say 50%, to determine the cycles to failure. Reese (1997) used the peak phase angle during cyclic loading, which appeared to correspond to cracking localization (macrocracking). This method is used experimentally in the AASHTO TP107 (2014) protocol for direct tension cyclic testing in the AMPT, but a stiffness-based approach was preferred due to difficulties in measuring true phase angle throughout the test procedure due to distortion of the response due to damage. Hou et al. (2010) used the pseudostiffness at failure (C_f) from the S-VECD analysis to compare fatigue performance of mixtures, but due to high levels of experimental variability, this method was not ideal (Sabouri, 2014). Dissipated energy approaches have also been discussed as possible failure criteria, but the applicability to the S-VECD requires additional considerations, primarily due to the model's inability to capture true phase angle variation. Sabouri and Kim (2014) were able to develop a loading mode-independent failure criterion by using the average rate of dissipated pseudo strain energy per cycle (G^R), which addresses shortcomings of a similar method by Zhang et al. (2013).

184

However, due to the mechanisms governing fatigue cracking, it is critical that the pavement system as a whole is accounted for in any performance rankings or assessments. As the research shows, asphalt pavements behave differently with respect to fatigue based on layer thickness and stiffness (Epps and Monismith, 1969; Huang, 2004; Brown et al., 2009; Mallick and El-Korchi, 2013). Linear elastic structural response models have been developed to determine system characteristics, such as the WinJULEA platform used in the Mechanistic-Empirical Pavement Design Guide (ARA, Inc., 2004). Current research is moving towards linear viscoelastic analysis of multilayer systems, which is believed to be more representative of pavement response under stress and strain (Eslaminia et al., 2012). While the work in this paper focuses on WinJULEA simulations, the direction moving forward will likely follow the most appropriate platform for a state agency. It is possible that an agency is comfortable with the predictions from a linear elastic analysis and may not implement a linear viscoelastic approach. The method outlined in the following sections should be adaptable to either structural response model type and to the controlled strain (thin pavements) and controlled stress (thick pavements) modes of analysis.

A combination of asphalt mixture and pavement system characteristics will allow for a more accurate performance-based approach to design and construction and increase communication between pavement designers and mixture designers. Additionally, if the methodology to relate mixture and pavement structure to classify fatigue performance is simplistic and inexpensive long-term, it brings with it higher chances of being implemented by state and local agencies.

7.2 Objectives

The primary objectives of this paper are outlined below. By addressing these points, a framework will be available for further expansion and refinement with additional materials on a more localized level per state agency. The objectives are to:

1. Relate mixture stiffness, fatigue, and pavement system characteristics together to develop a material space for use in performance-based mixture design;

2. Identify an S-VECD output parameter which produces the most separation among poorly performing structures and satisfactory performing structures when combined with dynamic modulus ($|E^*|$) information;

3. Evaluate the impact of reclaimed asphalt pavement (RAP) on the performance of the material space;

4. Develop an alternate approach to fatigue characterization that requires only use of the AMPT.

7.3 Materials and Testing Methods

The materials used in this study come from two primary sources. Fourteen plant-produced mixtures are used from Phase I of Transportation Pooled Fund Study TPF5-230: Evaluation of Plant-Produced High-Percentage RAP Mixtures in the Northeast. These mixtures underwent a variety of laboratory tests, including dynamic modulus (AASHTO TP79) at 4, 20, and 35°C using frequencies of 25, 10, 5, 1, 0.5, 0.1, and 0.01 (at 35°C only) Hz and direct tension cyclic testing in the AMPT at 25°C (AASHTO 2012i). It is important to note that since the testing was completed in 2012, modifications to the desired testing temperature have been made to the AASHTO TP107 method for direct tension cyclic testing to lessen the potential for viscoplastic

186

effects during the test (AASHTO, 2014). Tables 7.1 and 7.2 detail the mixture properties of the Pooled Fund materials used in this study. Note that one RAP source was used for the NH mixtures, one source for the NY mixtures, and one source for the VT mixtures. The naming convention for the materials is as follows: NH, NY, or VT denotes the production location, a lowercase letter after the state abbreviation indicates the virgin binder grade, and the number indicates the RAP percentage by weight of mixture. For example, NYb30 is a mixture produced in New York with a PG 58-28 virgin binder and 30% RAP by weight of mixture. Note in Table 7.2, the measured binder percentage is found from the extraction procedure, and the RAP percentage by weight of binder was calculated from the design binder content.

In order to simulate a pavement structure representing local conditions, a cross-section located in New York was selected from the Long-Term Pavement Performance database. Since many of the Pooled Fund materials were not placed in the field, two simulated pavement structures (thick and thin HMA layers) are developed later on in this paper.

Table 7.1: Continuous PG grades and mixture gradations

Mix	Virgin Continuous PG Grade	Percent Passing									
		19.0	12.5	9.5	#4	#8	#16	#30	#50	#100	#200
NHe00	66.3-29.7	100	99	86	58	43	32	25	16	7	3.6
NH RAP	85.5-13.2	100	100	98	74	56	44	33	22	12	7.4
NYb30	61.0-34.6	100	97.5	91	60	33	21	15	10	6	5.3
NYd00	67.0-25.5	100	100	91	68	42	27	19	13	5	3.8
NYd20		100	99	91	59	31	19	12	8	7	3.8
NYd30		100	95	86	54	30	23	17	12	8	6.0
NYd40		100	98	89	53	31	19	14	10	6	4.3
NY RAP	87.2-19.9	100	98	93	66	47	32	22	13	7	4.5
VTa00	56.3-32.5	100	100	99	79	51	31	19	11	6	3.8
VTa20		100	100	98	79	51	31	19	12	7	4.6
VTa30		100	100	99	75	48	30	19	12	7	4.5
VTa40		100	100	98	77	49	29	18	12	8	4.6
VTe00	64.4-30.2	100	100	100	77	49	30	18	10	6	3.3
VTe20		100	100	99	81	54	32	20	12	7	4.3
VTe30		100	100	98	78	49	29	18	11	7	4.3
VTe40		100	100	99	75	47	27	16	9	5	4.5
VT RAP	73.8-25.2	100	99	90	72	52	36	24	16	11	8.3

Table 7.2: Mixture design and production information

Mix	Nominal Maximum Aggregate Size (NMAS) (mm)	% Total Binder (design/ measured)	% RAP by weight of mix/by weight of binder	RAP Binder Content (%)	Voids in Mineral Aggregate (VMA)	Voids Filled with Asphalt (VFA)	Aggregate Temp. (ºC)	Discharge Temp. (ºC)	Compaction Temp. (ºC)	Silo Storage Time (h)
NHe00	12.5	5.7/5.8	0/0	--	14.9	74.8	n/a	165.6	148.9	6.00
NYb30		5.2/5.0	30.0/28.4	4.93	13.7	81.1	210.0	151.7	135.0	3.50
NYd00		5.2/5.0	0/0	--	12.6	89.3	191.0	154.4	143.3	2.75
NYd20	12.5	5.2/5.2	20.0/19.0	4.95	14.1	79.9	210.0	160.0	143.3	0.75
NYd30		5.2/5.5	30.0/28.4	4.93	13.0	85.1	210.0	151.7	143.3	2.75
NYd40		5.2/5.1	40.0/37.7	4.90	12.5	87.9	232.0	165.6	143.3	3.00
VTa00		6.7/6.3	0/0	--	20.2	76.3		171.1	171.1	
VTa20		6.8/6.2	20.0/15.9	5.41	18.8	81.9		162.2	162.2	
VTa30		6.6/6.2	30.0/24.6	5.41	17.7	82.5		160.0	160.0	
VTa40	9.5	6.6/6.3	40.0/32.8	5.41	18.0	77.8	n/a	148.9	146.1	n/a
VTe00		6.5/6.6	0/0	--	20.3	71.5		165.6	148.9	
VTe20		6.7/6.3	20.0/16.1	5.41	18.7	79.7		148.9	148.9	
VTe30		6.6/6.1	30.0/24.6	5.41	19.1	75.9		161.1	154.4	
VTe40		6.6/6.1	40.0/32.8	5.41	18.2	76.4		146.1	146.1	

7.4 Experimental Approach

This section outlines the details for simulation of pavement structures, as well as a discussion on linear viscoelastic characterization (through |E*| master curves) and targeted fatigue parameters for the material space which holds potential for a performance-based mixture design and acceptance tool.

7.4.1 Pavement Structure Simulation

As mentioned previously, a LTPP project cross-section from Orleans County, New York was selected to model a base and subgrade layer for simulation. This project was selected due in part to the availability of resilient modulus data for input into WinJULEA and its relatively simplistic structure. Figure 7.1 details the pavement structures used in this paper.

76 or 203 mm (3 or 8 inch) ← HMA

203 mm (8 inch) ← Crushed gravel subbase (M_R = 193 MPa)

← Silty sand subgrade (M_R = 55 MPa)
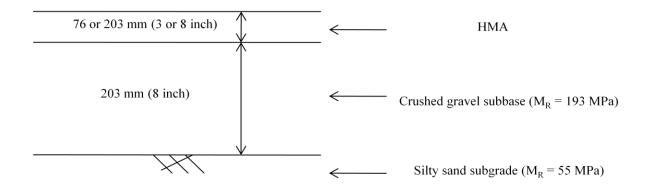
Figure 7.1: Simulated pavement cross-section

With the pavement thicknesses and moduli of the underlying layers defined, the asphalt modulus must be characterized. In this study, the Odemark transformation method is used to calculate an effective depth which corresponds to the thickness needed should the layer be represented only by the subgrade modulus. Equation 7.1 below provides the form of the Odemark transformation used in this paper, where the point of calculation is at the midpoint of a sublayer. The

sublayering technique follows the method used in the NCHRP 1-37A final report for a 76 mm lift (12.7-12.7-25.4-25.4 mm thicknesses) and a 203 mm lift (12.7-12.7-25.4-25.4-25.4-101.6 mm thicknesses).

$$Z_{eff} = \sum_{i=1}^{n-1} h_i \sqrt[3]{\frac{E_i}{E_{SG}}} + \frac{h_n}{2} \sqrt[3]{\frac{E_n}{E_{SG}}}$$ [7.1]

where,

Z_{eff} = effective depth;

h_i = thickness of sublayer i;

E_i = modulus of sublayer i;

E_{SG} = modulus of subgrade;

h_n = thickness of sublayer n;

E_n = modulus of sublayer n.

The effective depth is then used to calculate the effective length (L_{eff}) of the load pulse, which is assumed to have a stress zone protruding through the pavement structure at an angle of 45°. The L_{eff} is represented by two times the sum of the tire contact radius and Z_{eff}. The L_{eff} is then needed to calculate the loading time which can then be converted to loading frequency (in Hz). The loading frequency can be found using Equation 7.2 (Fugro Consultants and Arizona State University, 2011). Please note the calculations were done in Imperial units and converted to metric for the preparation of results.

$$f = 17.6 \left(\frac{v}{L_{eff}} \right)$$ [7.2]

where,

f = loading frequency (Hz);

v = velocity (mph).

With the frequency known, the effective temperature (T_{eff}) can be found to allow the user to determine the appropriate |E*| of the asphalt sublayer. The model for T_{eff} was refined in NCHRP Report 704 and is shown in Equation 7.3 (Fugro Consultants and Arizona State University, 2011).

$$T_{eff} = -13.995 - 2.332\sqrt{f} + 1.006MAAT + 0.876\sigma MAAT - 1.186Wind +$$
$$0.549Sunshine + 0.071Rain \qquad [7.3]$$

where,

$MAAT$ = mean annual air temperature (°F);

$\sigma MAAT$ = standard deviation of mean annual air temperature (°F);

$Wind$ = mean annual wind speed (mph);

$Sunshine$ = mean annual percentage sunshine (%);

$Rain$ = annual cumulative rainfall depth (in.).

To calculate effective temperature for the Pooled Fund mixtures, climate sites from the Enhanced Integrated Climatic Model (EICM) near to the production plant were used. Climate information is shown in Table 7.3.

Table 7.3: Climate details for effective temperature calculation

Location	MAAT (°C/°F)	σMAAT (°C/°F)	Wind (kph/mph)	Sunshine (%)	Rain (cm/in.)
Lebanon, NH	7.33/45.20	10.05/18.09	6.44/4.00	48.14	93.09/36.65
Albany, NY	9.38/48.88	9.66/17.38	10.54/6.55	55.77	96.22/37.88
Burlington, VT	8.13/46.64	10.26/18.47	10.80/6.71	44.32	91.85/36.16

It is important to note that the determination of the |E*| for WinJULEA input is an iterative process, where an initial Z_{eff} must be guessed to ultimately calculate |E*| and revise accordingly. In this work, a maximum of ten iterations or a 0.1 psi change in |E*| were selected as criteria to cease the calculation. In most cases, the convergence of |E*| was observed on or about the third iteration.

Once the inputs were gathered, WinJULEA simulations were executed at a full slip, no slip, and midpoint slip condition. The data used in subsequent sections is from the midpoint slip condition. This condition was selected since complete bonding and the complete absence of bonding are not indicative of field conditions. Agency priority may dictate which bonding condition to use in future work. WinJULEA utilizes multilayer elastic theory to calculate deflections, stresses, and strains at various points in the pavement structure under a variety of loading conditions. Table 7.4 outlines the input assumptions for WinJULEA analysis.

Table 7.4: Input parameters for WinJULEA simulation

Vehicle speed	100 kph (60 mph)
Bonding value (0 to 100,000)	50,000
Poisson's ratio	0.35
Tire load	40 kN (9000 lb)
Tire pressure	0.759 MPa (110 psi)
Tire imprint shape	Circular
Analysis locations	Center of load, tire edge, 12.7 mm outside tire edge
Analysis depths	0, 12.7, 25.4, 76.2 (for thin section), 203 mm (for thick section)

7.4.2 Linear Viscoelastic Characterization

In obtaining the dynamic modulus master curve for the Pooled Fund materials, the test data was fit to the modified Kaelble shift factor function and the Richards sigmoidal function to predict dynamic modulus along the reduced frequency axis. Recall reduced frequency is simply the actual frequency (i.e., 10 Hz) multiplied by the time-temperature shift factor (a_T) to convert to

193

the reference temperature. Equations 7.4-7.6 display the modified Kaelble, the Richards curve

function and its differential (to obtain phase angle), respectively, which were executed by

Abatech, Inc.'s RHEA software (Kaelble, 1985; Richards, 1959; Rowe, 2009).

$$\log a_T = -C_1 \left(\frac{T-T_d}{C_2+|T-T_d|} - \frac{T_R-T_d}{C_2+|T_R-T_d|} \right) \tag{7.4}$$

$$\log |E^*| = \delta + \frac{\alpha}{[1+\lambda e^{\beta+\gamma \log(\omega)}]^{1/\lambda}} \tag{7.5}$$

$$\delta(\omega) = 90\alpha\gamma \frac{\alpha}{[1+\lambda e^{\beta+\gamma \log(\omega)}]^{(1+\frac{1}{\lambda})}} \tag{7.6}$$

where,

a_T	=	time-temperature shift factor;
C_1, C_2	=	Kaelble fit parameters;
T	=	temperature;
T_d	=	defining temperature;
T_R	=	reference temperature (15°C);
$|E^*|$	=	dynamic modulus;
$\delta, \alpha, \beta, \lambda, \gamma$	=	fit coefficients;
ω	=	angular frequency;
$\delta(\omega)$	=	phase angle.

The Richards curve and modified Kaelble representation of the |E*| will be used in a subsequent

section to identify the asphalt moduli to use with the WinJULEA simulation of the pavement

structures. However, the software platform (ALPHA-Fatigue) used for the S-VECD analysis

uses a Verhulst (or standard logistic) function to calculate |E*|. The shift factor function was

194

originally described using the polynomial method (Kim et al., 2011). Equations 7.7 and 7.8 provide the form of the Verhulst and shift factor functions. This introduces a source of error in the data which has not been quantified to date. It is acknowledged that future work will identify the variation in |E*| in using the two methodologies or focus on using one method for all calculations.

$$\log|E^*| = \delta + \frac{\alpha}{1+e^{\beta+\gamma\log(\xi)}} \qquad [7.7]$$

$$\log a_T = a_1 T^2 + a_2 T + a_3 \qquad [7.8]$$

where,

$|E^*|$	=	dynamic modulus;
$\delta, \alpha, \beta, \gamma$	=	fit coefficients;
ξ	=	reduced time $= \frac{t}{a_T}$;
a_T	=	time-temperature shift factor;
a_1, a_2, a_3	=	shift factor coefficients;
T	=	temperature.

To obtain the relaxation modulus for S-VECD analysis, the Prony (or Dirichlet) series of decaying exponentials is used. It has also been found that the Prony series applies to a wide range of linear viscoelastic conditions and has a physical meaning in terms of the generalized Voigt (for creep compliance) and generalized Maxwell or Wiechert (for relaxation modulus) mechanical models (Kim, 2009). Equation 7.9 represents the generalized Maxwell formulation of the Prony series.

$$E(t) = E_\infty + \sum_{i=1}^{m} E_i e^{\frac{t}{\rho_i}} \qquad [7.9]$$

where,

$E(t)$ = relaxation modulus;

E_∞ = equilibrium (long-time) modulus;

E_i = relaxation strength;

ρ_i = relaxation time;

t = time.

While several methods to fit the Prony coefficients exist, the data presented in this work are fit to 21 relaxation strengths and 21 relaxation times. The relaxation modulus' role in the S-VECD calculations will be described later on.

7.4.3 Simplified Viscoelastic Continuum Damage Model

The S-VECD calculation procedure, like the VECD model, still relies on three foundational premises to assess changes in material integrity due to repeated loading: the elastic-viscoelastic correspondence principle, Schapery's work potential theory, and the TTSP. The elastic-viscoelastic correspondence principle separates the time-dependency of viscoelastic materials (i.e., asphalt) by using pseudostrain (ε^R) and a corresponding reference modulus to form a variation of the classic Hooke's Law, as shown in Equation 7.10:

$$\sigma = E_R \varepsilon^R \qquad [7.10]$$

where,

σ = stress;

E_R = reference modulus (usually set to unity);

ε^R = pseudostrain.

By separating the time effects from the damage effects, any change in the slope of the stress-pseudostrain curve can be directly tied to damage induction. The change in slope (or change in the E^R term) is usually represented by the DCC, or the pseudostiffness (or pseudo secant modulus) function with growing damage. The pseudostrain relation is captured by the relaxation modulus convolution integral (calculated here via Prony series), which explains the VECD requirement of developing a linear viscoelastic master curve.

Based on Schapery's (1990) work potential theory, which used the method of thermodynamics of irreversible processes, a rate type damage evolution law can be found to determine S as it relates to ε^R. Note that S is an internal state variable designed to account for microstructural damage in the specimen. The formulation of a damage evolution law is shown by Equations 7.11-7.13:

Pseudo strain energy density function

$$W^R = f(\varepsilon^R, S) \tag{7.11}$$

Stress-pseudo strain relationship

$$\sigma = \frac{\partial W^R}{\partial \varepsilon^R} \tag{7.12}$$

Damage evolution law

$$\frac{dS}{dt} = \left(-\frac{\partial W^R}{\partial S}\right)^\alpha \tag{7.13}$$

where,

α =   material property based on viscoelastic behavior, function of log-log slope of relaxation modulus with respect to reduced time.

Lastly, the concept of TTSP with growing damage is paramount to the VECD theory as it reinforces the validity of the linear viscoelastic master curves at high levels of damage, reduces testing time, and confirms the notion that damage is a universal property of asphalt concrete (Chehab et al., 2002; Gibson et al., 2003; Underwood et al., 2006).

The simplified model is detailed in Underwood et al. (2010) and offers two calculation approaches: the transient (first cycle of loading) realm where damage growth is not constant, and the steady state or cyclic calculations where damage growth per cycle is small and only manifested in the tensile portion of loading. The primary relations needed to determine the DCC are shown in Equations 7.14-7.16 (Underwood, 2011):

$$\varepsilon^R = \begin{cases} \varepsilon^R = \dfrac{1}{E_R} \displaystyle\int_0^{\xi} E(\xi - \tau)\dfrac{d\xi}{d\tau}\, d\tau & \xi \leq \xi_p \\[2ex] \varepsilon^R_{0,ta_{cycle\ i}} = \dfrac{1}{E_R}\dfrac{\beta + 1}{2}\left((\varepsilon_{0,pp})_i |E^*|_{LVE}\right) & \xi > \xi_p \end{cases} \qquad [7.14]$$

$$C = \begin{cases} C = \dfrac{\sigma}{\varepsilon^R DMR} & \xi \leq \xi_p \\[2ex] C^* = \dfrac{\sigma_{0,ta}}{\epsilon^R_{0,ta} DMR} & \xi > \xi_p \end{cases} \qquad [7.15]$$

$$dS = \begin{cases} (dS_{transient})_{timestep\ j} = (-\dfrac{DMR}{2}(\varepsilon^R)_j \Delta C_j)^{\frac{\alpha}{1+\alpha}}(\Delta\xi_j)^{\frac{1}{1+\alpha}} & \xi \leq \xi_p \\[2ex] (dS_{cyclic})_{cycle\ i} = (-\dfrac{DMR}{2}(\varepsilon^R_{0,ta})^2 \Delta C_i)^{\frac{\alpha}{1+\alpha}}(\Delta\xi_p K_1)^{\frac{1}{1+\alpha}} & \xi > \xi_p \end{cases} \qquad [7.16]$$

where,

$E(\xi - \tau)$ = relaxation modulus function;

ξ = reduced time;

τ = integration variable;

ξ_p = pulse time;

198

$\varepsilon_{0,ta}^R$ = tension amplitude of pseudo strain for given cycle;

β = quantity to determine proportion of tensile loading in cycle;

$\varepsilon_{0,pp}$ = peak to peak strain in cycle;

$|E^*|_{LVE}$ = dynamic modulus;

C = pseudostiffness for transient realm;

DMR = dynamic modulus ratio;

C^* = pseudostiffness in cyclic portion;

$\sigma_{0,ta}$ = tension amplitude of stress for given cycle;

dS = change in damage;

ΔC = change in pseudostiffness;

$\Delta \xi$ = change in reduced time;

K_1 = form adjustment factor.

Once the pseudo strain, pseudo secant modulus, and damage evolution characteristics are determined, a fit can be applied to determine the DCC. The S-VECD is capable of fitting the DCC in exponential or power law form. For all 14 mixtures, the exponential fit (Equation 7.17) provided a lower mean square error than the power law form and hence was selected for the DCC representation.

$$C(S) = e^{aS^b} \qquad [7.17]$$

where,

a, b = fit coefficients.

As mentioned previously, the failure criterion is an important tool for objectifying fatigue resistance of mixtures. The most current failure criterion is the G^R term developed by Sabouri

and Kim (2014). This parameter is found by calculating the average amount of pseudostrain energy released per cycle throughout the fatigue test. Equations 7.18 and 7.19 describe the formulation, which begins by determining the level of pseudostrain energy released per cycle (W_C^R). The average value is then found by integrating the W^R function and normalizing by the number of cycles to failure (N_f).

$$(W_C^R)_i = \frac{1}{2}(1 - C^*{}_i)(\varepsilon_{0,ta}^R)_i^2 \qquad\qquad [7.18]$$

$$G^R = \frac{\int_0^{N_f} W_C^R}{N_f{}^2} \qquad\qquad [7.19]$$

7.5 Results and Discussion

In order to develop a framework for performance-based mixture design, a test procedure and relevant material indices are needed. The method proposed in this section can be completed using only the AMPT, which allows for contractors and agencies to purchase a single piece of equipment. The results shown below are from plant-produced, laboratory-reheated samples and separate indices are proposed for controlled stress and controlled strain conditions.

7.5.1 Identifying Critical Strain Locations

The first part of this investigation pertains to identifying the critical strain and its location. Once the critical strain is identified, a fatigue life corresponding to the simulated pavement structure for each mixture can be predicted. Generally, for the included pavement sections it is expected that the tensile strain at the bottom of the asphalt layer will be the critical design strain. However, it is important to determine the maximum shear strain criteria at or near the surface for top-down cracking considerations. Since WinJULEA calculates the maximum shear stress and strain at any location, a p-q diagram was used to determine if the stress levels exceed the

threshold of the material. A p-q diagram is commonly used in soil mechanics as an alternative to the traditional Mohr-Coulomb space and has been used to analyze tire stresses at or near the surface by past researchers (Wang and Al-Qadi, 2010). Refer to Equations 7.20-7.24 display the manipulations required for the p-q manipulations.

$$p = \frac{\sigma_1 + \sigma_3}{2} \tag{7.20}$$

$$q = \frac{\sigma_1 - \sigma_3}{2} \tag{7.21}$$

$$q_{fail} = a + p * tan\psi \tag{7.22}$$

$$a = c * cos\varphi \tag{7.23}$$

$$tan\psi = sin\varphi \tag{7.24}$$

where,

p =   normal stress;

σ_1 =   maximum principal stress;

σ_3 =   minimum principal stress;

q =   shear stress;

q_{fail} =   critical shear stress;

a =   cohesive strength in p-q diagram;

ψ =   angle of friction in p-q diagram;

c =   cohesive strength in Mohr-Coulomb space;

φ =   angle of friction in Mohr-Coulomb space.

Using Wang and Al-Qadi (2010) as a guide, the cohesive strength and angle of friction (c and φ) were assumed to be 600 kPa and 40° at 25°C respectively. Although the effective temperature values in the pavement sections are colder than 25°C, it is unlikely that these values vary

drastically over the range of effective temperatures used. Looking at the thick pavement sections in this study, the shear stress at various points along the 25.4 mm depth line exceeds the allowable using the p-q diagram. However, the magnitude of shear strain is lower than that of the horizontal tensile strain at the bottom of the asphalt layer. Work to characterize top-down cracking is ongoing in the industry, where some believe the shear strains under certain conditions are increased due to temperature gradients throughout the pavement system, aging, or a soft substructure, and it has even been postulated that bottom-up cracking may be a myth in thick pavements (Myers, Roque, and Ruth, 1998; Yoo and Al-Qadi, 2008). A more complete investigation is outside the scope of this paper.

7.5.2 Fatigue Output Analysis

In this portion of the study, outputs from the S-VECD are examined to couple with pavement system effects and mixture stiffness ($|E^*|$). Figure 7.2 presents the mixture DCCs for the 14 sets of Pooled Fund materials. The NY mixture curves are above the others in the C*-S space. Generally, a curve with a higher C value at a given S represents a better degree of material integrity. However, it is not optimal to assign objective mixture resistance ratings based only on the DCC curve because of the lack of a failure criterion at this stage of the analysis, the undefined physical meaning of the damage internal state variable, and the absence of the controlling mechanism (stress or strain).
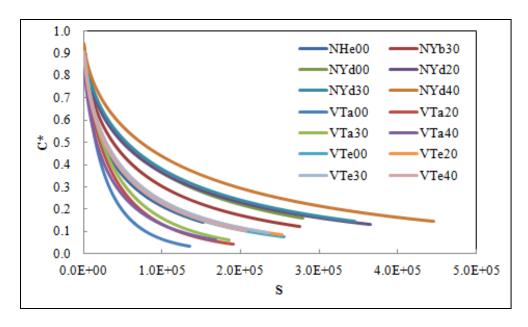
Figure 7.2: Damage characteristic curves for Pooled Fund mixtures

7.5.2.1 Controlled Strain

To determine the parameters for a performance-based mixture design framework, three elements must be considered for the fatigue distress mode: 1) a value from the S-VECD model since this type of testing would be prescribed, 2) a value that captures mixture stiffness, and 3) a value that relates to the components of the pavement system on a whole. Given the approach described above, the mixture stiffness and pavement system can be described in a single term: cycles to failure (N_f). For controlled strain, it is expected that the material's flexibility or relaxation capabilities will influence the response under loading rather than strictly the stiffness. It is important to note that the pavement cross section produced high strains for the thin pavement when run through the WinJULEA simulation. These strains, along with the predicted cycles to failure based on the traditional fatigue laws, are shown in Table 7.5. As expected, the stiffer the mixture, the lower the predicted strain level. However, the strain level does not directly correlate to the rank or the magnitude of the cycles to failure in controlled strain mode ($N_{f,\ strain}$). This

reinforces the need for a fatigue-related parameter. In this paper, the targeted value to assess fatigue properties is the current failure criterion in the S-VECD methodology, G^R.

Table 7.5: Horizontal tensile strain at bottom of asphalt layer and cycles to failure

Mixture	Critical microstrain	Cycles to failure ($N_{f, strain}$)	Rank by cycles to failure
NHe00	426	59,767	10
NYb30	389	62,201	9
NYd00	364	101,512	6
NYd20	365	21,376	14
NYd30	367	51,320	11
NYd40	358	222,100	3
VTa00	486	433,867	2
VTa20	453	121,393	5
VTa30	442	818,948	1
VTa40	446	191,919	4
VTe00	411	48,608	12
VTe20	414	94,178	7
VTe30	404	68,340	8
VTe40	408	26,298	13

Figure 7.3 shows the G^R-N_f curves from the experimental data, for which a higher G^R value implies more energy is dissipated during loading. This trait should be indicative of a well-performing mixture. Generally, the VTa materials exhibit the highest G^R for a particular N_f, with the NHe00 mixture dissipating the least amount of energy in the N_f range shown. An index that was recently discussed at an industry meeting will be employed to normalize the G^R values instead of using the G^R corresponding to the $N_{f, strain}$, which will vary across mixtures (Sabouri et al., 2015). This index uses the N_f corresponding to a G^R of 100, which incorporates a degree of extrapolation from the data shown in the figure below. However, most of the available data points failed within or close to 20,000 cycles based on a previous recommendation in the test protocol. In the current AASHTO TP107, the ideal approach is to capture four replicates with varying cycles to failure that span across several decades in log space.
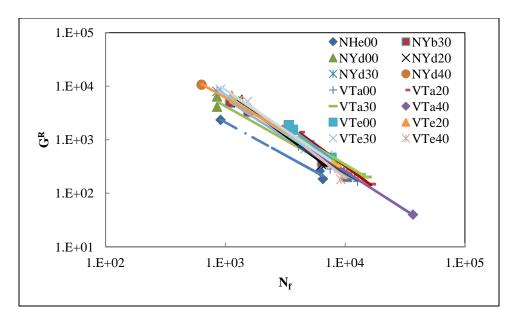
Figure 7.3: Energy-based failure criterion with experimental cycles to failure for Pooled Fund mixtures

The next step is to determine if there is a correlation between the proposed parameter to capture fatigue effects ($N_{G_{100}^R}$) and the parameter to capture stiffness and structural effects ($N_{f, \text{strain}}$). Figure 7.4 shows the expected trend that as $N_{G_{100}^R}$ increases (rank goes to 1), more energy is dissipated per loading cycle and the pavement's overall fatigue life should increase (rank goes to 1). However, Figure 7.5 shows that the correlation between the actual values as opposed to ranks is modest at best. The general trend is confirmed however that the higher $N_{G_{100}^R}$ leads to a higher $N_{f, \text{strain}}$. The correlation among the rank of parameters with respect to the fatigue life rank is also captured through Kendall's tau coefficient, which varies from -1 (complete disagreement) to 1 (complete agreement), with a value of zero corresponding to no relationship. The coefficient is based on the premise of concordant and discordant pairs, which relate to the rank of a value relative to the position in a master list. In this case, the master list is the $N_{f, \text{strain}}$ rank. For example, a ranking of $N_{f, \text{strain}} = 1$ and $N_{G_{100}^R} = 2$ would generate a concordant pair when $N_{f, \text{strain}} > 1$ and $N_{G_{100}^R} > 2$ and a discordant pair if $N_{f, \text{strain}} > 1$, but $N_{G_{100}^R} < 2$. This parameter is not

influenced by isolated data points and is better suited for small datasets, such as the one used in

this work. Equations 7.25 and 7.26 show the Kendall's tau formulation as well as the method to

calculate the Z-statistic for statistical significance testing (Gibson et al., 2012; Abdi, 2007). The

Kendall's tau for the $N_{G_{100}^R}$ parameter is 0.626, which shows a significant agreement (with α =

0.05) with fatigue life of the controlled strain pavement.

$$\tau_K = \frac{N_C - N_D}{\frac{n}{2}(n-1)} \qquad [7.25]$$

$$Z_K = \frac{3\tau_K\sqrt{n(n-1)}}{\sqrt{2(2n+5)}} \qquad [7.26]$$

τ_K = Kendall's tau rank coefficient;

N_C = number of concordant pairs;

N_D = number of discordant pairs;

n = sample size;

Z_K = Z-statistic for Kendall's tau rank coefficient.
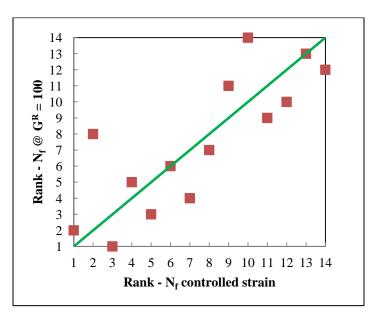
Figure 7.4: Comparing ranks of energy-based index and fatigue life of pavement in controlled strain, with line of equality shown
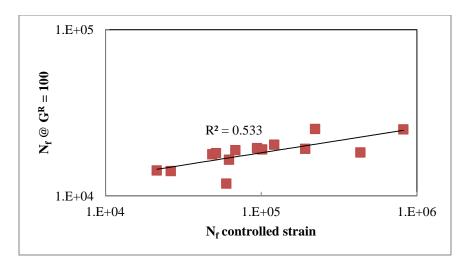
Figure 7.5: Correlation of energy-based fatigue life and pavement fatigue life in controlled strain mode

The analysis shown here is preliminary in nature because there is no field performance data available to confirm the fatigue predictions. Due to the complexity of the fatigue phenomenon, it is important to capture field performance data to develop transfer functions for calibration with S-VECD predictions. However, the $N_{G^R_{100}}$ term shows promise as it relates to pavement fatigue life in controlled strain mode over a spread of nearly 800,000 cycles to failure from the worst performing to best performing mixture. Several other parameters were compared to the pavement system fatigue life, including the C_f failure criterion, the α term relating to the relaxation modulus master curve, and a variety of $|E^*|$-based terms which sought to quantify energy dissipation through combination with phase angle (δ). These terms were the $|E^*|$ by itself, the storage and loss moduli, $|E^*| \tan \delta$ for damping effects, and a modified-Glover-Rowe term used in a previous paper for mixture (Mensching et al., 2015). The $|E^*|$ and δ terms correspond to the measured test point that most closely corresponds to the calculated $|E^*|$ and δ at the bottom of the simulated pavement structure, which for controlled strain is at the 4°C-5 Hz condition.

7.5.2.2 Controlled Stress

A similar series of steps were done for the controlled stress scenario. A constant stress of 0.759 MPa was simulated for the pavement system, with the cycles to failure and corresponding rank shown in Table 7.6. The ranking by controlled stress expectedly follows the trends in |E*| stiffness among the 14 mixtures more closely as opposed to the controlled strain predictions.

For the controlled stress predictions, there was no noticeable trend between $N_{G_{100}^R}$ and the $N_{f, \text{stress}}$ values. Using the α term did not show any stable trend with the stress-controlled fatigue life as well. With the energy-based and relaxation-based terms not generating suitable fits to the predicted fatigue life, the use of a stiffness-based parameter was examined. Table 7.7 displays the coefficient of variation (COV) of the root mean square error (RMSE) and the coefficient of determination (R^2) when comparing the values of each parameter to the cycles to failure prediction using a power law function. Note the closest measured |E*| and δ to the calculated values at the bottom of the asphalt layer correspond to a test condition of 4°C-1 Hz.

Table 7.6: Cycles to failure in controlled stress mode

Mixture	Cycles to failure ($N_{f, \text{stress}}$)	Rank by cycles to failure
NHe00	1,209,947	7
NYb30	1,560,724	6
NYd00	6,219,927	2
NYd20	1,208,766	8
NYd30	3,821,705	3
NYd40	21,761,174	1
VTa00	122,702	14
VTa20	332,508	13
VTa30	670,466	10
VTa40	415,221	12
VTe00	775,513	9
VTe20	1,948,420	4
VTe30	1,829,788	5
VTe40	517,585	11

Table 7.7: Determining a stiffness-based parameter for controlled stress predictions

Parameter	COV of RMSE (%)	R^2
$\|E^*\| \tan \delta$	11.6	0.616
$\|E^*\| \cos \delta$	21.6	0.738
$\|E^*\| \sin \delta$	12.3	0.634
Modified Glover-Rowe for mixture ($\|E^*\| \cos^2 \delta / \sin \delta$)	32.2	0.753
C_f	17.3	0.492
$\|E^*\|$ at 4°C-1 Hz	20.7	0.737

Based on the results above, the $\|E^*\| \tan \delta$ may best describe the trend in cycles to failure for the pavement system given its low COV of RMSE value. The $\tan \delta$ term is commonly used in viscoelasticity to describe damping or the ability to absorb and release energy, which seems feasible given that cracking behavior is often tied to a combination of stiffness, relaxation, and ability to dissipate energy under loading. Figure 7.6 shows how well the parameter rankings match with the $N_{f, stress}$ rankings, while Figure 7.7 shows the correlation with the actual values. As $\|E^*\| \tan \delta$ increases (rank towards 1), the cycles to failure for the pavement system increases (rank towards 1), but in the controlled strain state it is expected that the energy dissipation drives the response. The Kendall's tau coefficient for the stiffness-based terms range from 0.467-0.670 and were found to be statistically significant, while the Kendall's tau coefficient for the $N_{G^R_{100}}$ parameter is 0.099 (close to no relationship). In the controlled stress mode, the stiffness is likely more prevalent in the material behavior since the phase angle should decrease as stiffness increases in this region of linear viscoelastic behavior. The decrease in phase angle corresponds to a decreased ability to dissipate energy, which could be detrimental to performance, especially in the controlled strain mode.
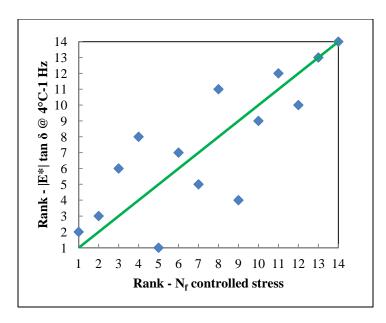
Figure 7.6: Ranks of |E*| tan δ versus the pavement system cycles to failure in controlled stress mode, with line of equality shown
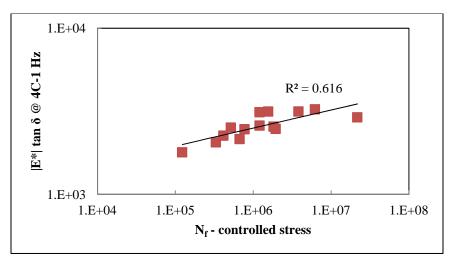
Figure 7.7: |E*| tan δ versus the pavement system cycles to failure in controlled stress mode

7.6 Conclusions

The research conducted in this paper is intended to be a first step in the process of defining an index for the identification of poorly performing fatigue mixtures. While the study has its share of limitations, an expanded dataset should find that the targeted parameters present value to contractors and owner agencies as the mixture design paradigm shifts from a volumetric-based

approach to a performance-based methodology. The authors provide the following conclusions and recommendations for further study:

1. Fatigue performance cannot be adequately described without incorporation of the pavement structure properties. A multilayer linear elastic platform is used to model a subbase and subgrade layer from an LTPP project in New York. A thin asphalt layer was used to capture controlled strain behavior, where the flexibility of the asphalt is expected to govern, and a thick pavement represented the controlled stress situation where mixture stiffness is expected to dominate the fatigue behavior. It is recommended some sense of viscoelasticity is incorporated into the considerations of the assignment of structural response model inputs. The approach outlined here has been used in the Mechanistic-Empirical Pavement Design Guide software, as well as the Quality Related Specification Software. This type of research lends itself well to the upcoming Layered Viscoelastic Continuum Damage (LVECD) approach as the stress and strain outputs are used to calculate the appropriate parameter terms. It may be worthwhile to obtain pavement structure information and evaluate stress and strain outputs from the LVECD and linear elastic methods and assess the difference in fatigue life as it relates to the proposed parameters in the future.

2. When calculating the DCC and G^R failure criterion, there was not a clear trend between RAP increases and a change in fatigue performance of the mixture. Generally, the stiffer mixtures produced less tensile strain at the bottom of the asphalt layer, but this was not necessarily a function of RAP percentage. Agencies and future researchers are encouraged to investigate the changes and trends of the DCC and G^R parameter to identify critical RAP levels for similar performance to low-RAP or

211

virgin mixtures. It may be of interest to conduct fatigue testing and S-VECD analysis on extracted and recovered RAP binders to learn more about fatigue predictions between a fully-blended condition and conditions more indicative of field mixture.

3. For controlled strain pavements, the average rate of dissipated energy per cycle (G^R) was used to rank performance. The G^R was set to 100 J/m^3 and the predicted cycles to failure was selected as a measure of the mixture's fatigue performance. When compared to the N_f prediction for the pavement system there was a degree of separation and a general trend stating that an increase in dissipated energy results in an increase in fatigue life.

4. For controlled stress pavements, the G^R approach did not show a trend with the fatigue life of the pavement system. Instead, several stiffness-based approaches were examined, with $|E^*| \tan \delta$ exhibiting the smallest degrees of variation among the range of N_f values when compared to a power law regression equation. This parameter holds promise because it captures stiffness and also a degree of energy dissipation through the damping term, $\tan \delta$. Ideally, the phase angle of the mixture could be investigated over the course of the direct tension fatigue test to determine level of damping, but due to phase angle distortion with microcrack coalescence the true phase angle is not found via the S-VECD model.

5. While a few parameters are targeted as a performance-based framework for fatigue, there are shortcomings to the approach in this paper that must be addressed. Future work must use field performance data to distinguish poorly performing materials from satisfactorily performing materials. Many of the mixtures in this study were not placed in the field, so an expansion study is needed to capture field performance and

assess the validity of the fatigue life predictions used throughout asphalt materials research. This would involve a detailed literature review of past project data (when applicable) or coordination with other agencies and researchers, such as the National Center for Asphalt Technology's test track. The first step of this process would be to plot the performance measure or ranking with S-VECD outputs and representative stiffness values to analyze the correlation. At this stage, separation can be evaluated and a failure line threshold and formulation determined. With this approach, there is a need to identify changes in these parameters and performance with respect to reasonable volumetric changes. This concept is paramount to the integration of a performance-based design and acceptance methodology, as confidence in materials can be established when the relationship between volumetric variation and performance is captured.

6. The approach in general holds promise because of its reliance on material attributes that can be tested from one specimen type on one testing machine. While the direct tension cyclic test is time-consuming, the constitutive model parameters that can be found from a test are powerful and are applicable not only to fatigue, but to low temperature performance. Future work may analyze the effects of damage on low temperature parameters such as modulus, phase angle, or fracture energy. For example, UTSST data can be analyzed in the VECD model by using the thermal stress and strain history. It is anticipated that damage characterization at low temperatures causes changes in the fracture temperature of the mixture, which could introduce errors when using LVE properties to emulate failure conditions (Alavi, 2014). By quantifying relevant material properties over a wide range of materials

with differing amounts of additives, the movement towards performance thresholds will be made easier for owner agencies. The implications of this work for the industry are evident when considering general fatigue analyses in asphalt materials research. Researchers must include structural considerations in examining fatigue resistance and this is shown through different properties best representing thick and thin pavement performance. Future work may help to reinforce the power behind the S-VECD model, which will come with accurate performance prediction.

7.7 Acknowledgements

CHAPTER 8

CONCLUDING REMARKS

Throughout this dissertation, work has been done to identify trends and tools which will aid in the shift from volumetric-based to performance-based design. A short summary of each technical chapter is provided below, as well as a number of closing remarks relating to future work and an explanation of how an agency would use this dissertation as a guide to exploring and potentially implementing a new design specification.

As shown in Figure 8.1, the motivation from this work stems from funding gaps, a paradigm shift in administration of federal funds to state agencies, and a general desire to use more alternate materials in asphalt pavement design and construction. Five technical chapters were developed to investigate elements which would be of interest to an agency looking to implement a performance-based mixture design or acceptance methodology. The overall goals of these studies were to identify differences in binder and mixture performance, select potential test and analysis methodologies, and evaluate the effectiveness of these analysis approaches with available virgin, RAP, field-aged, and laboratory-conditioned materials for a performance-based framework for low temperature and fatigue cracking.

The proposed parameters exhibit trends with performance measures of the evaluated mixtures and are operationally efficient since only use of the AMPT is required at this time. The general simplicity for the user in modeling of dynamic modulus and S-VECD properties for these

mixtures and their relationship to performance allows for the expansion of testing among length scales (e.g., fine aggregate matrix and mastic) to further understanding of each component's role in construction and design.
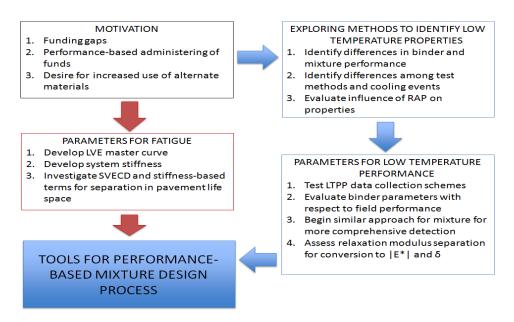
Figure 8.1: Schematic showing motivation and goals of performance-based mixture design framework

In Chapter 3, the influence of cooling rate, starting temperature, blending, and RAP percentage were examined with respect to low temperature cracking resistance of asphalt binders and mixtures. The findings show that cooling rate has an impact on critical cracking temperature of materials, due to changes in relaxation capabilities. Generally, an increase in RAP percentage results in a warmer critical cracking temperature, but the effect of changing binder grade to account for higher levels of recycled material was prediction or test method-dependent. The importance of this chapter is obvious when considering how many different testing and prediction models exist for low temperature characterization. It also shows that there may be differences in binder predictions versus mixture predictions, which is exacerbated by the question of mobilization in RAP materials.

In the next chapter of the dissertation, three rheological parameters were investigated for use as an indicator for poorly performing materials using field performance values from the LTPP database coupled with BBR and DSR data for field extracted binders. For the included data, the Superpave parameters $S(60)$ and $m(60)$ correlated best with the field performance, but the intermediate temperature Glover-Rowe parameter and crossover frequency-rheological index space show promise for detecting poorly performing materials and material property changes due to aging. A discussion of data limitations found in the LTPP database is provided, which may help agencies identify the need for more robust and consistent recording and testing practices of asphalt materials to secure useful information for a performance-based approach to construction.

Chapter 5 begins the process of determining mixture-based parameters to identify separations in performance among a set of materials. The paper evaluated the Glover-Rowe parameter for both intermediate and low temperature considerations for three different sets of binders where field and laboratory performance measures were available. The intermediate parameter showed mixed results when comparing the location in Black Space to low temperature performance, while the low temperature approach, which is being developed as a surrogate to the BBR-based Superpave binder specification, showed very good agreement with field performance and the traditionally measured continuous low temperature grade. The second portion of the study was an exploration of a Black Space-based mixture parameter for low temperature cracking, where results show separation between mixtures in Black Space grows as frequency moves from high reduced frequencies towards the inflection point frequency.

A continuation of the Black Space mixture parameter development is presented in Chapter 6. A location on the relaxation modulus master curve along the reduced time axis is then brought to the frequency domain to determine the representative temperature-frequency combination for

217

plotting in Black Space. The Pooled Fund materials showed agreement and separation in Black Space between the failed or high-risk materials and the satisfactory performers, while there was no clear trend among the LTPP mixtures. The lack of clear separation in the LTPP materials may be a result of aging effects or data collection shortcomings in the database.

The final technical chapter of the dissertation relates to a preliminary effort to develop indicators for fatigue cracking using a combination of mixture stiffness, pavement system elements, and S-VECD outputs. For the controlled strain application, the cycle number corresponding to a rate of average dissipated energy per cycle of 100 J/m^3 showed a promising trend with respect to the fatigue life of the thin pavement system. For controlled stress, the fatigue life of the thick system showed the most stable trend with a $|E^*| \tan \delta$ parameter. Future work in this line of research would require field performance to correlate to the fatigue life predictions and to ensure the parameters identified in this study can apply to real-life conditions.

It is important to note the research efforts included in this document are intended to serve as pieces in the progression to measuring material properties to classify design of asphalt pavements. Opportunities exist for future work primarily by expanding the dataset and refining the parameter definitions and input assumptions. Should an agency look to implement this framework, the following procedure is likely to be executed:

- Identify critical distress modes for the agency, in this case low temperature and fatigue cracking.
- Develop a materials catalog comprised of common mixture designs with relevant information regarding the engineering-related properties of the component materials.

- Develop a process to evaluate performance of mixtures, whether it is field or laboratory-based. Include service life considerations for full-scale pavement construction, overlays, and so on. This is critical to compare the desired material properties of the mixture to establish satisfactory versus poor performer relationship.

- Identify material properties required for performance-based thresholds. These properties should be derived from a trend with performance data. In this dissertation, $|E^*|$ and δ are used for low temperature cracking and controlled stress pavements, while the cycles to failure when the S-VECD energy-based failure criterion is equal to 100 J/m^3 is used for controlled strain pavements.

- Assess relationship between mixture condition (i.e., production and compaction location, field cores, mat samples, aging level) and performance measure to better establish specification attributes. This may rely on current QA/QC sampling processes, which would be the least invasive method given a sufficiently accurate correlation to performance when analyzing the desired material properties.

- Monitor and document changes to the material property and proposed performance indication (i.e., pass or fail) with the volumetric targets and with reasonable volumetric changes. The inclusion of volumetrics will be needed early-on to compare to material property thresholds and establish a better sense of the spread in data across common mixture types, especially when considering impacts due to addition of alternate materials. This will test the quality of the current mixture designs and specifications (both volumetric and performance-based) and begin the movement towards a QA/QC method using the performance-based thresholds. For a QA/QC process, sampling frequency and a pay factor equation should be developed.

- Monitor pavement condition and track changes in relevant material properties of the mixture throughout the pavement life. This will strengthen the pavement management system of the agency and allow the agency to refine the performance-based specification if the critical material properties are not adequately capturing performance and degradation over the service life of the constructed pavements.

In closing, it is the author's opinion that designing asphalt mixtures through performance testing thresholds will also encourage increased usage of recycled materials, which will reduce the space and cost needed for transport of waste material. And most importantly, the design, production, and maintenance of mixtures based on material properties should lead to increased pavement life, more informed programming decisions for assignment of rehabilitation funds, and a better infrastructure investment for taxpayers. These attributes will help move society forward and alleviate some of the budgetary challenges in the current engineering landscape.

CHAPTER 9

REFERENCES

Abdi, H., "The Kendall Rank Correlation Coefficient," Encyclopedia of Measurement and Statistics (Edited by Salkind), Sage Publications, Thousand Oaks, CA, 2007.

Airey, G.D., "Use of Black Diagrams to Identify Inconsistencies in Rheological Data," Journal of Road Materials and Pavement Design, Vol. 3, No. 4, 2002, 403-424.

Alavi, S.M.Z., "Comprehensive Methodologies for Analysis of Thermal Cracking in Asphalt Pavements," Ph.D. Dissertation, University of Nevada, Reno, Reno, NV, 2014.

Alavi, M.Z., and Hajj, E.Y., Evaluation of Thermo-Viscoelastic Properties of Asphalt Mixtures with High RAP Contents, Final Report, University of Nevada-Reno, 2013.

Alavi, M.Z., Hajj, E.Y., Morian, N.E., and Sebaaly, P.E., "Low Temperature Characterization of Asphalt Mixtures by Measuring Viscoelastic Properties under Thermal Loading," Proceedings of ISCORD 2013: Planning for Sustainable Cold Regions, 2013, 404-415.

Al-Qadi, I.L., Ozer, H., Lambros, J., Lippert, D.L., Elkhatib, A., Khan, T., and Sighn, P., "Testing Protocols to Ensure Mix Performance with High RAP and RAS," presented at North Central Asphalt User/Producer Group and Illinois Bituminous Paving Joint Conference, Champaign, IL, 2015.

American Association of State Highway and Transportation Officials, "Determination of Low-Temperature Performance Grade (PG) of Asphalt Binders," AASHTO R49, Washington, D.C., 2012a.

American Association of State Highway and Transportation Officials, "Method for Thermal Stress Restrained Specimen Tensile Strength," AASHTO TP10, Washington, D.C., 2012b.

221

American Association of State Highway and Transportation Officials, "Mixture Conditioning of Hot Mix Asphalt (HMA)," AASHTO R30, Washington, D.C., 2012c.

American Association of State Highway and Transportation Officials, "Quantitative Extraction of Asphalt Binder from Hot Mix Asphalt (HMA)," AASHTO T164, Washington, D.C., 2012d.

American Association of State Highway and Transportation Officials, "Quantitative Grading or Verifying the Performance Grade of an Asphalt Binder," AASHTO R29, Washington, D.C., 2012e.

American Association of State Highway and Transportation Officials, "Quantitative Recovery of Asphalt from Solution by Abson Method," AASHTO T170, Washington, D.C., 2012f.

American Association of State Highway and Transportation Officials, "Standard Method of Test for Determining Dynamic Modulus of Hot-Mix Asphalt Concrete Mixtures," AASHTO T342, Washington, D.C., 2012g.

American Association of State Highway and Transportation Officials, "Standard Method of Test for Determining the Creep Compliance and Strength of Hot-Mix Asphalt (HMA) Using the Indirect Tensile Test Device," AASHTO T322, Washington, D.C., 2012h.

American Association of State Highway and Transportation Officials, "Standard Method of Test for Determining the Dynamic Modulus and Flow Number for Hot Mix Asphalt (HMA) Using the Asphalt Mixture Performance Tester (AMPT)," AASHTO TP79, Washington, D.C., 2012i.

American Association of State Highway and Transportation Officials, "Standard Method of Test for Determining the Flexural Creep Stiffness of Asphalt Binder Using the Bending Beam Rheometer (BBR)," AASHTO T313, Washington, D.C., 2012j.

American Association of State Highway and Transportation Officials, "Standard Method of Test for Determining the Fracture Properties of Asphalt Binder in Direct Tension (DT)," AASHTO T314, Washington, D.C., 2012k.

American Association of State Highway and Transportation Officials, "Standard Method of Test for Determining the Permanent Shear Strain and Stiffness of Asphalt Mixtures Using the Superpave Shear Tester (SST)," AASHTO T320, Washington, D.C., 2012l.

American Association of State Highway and Transportation Officials, "Standard Method of Test for Determining the Rheological Properties of Asphalt Binder Using a Dynamic Shear Rheometer (DSR)," AASHTO T315, Washington, D.C., 2012m.

American Association of State Highway and Transportation Officials, "Standard Specification for Performance-Graded Asphalt Binder," AASHTO M320, Washington, D.C., 2012n.

American Association of State Highway and Transportation Officials, "Determining the Damage Characteristic Curve of Asphalt Concrete from Direct Tension Cyclic Fatigue Tests," AASHTO TP 107, Washington, D.C., 2014.

American Society of Testing and Materials, "Standard Practice for Determining Low-Temperature Performance Grade (PG) of Asphalt Binders," ASTM D6816, West Conshohocken, PA, 2002.

American Society of Testing and Materials, "Standard Test for Determining Fracture Energy of Asphalt-Aggregate Mixtures Using the Disk-Shaped Compact Tension Geometry," ASTM D7313, West Conshohocken, PA, 2013.

American Society of Civil Engineers, "2013 Report Card for America's Infrastructure," < http://www.infrastructurereportcard.org/a/#p/roads/overview>, Reston, VA, 2013.

Anderson, D.A., Christensen, D.W., Bahia, H.U., Dongré, R.N., Sharma, M.G., Antle, C.E., and Button, J., "Binder Characterization and Evaluation," SHRP A-369, Vol. 3 Physical Characterization, Strategic Highway Research Program, National Research Council, Washington, D.C., 1994.

Anderson, D.A., Lapalu, L., Marasteanu, M.O., Le Hir, Y.M., Planche, J-P., and Martin, D., "Low Temperature Thermal Cracking of Asphalt Binders as Ranked by Strength and Fracture Properties," Transportation Research Record, Vol. 1766, 2001, 1-6.

Anderson, M., Anderson, D., Bahia, H., Baumgardner, G., McGennis, B., Planche, J-P., Reinke, G., and Rowe, G., "Asphalt Binder ETG Intermediate Temperature Parameter Task Force," Status Report to Asphalt Binder ETG, 2013.

Anderson, R.M., King, G.N., Hanson, D.I., and Blankenship, P.B., "Evaluation of the Relationship between Asphalt Binder Properties and Non-Load Related Cracking," Journal of the Association of Asphalt Paving Technologists, Vol. 80, 2011, 615-663.

ARA, Inc., "Guide for Mechanistic-Empirical Design of New and Rehabilitated Pavement Structures," Final Report, NCHRP Project 1-37A, National Cooperative Highway Research Program, National Research Council, Washington, D.C., 2004.

Asphalt Research Consortium, December 2007 Newsletter, <http://www.arc.unr.edu/newsletter/dec07/index_files/page324.htm>, Accessed September 29, 2014.

Baburamani, P., "Asphalt Fatigue Life Prediction Models – A Literature Review," Report ARR 334, ARRB Transport Research Limited, Vermont South, Victoria, Australia, 1999.

Baumgaertel, M., and Winter, H.H., "Determination of Discrete Relaxation and Retardation Time Spectra from Dynamic Mechanical Data," Rheologica Acta, Vol. 28, 1989, 511-519.

Behnia, B., Dave, E.V., Ahmed, S., Buttlar, W.G., and Reis, H., "Effects of Recycled Asphalt Pavement Amounts on Low-Temperature Cracking Performance of Asphalt Mixtures Using Acoustic Emissions," Transportation Research Record: Journal of the Transportation Research Board, Vol. 2208, Transportation Research Board of the National Academies, Washington, D.C., 2011, 64-71.

Bennert, T., "Rejuvenating Agents with RAP in HMA – Quarterly Meeting Presentation," New Jersey Department of Transportation, 2014.

Bennert, T., and Maher, A., "Forensic Study on the Cracking Distress of New Jersey's LTPP SPS-5 Sections – 30% RAP vs. Virgin Hot Mix Asphalt (HMA)," Presented at 92nd Annual Meeting of the Transportation Research Board, Washington, D.C., 2013.

Bennert, T., and Maher, A., "Forensic Study on the Cracking of New Jersey's Long-Term Pavement Performance Specific Pavement Study Sections," Transportation Research Record: Journal of the Transportation Research Board, Vol. 2371, Transportation Research Board of the National Academies, Washington, D.C., 2014, 74-86.

Bhattacharjee, S., Swamy, A.K., and Daniel, J.S., "Continuous Relaxation and Retardation Spectrum Method for Viscoelastic Characterization of Asphalt Concrete," Journal of Mechanics of Time-Dependent Materials, DOI: 10.1007/s11043-011-9162-9, 2011.

Bonaquist, R., "Laboratory Evaluation of Hot Mix Asphalt (HMA) Mixtures Containing Recycled or Waste Product Materials Using Performance Testing," Report FHWA-PA-2005-006+98-32(19), Pennsylvania Department of Transportation, Harrisburg, PA, 2005.

Bouldin, M.G., Dongre, R., Sharrock, M.J., Rowe, G.M., Anderson, D.A., Marasteanu, M., Dunn, L., Zanzotto, L., and Kluttz, R.Q., "A Comprehensive Evaluation of the Binders and Mixtures Placed on the Lamont Test Sections," Report for the Federal Highway Administration Binder Expert Task Group, 1999.

Bouldin, M.G., Dongre, R., Rowe, G.M., Sharrock, M.J., and Anderson, D.A., "Predicting Thermal Cracking of Pavements from Binder Properties: Theoretical Basis and Field Validation," Journal of the Association of Asphalt Paving Technologists, Vol. 69, 2000, 455-496.

Braham, A.F., "Fracture Characteristics of Asphalt Concrete in Mode-I, Mode-II, and Mixed-Mode," Ph.D. Dissertation, University of Illinois at Urbana-Champaign, Urbana, IL, 2008.

Brown, E.R., Kandhal, P.S., Roberts, F.L., Kim, Y.R., Lee, D., and Kennedy, T.W., "Hot Mix Asphalt Materials, Mixture Design, and Construction," 3rd Edition, National Center for Asphalt Technology at Auburn University, National Asphalt Pavement Association, Latham, MD.

Buttlar, W.G., and Roque, R. "Evaluation of Empirical and Theoretical Models to Determine Asphalt Mixture Stiffnesses at Low Temperatures," Journal of the Association of Asphalt Paving Technologists, Vol. 65, 1996, 99-141.

Chehab, G.R., "Characterization of Asphalt Concrete in Tension Using a Viscoelastoplastic Model," Ph.D. Dissertation, North Carolina State University, Raleigh, NC, 2002.

Chehab, G.R., Kim, Y.R., Schapery, R.A., Witczak, M.W., and Bonaquist, R., "Time-Temperature Superposition Principle for Asphalt Concrete with Growing Damage in Tension State," Journal of Association of Asphalt Paving Technologists, Vol. 71, 2002, 559-593.

Chong, K.P., and Kuruppu, M.D., "New Specimen for Fracture Toughness Determination for Rock and Other Materials," International Journal of Fracture, Vol. 26, 1984, R59-R62.

Christensen, D.W., "Mathematical Modeling of the Linear Viscoelastic Behavior of Asphalt Cements," Ph.D. Dissertation, Pennsylvania State University, State College, PA, 1992.

Christensen, D., "Analysis of Creep Data from Indirect Tension Test on Asphalt Concrete," Journal of the Association of Asphalt Paving Technologists, Vol. 67, 1998, 458-492.

Christensen, D.W., Pellinen, T. and Bonaquist, R., "Hirsch Model for Estimating the Modulus of Asphalt Concrete," Journal of the Association of Asphalt Paving Technologists, Vol. 72, 2003, 97-121.

Christensen, R.M., "Theory of Viscoelasticity," 2nd edition, Academic Press, New York, NY, 2003.

Clark, R.C., "Practical Results of Asphalt Hardening on Pavement Life," Journal of the Association of Asphalt Paving Technologists, Vol. 27, 1958, 196-208.

Clendennen, C.R., and Romero, P., "Evaluating the Representative Volume Element of Asphalt Concrete Mixture Beams for Testing in the Bending Beam Rheometer," Multi-Scale Modeling and Characterization of Materials: Proceedings of the 8th International RILEM Symposium, Stockholm, Sweden, 2013, 13-30.

Clyne, T., "Specifying Low-Temperature Cracking Performance for Hot-Mix Asphalt," Minnesota Department of Transportation, < http://www.dot.state.mn.us/mnroad/projects/Low_Temp_Cracking/pdfs/TRB%20Article%20-%20LTC%20(clyne).pdf>, 2012, Accessed September 30, 2014.

Cortez, E., and Hajj, E.Y., "Pavement Temperature Rates in Hot Mix Asphalt Layers," Report as part of Contract DTFH61-07-H-00009, Federal Highway Administration, Washington, D.C., 2011.

Daniel, J.S., "Development of a Simplified Fatigue Test and Analysis Procedure Using a Viscoelastic, Continuum Damage Model and its Implementation to WesTrack Mixtures," Ph.D. Dissertation, North Carolina State University, Raleigh, NC, 2001.

Daniel, J.S., Bennert, T., Kim, Y.R., Mogawer, W., Congalton, A., Mensching, D., Sabouri, M., and Elwardany, M., "Evaluation of Plant Produced RAP Mixtures in the Northeast: Phase I Interim Report." Transportation Pooled Fund Study 5(230), Federal Highway Administration, 2014.

Daniel, J.S., Pochily, J., and Boisvert, D. "Can More Reclaimed Asphalt Pavement Be Added? Study of Extracted Binder Properties from Plant Produced Mixtures with up to 25% Reclaimed Asphalt Pavement," Transportation Research Record: Journal of the Transportation Research Board, Vol. 2180, Transportation Research Board of the National Academies, Washington, D.C., 2010, 19-29.

Daniel, J.S., and Kim, Y.R., "Development of a Simplified Fatigue Test and Analysis Procedure Using a Viscoelastic Damage Model," Journal of the Association of Asphalt Paving Technologists, Vol. 71, 2002, 619-650.

Dongré, R., and D'Angelo, J., "Development of New Standard Test Methods for Characterizing Low Temperature Properties of Asphalt Binders," American Society of Testing and Materials Standardization News, November 2003.

Doyle, P.C., "Cracking Characteristic of Asphalt Cement," Journal of the Association of Asphalt Paving Technologists, Vol. 27, 1958, 581-597.

DriverLayer.com, Inc., < http://driverlayer.com/img/usa%20northeast%20region%20map/20/any >, Accessed February 6, 2015.

Dukatz, E., Hanz, A., and Reinke, G., "Implementation of Asphalt Mixture Cracking Tests in Wisconsin DOT Specification," Presented at 94th Annual Meeting of the Transportation Research Board, Washington, D.C., 2015.

Elwardany, M.D., "Performance of Plant Produced HMA Mixtures with High RAP Content in Terms of Low Temperature Cracking, Fatigue Cracking, and Moisture Induced Damage," M.S. Thesis, University of New Hampshire, 2012.

Epps, J., and Monismith, C.L., "Influence of Mixture Variables on the Flexural Fatigue Properties of Asphalt Concrete," Journal of the Association of Asphalt Paving Technologists, Vol. 38, 1969, 423-464.

Eslaminia, M., Thirunavukkarasu, S., Guddati, M.N., and Kim, Y.R., "Accelerated Pavement Performance Modeling Using Layered Viscoelastic Analysis," 7th RILEM International Conference on Cracking in Pavements, Delft, The Netherlands, 2012, 497-506.

Findley, W.N., Lai, J.S., and Onaran, K., "Creep and Relaxation of Nonlinear Viscoelastic Materials: With an Introduction to Linear Viscoelasticity," Dover Publications, Inc., Minneola, NY, 1976.

Fromm, H.J., and Phang, W.A., "Temperature Susceptibility Control in Asphalt Cement Specifications," Report IR35, Ontario Department of Highways, 1970.

Fromm, H.J., and Phang, W.A., "A Study of Transverse Cracking of Bituminous Pavements," Journal of the Association of Asphalt Paving Technologists, Vol. 41, 1972, 383-423.

Fugro Consultants, Inc., and Arizona State University, "A Performance-Related Specification for Hot-Mixed Asphalt," Report 704, National Cooperative Highway Research Program, National Research Council, Washington, D.C., 2011.

Gibson, N.H., "A Viscoelastoplastic Continuum Damage Model for the Compressive Behavior of Asphalt Concrete," Ph.D. Dissertation, University of Maryland, College Park, MD, 2006.

Gibson, N.H., Schwartz, C.W., Schapery, R.A., and Witczak, M.W., "Viscoelastic, Viscoplastic, and Damage Modeling of Asphalt Concrete in Unconfined Compression," Transportation Research Record, Vol. 1860, 2003, 3-15.

Gibson, N.H., Qi, X., Shenoy, A., Al-Khateeb, G., Kutay, M.E., Andriescu, A., Stuart, K., Youtcheff, J., and Harman, T., "Performance Testing for Superpave and Structural Validation," Report FHWA-HRT-11-045, Federal Highway Administration, McLean, VA, 2012.

Glover, C.J., Davison, R.R., Domke, C.H., Ruan, Y., Juristyarini, P., Knorr, D.B., and Jung, S.H., "Development of a New Method for Assessing Binder Durability with Field Validation," Report FHWA/TX-05/1872-2, Texas Department of Transportation, Austin, TX, 2005.

Griffith, A.A., "The Phenomena of Rupture and Flow in Solids," Philosophical Transactions of the Royal Society of London, Series A: Containing Papers of a Mathematical or Physical Character, Vol. 221, 1921, 163-198.

Gordon, G.V., and Shaw, M.T., "Computer Programs for Rheologists," Hanser/Gadner Publications, Cincinnati, OH, 1994.

Harvey, J.T., Deacon, J.A., Tsai, B., and Monismith, C.L., "Fatigue Performance of Asphalt Concrete Mixes and its Relationship to Asphalt Concrete Pavement Performance in California," Report RTA-65W485-2, California Department of Transportation, Sacramento, CA, 1995.

Heukelom, H., "Observations on the Rheology and Fracture of Bitumens and Asphalt Mixes," Journal of Association of Asphalt Paving Technologists, Vol. 36, 1966, 358-396.

Hills, J.F., and Brien, D., "The Fracture of Bitumens and Asphalt Mixes by Temperature Induced Stresses," Journal of Association of Asphalt Paving Technologists, Vol. 35, 1966, 292-309.

Hiltunen, D.R., and Roque, R. "A Mechanics-Based Prediction Model for Thermal Cracking of Asphaltic Concrete Pavements," Journal of the Association of Asphalt Paving Technologists, Vol. 63, 1994, 81-117.

Hopkins, I.L., and Hamming, R.W., "On Creep and Relaxation," Journal of Applied Physics, Vol. 28, No.8, 1957, 906-909.

Hou, T., Underwood, B.S., and Kim, Y.R., "Fatigue Performance Prediction of North Carolina Mixtures Using Simplified Viscoelastic Continuum Damage Model," Journal of the Association of Asphalt Paving Technologists, Vol. 79, 2010, 35-80.

Huang, B., Shu, X., and Zuo, G., "Using Notched Semi Circular Bending Fatigue Tests to Characterize Fracture Resistance of Asphalt Mixtures," Journal of Engineering Fracture Mechanics, Vol. 109, 2013, 78-88.

Huang, Y.H., "Pavement Analysis and Design," 2nd Edition, Prentice Hall, Inc., LOCATION, 2004.

Irwin, G.R., "Analysis of Stresses and Strains near the End of a Crack Traversing a Plate," Journal of Applied Mechanics, Vol. 24, 1957, 361-364.

Jadoun, F., "Calibration of the Flexible Pavement Distress Prediction Models in the Mechanistic Empirical Pavement Design Guide (MEPDG) for North Carolina," Ph.D. Dissertation, North Carolina State University, Raleigh, NC, 2011.

Jones, G.M., Darter, M.I., and Littlefield, G., "Thermal Expansion-Contraction of Asphaltic Concrete," Journal of the Association of Asphalt Paving Technologists, Vol. 37, 1968, 56-97.

Jung, D.H., and Vinson, T.S., "Low-Temperature Cracking: Test Selection," SHRP A-400, Strategic Highway Research Program, National Research Council, Washington, D.C., 1994.

Kaelble, D.H., "Computer-Aided Design of Polymers and Composites," Marcel Dekker, New York, NY, 1985.

Kandhal, P.S., "Low-Temperature Ductility in Relation to Pavement Performance," Low Temperature Properties of Bituminous Materials and Compacted Bituminous Paving Mixtures, ASTM STP 628, American Society for Testing and Materials, 1977, 95-106.

Kim, M., Mohammad, L.N., and Elseifi, M.A., "Characterization of Fracture Properties of Asphalt Mixtures as Measured by Semicircular Bend Test and Indirect Tension Test," Transportation Research Record, Vol. 2296, Transportation Research Board of the National Academies, Washington D.C., 2012, 115-124.

Kim, M., Mohammad, L., Challa, H., and Elseifi, M., "A Simplified Performance-Based Specification for Asphalt Pavements," in press, Journal of Association of Asphalt Paving Technologists, Vol. 84, 2015.

Kim, S-S., Sargand, S., and Wargo, A., "A Simple Test Procedure for Evaluating Low Temperature Crack Resistance of Asphalt Concrete," Report FHWA/OH-2009/5, Ohio Department of Transportation, Columbus, OH, 2009.

Kim, S-S., Wargo, A., and Powers, D., "Asphalt Concrete Cracking Device to Evaluate Low Temperature Performance of HMA," Journal of Association of Asphalt Paving Technologists, Vol. 79, 2010, 157-187.

Kim, Y.R. (ed.), "Modeling of Asphalt Concrete," McGraw-Hill, New York, NY, 2009.

Kim, Y.R., Daniel, J.S., and Wen, H., "Fatigue Performance Evaluation of WesTrack Asphalt Mixtures Using Viscoelastic Continuum Damage Approach," Report FHWA/NC/2002-004, North Carolina Department of Transportation, Raleigh, NC, 2002.

Kim, Y.R., and Little, D.N., "One-Dimensional Constitutive Modeling of Asphalt Concrete," Journal of Engineering Mechanics, Vol. 116, No. 4, 1990, 751-772.

Kim, Y.R., Underwood, B., Sakhaei Far, M., Jackson, N., and Puccinelli, J., "LTPP Computer Parameter: Dynamic Modulus," Report FHWA-HRT-10-035, Turner-Fairbank Highway Research Center, Federal Highway Administration, McLean, VA, 2011.

Kim, Y.R., and Wen, H., "Fracture Energy from Indirect Tension Testing," Journal of the Association of Asphalt Paving Technologists, Symposium, 2002, 779-793.

King, G., Anderson, M., Hanson, D., and Blankenship, P., "Using Black Space Diagrams to Predict Age-Induced Cracking," 7th RILEM International Conference on Cracking in Pavements, Delft, The Netherlands, 2012, 453-464.

Labuz, J.F., and Dai, S., "Cracking of Asphalt Concrete at Low Temperatures," Final Report, Center for Transportation Studies, University of Minnesota, Minneapolis, MN, 1994.

Leahy, R.B., Harrigan, E.T., and Von Quintus, H., "Validation of Relationships between Specification Properties and Performance," SHRP A-409 Report, Strategic Highway Research Program, National Research Council, Washington, D.C., 1994.

Lee, H.J., and Kim, Y.R., "Viscoelastic Constitutive Model for Asphalt Concrete Under Cyclic Loading", Journal of Engineering Mechanics, Vol. 124, No. 1, 1998a, 32-40.

Lee, H.J., and Kim, Y.R., "A Viscoelastic Continuum Damage Model of Asphalt Concrete with Healing", Journal of Engineering Mechanics, Vol. 124, No. 11, 1998b, 1224-1232.

Lee, J., Gibson, N., and Kim, Y.R., "Investigation of Effects of Asphalt Mix Design Targets and Compaction on Fatigue Performance of Asphalt Mixtures Using Mechanistic Models," Presented at 94th Annual Meeting of the Transportation Research Board, Washington, D.C., 2015.

Li, X., "Evaluation of the Factors that Affect the Fracture Resistance of Asphalt Mixtures at Low Temperatures Using Mechanical Testing and Acoustic Emission Methods," Ph.D. Dissertation, University of Minnesota, Minneapolis, MN, 2006.

Lytton, R.L., Uzan, J., Fernando, E.G., Roque, R., Hiltunen, D., and Stoffels, S.M., "Development and Validation of Performance Prediction Models and Specifications for Asphalt Binders and Paving Mixes," SHRP-A-357 Report, Strategic Highway Research Program, National Academies, Washington, D.C., 1993.

Ma, W., "Proposed Improvements to Overlay Test for Determining Cracking Resistance of Asphalt Mixtures," M.S. Thesis, Auburn University, Auburn, AL, 2014.

Mallick, R.B., and El-Korchi, T., "Pavement Engineering: Principles and Practice," 2nd Edition, CRC Press, Boca Raton, FL, 2013.

Marasteanu, M.O., "Role of Bending Beam Rheometer Parameters in Thermal Stress Calculations," Transportation Research Record, Vol. 1875, 2004, 9-13.

Marasteanu, M.O., and Anderson, D.A., "Booji and Thoone Approximation and Bitumen Relaxation Spectrum Generation, Proceedings of Eurobitume Workshop on Performance Related Properties for Bituminous Binders, Luxembourg, 1999.

Marasteanu, M.O., and Anderson, D.A., "Improved Model for Bitumen Rheological Characterization," Eurobitume Workshop on Performance Related Properties for Bituminous Binders, Brussels, Belgium, 1999.

Marasteanu, M., Buttlar, W., Bahia, H., and Williams, C. et al., "Investigation of Low Temperature Cracking in Asphalt Pavements – Phase II", National Pooled Fund Study, Report MN/RC 2012-23, Minnesota Department of Transportation, St. Paul, MN, 2012a.

Marasteanu, M., Falchetto, A.C., Turos, M., and Le, J-L., "Development of a Simple Test to Determine the Low Temperature Strength of Asphalt Mixtures and Binders," National Cooperative Highway Research Program Innovations Deserving Exploratory Analysis Program 151, Final Report, National Research Council, Washington, D.C., 2012b.

Marasteanu, M.O., Li, X., Clyne, T.R., Voller, V.R., Timm, D.H., and Newcomb, D.E., "Low Temperature Cracking of Asphalt Concrete Pavements," Report MN/RC – 2004-23, Minnesota Department of Transportation, St. Paul, MN, 2004.

Marasteanu, M., Teshale, E.Z., Moon, K.H., Turos, M., Buttlar, W., Dave, E., and Ahmed, S., "Investigation of Low Temperature Cracking in Asphalt Pavements National Pooled Fund Study – Phase II," Task 3 Report, Minnesota Department of Transportation, St. Paul, MN, 2012c.

Marasteanu, M., Velasquez, R., Falchetto, A.C., and Zofka, A., "Development of a Simple Test to Determine Low Temperature Creep Compliance of Asphalt Mixtures," National Cooperative Highway Research Program Innovations Deserving Exploratory Analysis Program Project 133, Final Report, National Research Council, Washington, D.C., 2009.

Marasteanu, M., Zofka, A., Turos, M., Li, X. Velasquez, R., Li, X., Buttlar, W., Paulino, G., Braham, A., Dave, E., Ojo, J., Bahia, H., Williams, C., Bausano, J., Gallistel, A., and McGraw, J., "Investigation of Low Temperature Cracking in Asphalt Pavements," National Pooled Fund Study 776, Report MN/RC 2007-43, Minnesota Department of Transportation, St. Paul, MN, 2007.

McDaniel, R.S., Shah, A., and Huber, G., "Investigation of Low- and High-Temperature Properties of Plant Produced RAP Mixtures," Report FHWA-HRT-11-058, Federal Highway Administration, McLean, VA, 2012.

McDaniel, R.S., Soleymani, H., Anderson, R.M., Turner, P., and Peterson, R., "Recommended Use of Reclaimed Asphalt Pavement in the Superpave Mix Design Method," National Cooperative Highway Research Program Web Document 30, Project D9-12, National Research Council, Washington, D.C., 2000.

McLeod, N.W., "A 4-Year Survey of Low Temperature Transverse Pavement Cracking on Three Ontario Test Roads," Journal of Association of Asphalt Paving Technologists, Vol. 41, 1972, 424-493.

Medeiros, Jr., M.S., "Characterization of Low-Temperature Properties of Plant-Produced RAP Mixtures in the Northeast," Ph.D. Dissertation, University of New Hampshire, Durham, NH, 2012.

Mensching, D.J., Daniel, J.S., Bennert, T., Medeiros, Jr., M.S., Elwardany, M.D., Mogawer, W., Hajj, E.Y., and Alavi, M.Z., "Low Temperature Properties of Plant-Produced RAP Mixtures in the Northeast," Journal of Road Materials and Pavement Design, Vol. 15, Supplement 1, Special Issue: Papers from the 89th Association of Asphalt Paving Technologists' Annual Meeting, 2014, 1-27.

Mensching, D.J., Rowe, G.M., Daniel, J.S., and Bennert, T., "Exploring Low Temperature Performance in Black Space," in press, Journal of Association of Asphalt Paving Technologists, Vol. 84, 2015.

Mogawer, W., Bennert, T., Daniel, J.S., Bonaquist, R., Austerman, A., and Booshehrian A., "Performance Characteristics of Plant Produced High RAP Mixtures," Journal of Road Materials and Pavement Design, Vol. 13, Supplement 1, Special Issue: Papers from the 87th Association of Asphalt Paving Technologists' Annual Meeting, 2012, 183-208.

Molenaar, J.M., and Molenaar, A.A.A., "Fracture Toughness of Asphalt in the Semi-Circular Bend Test," Proceedings of the 2nd Eurasphalt and Eurobitume Congress, Barcelona, Spain, 2000.

Monismith, C.L., Alexander, R.L., and Secor, K.E., "Rheological Behavior of Asphalt Concrete," Journal of Association of Asphalt Paving Technologists, Vol. 35, 1966, 400-450.

Monismith, C.L., Secor, G.A., and Secor, K.E., "Temperature Induced Stresses and Deformations in Asphalt Concrete," Journal of Association of Asphalt Paving Technologists, Vol. 34, 1965, 248-285.

Myers, L.A., Roque, R., and Ruth, B.E., "Mechanisms of Surface-Initiated Longitudinal Wheel Path Cracks in High-Type Bituminous Pavements," Journal of Association of Asphalt Paving Technologists, Vol. 67, 1998, 401-432.

Oliver, J.W.H., "The Influence of the Binder in RAP on Recycled Asphalt Properties," International Journal of Road Materials and Pavement Design, Vol. 2, No. 3, 2001, 311-325.

Paris, P.C., and Erdogan, F., "A Critical Analysis of Crack Propagation Laws," Journal of Fluids Engineering, Vol. 85, No. 4, 1963.

Park, S.W., and Schapery, R.A., "Methods of Interconversion between Linear Viscoelastic Material Functions: Part I – a Numerical Method Based on the Prony Series," International Journal of Solids and Structures, Vol. 36, 1999, 1653-1675.

Pell, P.S., and Taylor, I.F., "Asphaltic Road Materials in Fatigue," Journal of the Association of Asphalt Paving Technologists, Vol. 38, 1969, 371-464.

Pellinen, T., Rowe, G., and Biswas, K., "Evaluation of Surface (Top Down) Longitudinal Wheel Path Cracking," Report FHWA/IN/JTRP-2004/6, Indiana Department of Transportation, Indianapolis, IN, 2004.

Perez, N., "Fracture Mechanics," Kluwer Academic Publishers, Norwell, MA, 2004.

Readshaw, E.E., "Asphalt Specifications in British Columbia for Low Temperature Performance," Journal of Association of Asphalt Paving Technologists, Vol. 43, 1972, 562-581.

Reese, R., "Properties of Aged Binder Related to Asphalt Concrete Fatigue Life," Journal of Association of Asphalt Paving Technologists, Vol. 66, 1997, 604-632.

Rice, J.R., "A Path Independent Integral and the Approximate Analysis of Strain Concentration by Notches and Cracks," Journal of Applied Mechanics, Vol. 35, 1968, 379-386.

Romero, P., and Jones, Z.L., "Implementation of Low Temperature Tests for Asphalt Mixtures to Improve the Longevity of Road Surfaces," Report MPC-13-260, North Dakota State University Upper Great Plains Transportation Institute, Fargo, ND, 2013.

Roque, R., Birgisson, B., Sangpetngam, B., and Zhang, Z., "Hot Mix Asphalt Fracture Mechanics: A Fundamental Crack Growth Law for Asphalt Mixtures," Journal of Association of Asphalt Paving Technologists, Vol. 70, 2001, 816-827.

Roque, R., Zhang, Z., and Sankar, B., "Determination of Crack Growth Rate Parameters of Asphalt Mixtures Using the Superpave IDT," Journal of the Association of Asphalt Paving Technologists, Vol. 68, 1999, 404-433.

Rowe, G., "Phase Angle Determination and Interrelationships within Bituminous Materials," 7th International RILEM Symposium on Advanced Testing and Characterization of Bituminous Materials, Book 1 (Edited by Loizos, Partl, Scarpas and Al-Qadi), Rhodes, Greece, 2009, 43-52.

Rowe, G., "Evaluation of the Relationship between Asphalt Binder Properties and Non-Load Related Cracking," Prepared Discussion, Journal of the Association of Asphalt Paving Technologists, Vol. 80, 2011, 649-663.

Rowe, G., "Interrelationships in Rheology for Asphalt Binder Specifications," submitted to Canadian Technical Asphalt Association, 2014.

Rowe G.M., and Sharrock, M.J., "Development of Standard Techniques for the Calculation of Master Curves for Linear Viscoelastic Materials," 1st International Symposium on Binder Rheology and Pavement Performance, University of Calgary, Alberta, Canada, 2000.

Rowe, G.M., and Sharrock, M.J., "Alternate Shift Factor Relationship for Describing the Temperature Dependency of the Viscoelastic Behavior of Asphalt Materials," Transportation Research Record, Vol. 2207, Transportation Research Board of the National Academies, Washington D.C., 2011, 125-135.

Rowe, G.M., Baumgardner, G., and Sharrock, M.J., "Application of Rheological Models to Modified Binders," Presentation to the 48th Petersen Asphalt Research Conference, Western Research Institute, Laramie, WY, 2011.

Rowe, G.M., King, G., and Anderson, M., "The Influence of Binder Rheology on the Cracking of Asphalt Mixes on Airport and Highway Projects," 4th International Conference on Asphalt Materials, Guangzhou, China, 2013.

Rowe, G.M., Sharrock, M.J., Bouldin, M.G., and Dongre, R.N., "Advanced Techniques to Develop Asphalt Master Curves from the Bending Beam Rheometer," Journal of Petroleum and Coal, Vol. 43, No. 1, 2001, 54-59.

Sabouri, M., "Development of a Unified Fatigue Failure Criterion for Asphalt Mixtures and Its Applications to Reclaimed Asphalt Pavements," Ph.D. Dissertation, North Carolina State University, Raleigh, NC, 2014.

Sabouri, M., and Kim, Y.R., "Development of Failure Criterion for Asphalt Mixtures under Different Modes of Fatigue Loading," in press, Transportation Research Record, Transportation Research Board of the National Academies, Washington, D.C., 2014.

Sabouri, M., Bennert, T., Daniel, J.S., and Kim, Y.R., "A Comprehensive Evaluation of the Fatigue Behavior of Plant-Produced RAP Mixtures," in press, Journal of Association of Asphalt Paving Technologists, Vol. 84, 2015.

Schapery, R.A., "A Simple Collocation Method for Fitting Viscoelastic Models to Experimental Data," Report GALCIT SM 61-23A, California Institute of Technology, Pasadena, CA, 1961.

Schapery, R.A., "Correspondence Principles and a Generalized J-integral for Large Deformation and Fracture Analysis of Viscoelastic Media," International Journal of Fracture, Vol. 25, 1984, 195-223.

Schapery, R.A., "A Theory of Mechanical Behavior of Elastic Media with Growing Damage and Other Changes in Structure," Journal of Mechanics of Physical Solids, Vol. 38, No. 2, 1990, 215-253.

Schapery, R.A., and Park, S.W., "Methods of Interconversion between Linear Viscoelastic Material Functions: Part II – an Approximate Analytical Method," International Journal of Solids and Structures, Vol. 36, 1999, 1677-1699.

Shah, A., McDaniel, R.S., Huber, G.A., and Gallivan, V.L., "Investigation of Properties of Plant-Produced Reclaimed Asphalt Pavement Mixtures," Transportation Research Record: Journal of the Transportation Research Board, Vol. 1998, Transportation Research Board of the National Academies, Washington, D.C., 2007, 103-111.

Soules, T.F., Busbey, R.F., Rekhson, S.M., Markovsky, A., and Burke, M.A., "Finite-Element Calculation of Stresses in Glass Parts Undergoing Viscous Relaxation," Journal of the American Ceramic Society, Vol. 70, Issue 2, 1987, 90-95.

Soleymani, H.R., Anderson, M., McDaniel, R., and Abdelrahman, M., "Investigation of the Black Rock Issue for Recycled Asphalt Mixtures," Journal of the Association of Asphalt Paving Technologists, Vol. 69, 2000, 366-390.

Stoffels, S.M., Roque, R., and Farwana, T., "Evaluation and Field Validation of Proposed SHRP Binder Specification for Thermal Cracking," Transportation Research Record: Journal of the Transportation Research Board, Vol. 1436, Transportation Research Board of the National Academies, Washington, D.C., 1994, 1-10.

Tabatabaee, H., Velasquez, R., Arshadi, A., and Bahia, H., "Investigation of Low Temperature Cracking in Asphalt Pavements National Pooled Fund Study – Phase II," Task 5 Report, University of Wisconsin-Madison, 2012.

Texas Department of Transportation, "Test Procedure for Overlay Test," Tex-248-F, Austin, TX, 2014.

Tschoegl, N.W., "The Phenomenological Theory of Linear Viscoelastic Behavior: An Introduction," Springer-Verlag, Berlin, Germany, 1989.

Underwood, B.S., "Multiscale Constitutive Modeling of Asphalt Concrete," Ph.D. Dissertation, North Carolina State University, Raleigh, NC, 2011.

Underwood, B.S., Kim, Y.R., Guddati, M., Thirunavukkarasu, S., and Savadatti, S., "Response and Fatigue Performance Modeling of ALF Pavements Using 3-D Finite Element Analysis and a Simplified Viscoelastic Continuum Damage Model," Journal of the Association of Asphalt Paving Technologists, Vol. 78, 2009, 829-868.

Underwood, B.S., Kim, Y.R., and Guddati, M.N., "Improved Calculation Method of Damage Parameter in Viscoelastic Continuum Damage Model," International Journal of Pavement Engineering, Vol. 10, No. 6, 2010, 459-476.

Underwood, B.S., Sakhaei Far, M.S., and Kim, Y.R., "Using Limited Purchase Specification Tests to Perform Full Linear Viscoelastic Characterization of Asphalt Binder," American Society for Testing and Materials Journal of Testing and Evaluation, Vol. 38, No. 5, 2010.

VanLandingham, M.R., "Lecture 9", Course Handout from Materials 370: Mechanical Behavior of Solids, <in.materials.drexel.edu/blogs/mate_370/attachment/3976.ashx>, Drexel University, Philadelphia, PA, 2009.

Vinson, T.S., Janoo, V.C., and Haas, R.C.G., "Summary Report on Low Temperature and Thermal Fatigue Cracking," SHRP A/IR-90-001, Strategic Highway Research Program, National Research Council, Washington, D.C., 1990.

Wagoner, M.P., Buttlar, W.G., and Paulino, G.H., "Disk-shaped Compact Tension Test for Asphalt Concrete Fracture," Journal of the Society for Experimental Mechanics, Vol. 45, No. 3, 2005, 270-277.

Wagoner, M.P., Buttlar, W.G., Paulino, G.H., and Blankenship, P., "Investigation of the Fracture Resistance of Hot-Mix Asphalt Concrete Using a Disk-Shaped Compact Tension Test," Transportation Research Record: Journal of the Transportation Research Board, Vol. 1929, Transportation Research Board of the National Academies, Washington, D.C., 2005, 183-192.

Walubita, L.F., Faruk, A.N., Das, G., Tanvir, H.A., Zhang, J., and Scullion, T., "The Overlay Tester: A Sensitivity Study to Improve Repeatability and Minimize Variability in the Test Results," Report FHWA/TX-12/0-6607-1, Texas Department of Transportation, Austin, TX, 2012.

Wang, H., and Al-Qadi, I.L., "Near-Surface Pavement Failure Under Multiaxial Stress State in Thick Asphalt Pavements," Transportation Research Record: Journal of the Transportation

Research Board, Vol. 2154, Transportation Research Board of the National Academies, Washington, D.C., 2010, 91-99.

West, R., Willis, J.R., and Marasteanu, M., "Improved Mix Design, Evaluation, and Materials Management Practices for Hot Mix Asphalt with High Reclaimed Asphalt Pavement Content," NCHRP 9-46 Final Report, National Cooperative Highway Research Program, National Research Council, Washington, D.C., 2013.

Williams, M.L., Landel, R.F., and Ferry, J.D., "The Temperature Dependence of Relaxation Mechanisms in Amorphous Polymers and Other Glass-forming Liquids," Journal of the American Chemical Society, Vol. 77, 1955, 3701-3706.

Witczak, M., "Simple Performance Tests: Summary of Recommended Methods and Database," Report 547, National Cooperative Highway Research Program, National Research Council, Washington, D.C., 2005.

Yoder, E.J., and Witczak, M.W., "Principles of Pavement Design," 2nd Edition, John Wiley and Sons, Inc., New York, NY, 1975.

Yoo, P.J., and Al-Qadi, I.L., "The Truth and Myth of Fatigue Cracking Potential in Hot-Mix Asphalt: Numerical Analysis and Validation," Journal of Association of Asphalt Paving Technologists, Vol. 77, 2008, 549-590.

Zeiada, W.A., Kaloush, K.E., Underwood, B.S., and Mamlouk, M.S., "Effect of Air Voids and Asphalt Content on Fatigue Damage Using the Viscoelastic Continuum Damage Analysis," Proceedings of the 2013 Airfield and Highway Pavement Conference, American Society of Civil Engineers, Los Angeles, CA, 2013, 1122-1133.

Zhang, J., Sabouri, M., Kim, Y.R., and Guddati, M.N., "Development of a Failure Criterion for Asphalt Mixtures under Fatigue Loading," Journal of Road Materials and Pavement Design, Vol. 14, Supplement 2, Special Issue: Papers from the 88th Association of Asphalt Paving Technologists' Annual Meeting, 2013, 1-15.

Zhang, Z., Roque, R., and Birgisson, B., "Evaluation of Laboratory Measured Crack Growth Rate for Asphalt Mixtures," Transportation Research Record: Journal of the Transportation Research Board, Vol. 1767, Transportation Research Board of the National Academies, Washington, D.C., 2001, 67-75.

Zhou, F., Hu, S., and Scullion, T., "Development and Verification of the Overlay Tester Based Fatigue Cracking Prediction Approach," Report FHWA/TX-07/9-1502-01-8, Texas Department of Transportation, Austin, TX, 2007.

Zofka, A., Marasteanu, M., Li, X., Clyne, T., and McGraw, J. "Simple Method to Obtain Asphalt Binders Low Temperature Properties from Asphalt Mixture Properties," Journal of the Association of Asphalt Paving Technologists, Vol. 74, 2005, 255-282.

Table A.1: Raw binder data for Black Space analysis – Michigan 1998 project (Chapter 4)

Bending Beam Rheometer Results			
Temperature (°C)	**Time (s)**	**Stiffness (MPa)**	**m-value**
-18	8	309	0.287
	15	255	0.315
	30	204	0.346
	60	159	0.378
	120	122	0.409
	240	91	0.440
-24	8	489	0.210
	15	425	0.236
	30	356	0.265
	60	294	0.294
	120	238	0.323
	240	188	0.351
Dynamic Shear Rheometer Results			
Temperature (°C)	**Frequency (rad/s)**	**G* (MPa)**	**δ (degrees)**
13	10	6,793	49.95
16		4,439	53.30
58		2.65	83.85
64		1.15	85.50

Table A.2: Raw binder data for Black Space analysis – Ontario 1998 project (Chapter 4)

Bending Beam Rheometer Results			
Temperature (°C)	Time (s)	Stiffness (MPa)	m-value
-18	8	370	0.231
	15	318	0.248
	30	266	0.267
	60	220	0.286
	120	179	0.305
	240	144	0.324
-24	8	673	0.189
	15	596	0.209
	30	510	0.230
	60	433	0.252
	120	360	0.269
	240	296	0.295
Dynamic Shear Rheometer Results			
Temperature (°C)	Frequency (rad/s)	G* (MPa)	δ (degrees)
58	10	12.60	73.90
64		5.90	77.00
70		3.20	79.25
76		2.00	78.60

Table A.3: Raw binder data for Black Space analysis – Quebec 2001 project (Chapter 4)

Bending Beam Rheometer Results			
Temperature (°C)	Time (s)	Stiffness (MPa)	m-value
-24	8	551	0.233
	15	470	0.258
	30	391	0.284
	60	319	0.311
	120	254	0.338
	240	199	0.365
-30	8	863	0.162
	15	775	0.186
	30	675	0.213
	60	576	0.240
	120	483	0.266
	240	399	0.293
Dynamic Shear Rheometer Results			
Temperature (°C)	Frequency (rad/s)	G* (MPa)	δ (degrees)
64	10	1.70	84.40
70		0.80	85.80
76		0.40	87.80

Table A.4: Raw binder data for Black Space analysis – Saskatchewan 1998 project (Chapter 4)

Bending Beam Rheometer Results			
Temperature (°C)	Time (s)	Stiffness (MPa)	m-value
-24	8	462	0.264
	15	389	0.291
	30	318	0.321
	60	254	0.351
	120	199	0.381
	240	152	0.411
-30	8	795	0.222
	15	680	0.249
	30	569	0.278
	60	467	0.307
	120	372	0.336
	240	292	0.365
Dynamic Shear Rheometer Results			
Temperature (°C)	Frequency (rad/s)	G* (MPa)	δ (degrees)
46	10	7.80	82.90
52		3.30	84.80
58		1.70	86.10

Table A.5: Raw binder data for Black Space analysis – Saskatchewan 1999 project (Chapter 4)

Bending Beam Rheometer Results			
Temperature (°C)	Time (s)	Stiffness (MPa)	m-value
-24	8	353	0.300
	15	288	0.334
	30	225	0.371
	60	173	0.408
	120	128	0.445
	240	93	0.483
-30	8	813	0.199
	15	708	0.230
	30	596	0.264
	60	492	0.299
	120	395	0.333
	240	309	0.368
Dynamic Shear Rheometer Results			
Temperature (°C)	Frequency (rad/s)	G* (MPa)	δ (degrees)
52	10	2.76	85.46
58		1.24	86.94

Table A.6: Raw binder data for Black Space analysis – Saskatchewan 2001 project (Chapter 4)

Bending Beam Rheometer Results			
Temperature (°C)	Time (s)	Stiffness (MPa)	m-value
-30	8	837	0.196
	15	732	0.228
	30	615	0.263
	60	509	0.298
	120	409	0.333
	240	319	0.368
Dynamic Shear Rheometer Results			
Temperature (°C)	Frequency (rad/s)	G* (MPa)	δ (degrees)
52	10	2.80	85.40
58		1.30	86.80

Table A.7: Christensen-Anderson-Marasteanu master curve and modified Kaelble shift factor coefficients for LTPP binders at 15°C reference temperature (Chapter 4)

Project	G_0 (MPa)	ω_0 (rad/s)	b	k	T_k (°C)	C1	C2
MI_1998	885.7	144.3	0.285	1.0	-24.0	28.8102	147.4
ON_1998	4,957.5	5.514	0.112	1.0	-24.0	27.7516	105.2
QC_2001	1,833.6	211.2	0.215	1.0	-26.0	26.0855	125.9
SK_1998	3,548.7	620.7	0.170	1.0	N/A	23.63*	184.81*
SK_1999	1,786.0	5,986.5	0.246	1.0	-24.0	17.8143	70.1
SK_2001	No functional fit available				N/A	19.90*	170.87*

  * - Williams-Landel-Ferry shift factor equation used

Table A.8: Christensen-Anderson-Marasteanu master curve and modified Kaelble shift factor coefficients for Indiana binders at 25°C reference temperature (Chapter 5)

Binder	G_0 (MPa)	ω_0 (rad/s)	b	k	T_k (°C)	C1	C2
Site 1	6,715	14.18	0.156	1.0	-18.0	35.1730	195.2
Site 2	4,937	69.29	0.197	1.0	-18.0	32.0529	192.3
Site 3	6,910	40.16	0.168	1.0	-12.0	25.7820	134.5

Table A.9: Christensen-Anderson-Marasteanu master curve and modified Kaelble shift factor coefficients for Lamont Test Road binders at 25°C reference temperature (Chapter 5)

Binder	G_0 (MPa)	ω_0 (rad/s)	b	k	T_k (°C)	C1	C2
L1	5,576	65.22	0.087	1.0	-19.5	38.0101	190.8
L2	1,912	1,906.6	0.140	1.0	-14.0	29.8591	149.8
L3	1,911	18,922	0.147	1.0	-14.0	16.8061	75.5
L4	1,263	438.31	0.149	1.0	-23.0	39.9651	184.4
L5	5,026	271.24	0.099	1.0	-33.0	30.7823	138.2
L6	930	0.0024	0.191	1.0	-30.0	12.5204	54.1
L7	1,181	1.65E-05	0.176	1.0	-30.0	9.1503	36.4

Table A.10: Richards master curve and modified Kaelble shift factor coefficients for New Jersey mixtures at 15°C reference temperature (Chapter 5)

Mixture	α	β	δ	γ	λ	T_k (°C)	C1	C2
0% RAP	3.407	-1.765	0.993	-0.586	0.997	20.0	15.869	115.890
30% RAP	4.293	-1.870	0.191	-0.418	0.957	3.9	25.950	170.830

Table A.11: Richards master curve and modified Kaelble shift factor coefficients for Indiana mixtures at 15°C reference temperature (Chapter 5)

Mixture	α	β	δ	γ	λ	T_k (°C)	C1	C2
Site 1	3.411	-1.504	0.783	-0.559	0.995	10.0	17.393	85.157
Site 2	4.991	-1.877	-0.817	-0.627	4.228	10.0	45.082	320.590
Site 3	4.298	-1.686	-0.001	-0.427	0.659	4.0	78.290	519.160

Table A.12: Richards master curve and modified Kaelble shift factor coefficients for Pooled Fund mixtures at 15°C reference temperature (Chapters 5, 6, and 7)

Mixture	α	β	δ	γ	λ	T_k (°C)	C1	C2
NHe00	3.493	-1.247	0.810	-0.530	0.999	3.9	34.136	261.300
NHe20	3.870	-1.387	0.526	-0.451	0.963	3.9	22.209	157.000
NHe30	3.992	-1.445	0.419	-0.428	0.964	3.9	23.389	161.400
NHe40	3.839	-1.358	0.634	-0.375	0.483	3.9	27.375	193.100
NYb30	3.470	-1.345	0.961	-0.494	0.999	3.9	16.339	109.300
NYd00	3.724	-1.577	0.763	-0.447	0.977	3.9	28.532	191.900
NYd20	3.915	-1.659	0.566	-0.436	0.952	3.9	30.751	213.200
NYd30	3.890	-1.634	0.592	-0.436	0.963	3.9	20.461	127.300
NYd40	3.671	-1.702	0.807	-0.424	0.935	3.9	26.963	181.500
VTa00	3.344	-0.738	0.979	-0.434	1.000	3.9	23.014	161.500
VTa20	3.469	-0.912	0.916	-0.407	0.968	3.9	21.171	143.300
VTa30	3.764	-0.998	0.673	-0.388	0.970	3.9	25.713	177.600
VTa40	4.123	-1.108	0.295	-0.391	0.964	3.9	24.710	161.814
VTe00	4.112	-1.300	0.318	-0.408	0.973	3.9	16.267	110.100
VTe20	3.916	-1.308	0.464	-0.434	0.944	3.9	23.574	162.800
VTe30	4.027	-1.444	0.363	-0.420	0.765	3.9	26.334	184.200
VTe40	3.859	-1.317	0.527	-0.440	0.960	3.9	20.041	133.300

Table A.13: Calculations for input of asphalt layer modulus for NH mixture (Chapter 7)

NHe00					
Depth (in.)	Effective depth (in.)	Effective length (in.)	Time (s)	Temperature (°F)	|E*| (psi)
0.25	1.57	13.3	0.013	51.0	1.96E+06
0.75	4.65	19.5	0.018	54.5	1.79E+06
1.50	9.12	28.4	0.027	57.5	1.63E+06
2.50	14.92	40.0	0.038	59.7	1.49E+06
3.50	20.57	51.3	0.049	61.1	1.39E+06
6.00	34.10	78.4	0.074	63.1	1.23E+06

Table A.14: Calculations for input of asphalt layer modulus for NY PG 64-22 mixtures (Chapter 7)

Depth (in.)	Effective depth (in.)	Effective length (in.)	Time (s)	Temperature (°F)	|E*| (psi)
NYd00					
0.25	1.77	13.7	0.013	55.6	2.83E+06
0.75	5.26	20.7	0.020	59.4	2.57E+06
1.50	10.29	30.8	0.029	62.4	2.34E+06
2.50	16.84	43.9	0.042	64.6	2.14E+06
3.50	23.22	56.6	0.054	65.9	2.00E+06
6.00	38.53	87.3	0.083	67.9	1.79E+06
NYd20					
0.25	1.76	13.7	0.013	55.6	2.79E+06
0.75	5.23	20.7	0.020	59.4	2.54E+06
1.50	10.25	30.7	0.029	62.3	2.32E+06
2.50	16.78	43.8	0.041	64.5	2.13E+06
3.50	23.15	56.5	0.054	65.9	2.00E+06
6.00	38.46	87.1	0.082	67.9	1.79E+06
NYd30					
0.25	1.76	13.7	0.013	55.6	2.78E+06
0.75	5.22	20.6	0.020	59.4	2.52E+06
1.50	10.22	30.6	0.029	62.3	2.29E+06
2.50	16.72	43.7	0.041	64.5	2.10E+06
3.50	23.06	56.3	0.053	65.9	1.97E+06
6.00	38.28	86.8	0.082	67.8	1.76E+06
NYd40					
0.25	1.78	13.8	0.013	55.6	2.86E+06
0.75	5.28	20.8	0.020	59.4	2.62E+06
1.50	10.36	30.9	0.029	62.4	2.41E+06
2.50	16.98	44.2	0.042	64.6	2.23E+06
3.50	23.46	57.1	0.054	66.0	2.11E+06
6.00	39.09	88.4	0.084	67.9	1.91E+06

Table A.15: Calculations for input of asphalt layer modulus for NY mixtures (Chapter 7)

			NYb30		
Depth (in.)	**Effective depth (in.)**	**Effective length (in.)**	**Time (s)**	**Temperature (°F)**	**|E*| (psi)**
0.25	1.69	13.6	0.013	55.5	2.47E+06
0.75	5.02	20.2	0.019	59.2	2.23E+06
1.50	9.81	29.8	0.028	62.1	2.01E+06
2.50	16.03	42.3	0.040	64.3	1.83E+06
3.50	22.08	54.4	0.051	65.7	1.71E+06
6.00	36.56	83.3	0.079	67.7	1.51E+06

Table A.16: Calculations for input of asphalt layer modulus for VT PG 52-34 mixtures (Chapter 7)

			VTa00		
Depth (in.)	**Effective depth (in.)**	**Effective length (in.)**	**Time (s)**	**Temperature (°F)**	**|E*| (psi)**
0.25	1.43	13.1	0.012	47.2	1.49E+06
0.75	4.23	18.7	0.018	50.6	1.32E+06
1.50	8.24	26.7	0.025	53.5	1.17E+06
2.50	13.41	37.0	0.035	55.7	1.04E+06
3.50	18.41	47.0	0.045	57.1	9.57E+05
6.00	30.28	70.8	0.067	59.1	8.29E+05
			VTa20		
Depth (in.)	**Effective depth (in.)**	**Effective length (in.)**	**Time (s)**	**Temperature (°F)**	**|E*| (psi)**
0.25	1.51	13.2	0.013	47.3	1.77E+06
0.75	4.48	19.2	0.018	50.8	1.57E+06
1.50	8.74	27.7	0.026	53.7	1.40E+06
2.50	14.24	38.7	0.037	55.9	1.26E+06
3.50	19.57	49.3	0.047	57.3	1.16E+06
6.00	32.27	74.7	0.071	59.3	1.02E+06
			VTa30		
Depth (in.)	**Effective depth (in.)**	**Effective length (in.)**	**Time (s)**	**Temperature (°F)**	**|E*| (psi)**
0.25	1.55	13.3	0.013	47.4	1.90E+06
0.75	4.59	19.4	0.018	50.9	1.68E+06
1.50	8.94	28.1	0.027	53.8	1.49E+06
2.50	14.55	39.3	0.037	56.0	1.34E+06
3.50	20.00	50.2	0.048	57.4	1.24E+06
6.00	32.97	76.2	0.072	59.4	1.08E+06

		VTa40			
Depth (in.)	**Effective depth (in.)**	**Effective length (in.)**	**Time (s)**	**Temperature (°F)**	**|E*| (psi)**
0.25	1.54	13.3	0.013	47.4	1.86E+06
0.75	4.56	19.3	0.018	50.9	1.65E+06
1.50	8.87	28.0	0.026	53.8	1.46E+06
2.50	14.44	39.1	0.037	56.0	1.31E+06
3.50	19.84	49.9	0.047	57.4	1.20E+06
6.00	32.68	75.6	0.072	59.4	1.05E+06

Table A.17: Calculations for asphalt layer modulus input for VT PG 64-28 mixtures (Chapter 7)

		VTe00			
Depth (in.)	**Effective depth (in.)**	**Effective length (in.)**	**Time (s)**	**Temperature (°F)**	**|E*| (psi)**
0.25	1.63	13.5	0.013	47.5	2.19E+06
0.75	4.82	19.9	0.019	51.1	1.98E+06
1.50	9.42	29.1	0.028	54.1	1.78E+06
2.50	15.40	41.0	0.039	56.3	1.62E+06
3.50	21.21	52.6	0.050	57.7	1.51E+06
6.00	35.13	80.5	0.076	59.6	1.34E+06
		VTe20			
Depth (in.)	**Effective depth (in.)**	**Effective length (in.)**	**Time (s)**	**Temperature (°F)**	**|E*| (psi)**
0.25	1.61	13.4	0.013	47.5	2.12E+06
0.75	4.77	19.7	0.019	51.1	1.92E+06
1.50	9.33	28.9	0.027	54.0	1.74E+06
2.50	15.26	40.7	0.039	56.2	1.59E+06
3.50	21.04	52.3	0.050	57.6	1.49E+06
6.00	34.88	80.0	0.076	59.6	1.32E+06
		VTe30			
Depth (in.)	**Effective depth (in.)**	**Effective length (in.)**	**Time (s)**	**Temperature (°F)**	**|E*| (psi)**
0.25	1.63	13.5	0.013	47.5	2.22E+06
0.75	4.85	19.9	0.019	51.1	2.02E+06
1.50	9.50	29.2	0.028	54.1	1.85E+06
2.50	15.55	41.3	0.039	56.3	1.69E+06
3.50	21.46	53.1	0.050	57.7	1.59E+06
6.00	35.65	81.5	0.077	59.7	1.43E+06

Table A.17 (continued): Calculations for asphalt layer modulus input for VT PG 64-28 mixtures (Chapter 7)

VTe40					
Depth (in.)	Effective depth (in.)	Effective length (in.)	Time (s)	Temperature (°F)	|E*| (psi)
0.25	1.63	13.5	0.013	47.5	2.20E+06
0.75	4.83	19.9	0.019	51.1	2.00E+06
1.50	9.46	29.1	0.028	54.1	1.81E+06
2.50	15.46	41.1	0.039	56.3	1.65E+06
3.50	21.32	52.8	0.050	57.7	1.55E+06
6.00	35.36	80.9	0.077	59.7	1.38E+06

Table A.18: Determination of closest measured dynamic modulus and phase angle to predicted properties at bottom of thin asphalt layer (Chapter 7)

Test temperature-frequency (°C-Hz)	Average distance in vector space	Number of instances distance in vector space < 1,500
4-1	866	4
4-5	455	13
4-10	687	12

Table A.19: Determination of closest measured dynamic modulus and phase angle to predicted properties at bottom of thick asphalt layer (Chapter 7)

Test temperature-frequency (°C-Hz)	Average distance in vector space	Number of instances distance in vector space < 1,500
4-0.5	631	7
4-1	1,032	16
4-5	1,038	7

Table A.20: Cycles to failure when $G^R = 100$, with function form $N_f = r(G^R)^s$ (Chapter 7)

Mixture	Fit parameter r	Fit parameter s	N_f at $G^R = 100$ J/m^3
NHe00	4.85E+05	-8.06E-01	11,838
NYb30	3.95E+05	-6.90E-01	16,491
NYd00	7.02E+05	-7.84E-01	19,014
NYd20	2.31E+05	-6.05E-01	14,203
NYd30	4.17E+05	-6.82E-01	18,061
NYd40	9.37E+05	-7.85E-01	25,248
VTa00	4.89E+05	-7.14E-01	18,224
VTa20	3.34E+05	-6.08E-01	20,302
VTa30	7.72E+05	-7.44E-01	25,101
VTa40	4.67E+05	-6.93E-01	19,171
VTe00	2.52E+05	-5.76E-01	17,776
VTe20	4.28E+05	-6.72E-01	19,366
VTe30	3.88E+05	-6.57E-01	18,818
VTe40	1.74E+05	-5.46E-01	14,085

Table A.21: Parameters used for controlled stress mixture fatigue indicator (Chapter 7)

Mixture	Alpha	C_f	$\|E^*\|$ at 4°C-1 Hz (MPa)	δ at 4°C-1 Hz (degrees)	Modified Glover-Rowe (MPa)	$\|E^*\|$ tan δ (MPa)	E' (MPa)	E'' (MPa)
NHe00	3.193	0.124	7,455	19.16	20,268	2,590	7,042	2,447
NYb30	3.388	0.102	11,103	15.82	37,695	3,147	10,683	3,027
NYd00	3.431	0.160	13,813	13.22	57,239	3,245	13,447	3,159
NYd20	3.400	0.120	13,494	13.01	56,922	3,117	13,148	3,037
NYd30	3.403	0.120	13,911	12.75	59,940	3,149	13,568	3,071
NYd40	3.608	0.117	14,548	11.29	71,475	2,904	14,267	2,848
VTa00	3.623	0.075	4,468	21.81	10,365	1,788	4,148	1,660
VTa20	3.815	0.079	5,831	19.40	15,619	2,053	5,500	1,937
VTa30	3.736	0.080	6,289	18.86	17,417	2,149	5,951	2,033
VTa40	3.509	0.084	6,659	18.69	18,643	2,253	6,308	2,134
VTe00	3.420	0.072	7,980	17.15	24,711	2,463	7,625	2,353
VTe20	3.366	0.093	7,817	17.57	23,543	2,475	7,453	2,359
VTe30	3.239	0.097	8,638	16.47	28,029	2,553	8,284	2,448
VTe40	3.323	0.108	8,350	16.79	26,499	2,519	7,994	2,412

Table A.22: Exponential parameters for damage characteristic curves (Chapter 7)

Mixture	Fit parameter a	Fit parameter b
NHe00	-2.27E-03	5.67E-01
NYb30	-1.89E-03	5.60E-01
NYd00	-1.24E-03	5.81E-01
NYd20	-1.93E-03	5.44E-01
NYd30	-1.58E-03	5.57E-01
NYd40	-1.20E-03	5.68E-01
VTa00	-6.19E-04	7.29E-01
VTa20	-7.52E-04	6.86E-01
VTa30	-7.87E-04	6.74E-01
VTa40	-1.80E-03	6.10E-01
VTe00	-1.79E-03	5.84E-01
VTe20	-1.75E-03	5.83E-01
VTe30	-1.81E-03	5.79E-01
VTe40	-1.81E-03	5.83E-01